The Dissertation Committee for Scott Garrett Miller
certifies that this is the approved version of the following dissertation:

Mutagenic Analysis of the Decarboxylases and Hydratases in Parallel Meta-Fission Pathways

Committee:

_____
Christian P. Whitman, Supervisor

_____
Sean M. Kerwin

_____
Hung-wen Liu

_____
Walter L. Fast

_____
Marvin L. Hackert

Mutagenic Analysis of the Decarboxylases and Hydratases in Parallel Meta-Fission Pathways

by

Scott Garrett Miller, B.S.

Dissertation

Presented to the Faculty of the Graduate School of

The University of Texas at Austin

in Partial Fulfillment

of the Requirements

for the Degree of

Doctor of Philosophy

The University of Texas at Austin

August 2008

Dedication

I would like to dedicate this dissertation to my Mom and Dad.

Thank you for the support and encouragement over the years. Your guidance has always been appreciated along this long road.

Acknowledgments

I would like to thank the National Institutes of Health (GM-41239), the Robert A. Welch Foundation (F-1334), and The University of Texas at Austin for their generous financial support these past years. Without their assistance this compilation of work would not have been possible. First and foremost I would like to express my gratitude to my advisor, Dr. Christian P. Whitman. His patience, encouragement, and guidance during my graduate studies have been essential in helping me establish a strong foundation for my professional career. I would like to thank Dr. Gerrit J. Poelarends, Dr. Susan C. Wang, and Dr. William H. Johnson, Jr. who not only introduced me to the laboratory, but were instrumental in teaching me all the techniques and giving good advice along the way. You have all been good friends and colleagues. Thank you to Hector Serrano for being a great friend and benchmate. We were always able to lend each other a helping hand during our time in the lab. A very special thank you goes to my son, Benjamin Miller, who has been an inspiration and an ever positive influence in my life. Finally, I would like to thank all the people who have helped me in some way during my studies at The University of Texas at Austin. These last few years have been interesting and rewarding.

Mutagenic Analysis of the Decarboxylases and Hydratases in Parallel Meta-Fission Pathways

Publication No. _____

Scott Garrett Miller, Ph.D.

The University of Texas at Austin, 2008

Supervisor: Christian P. Whitman

The catechol meta-fission pathway, a degradation pathway for simple aromatic compounds, is rich in enzyme chemistry and replete with structural and evolutionary diversity. Vinyl pyruvate hydratase (VPH) and MhpD catalyze the same reaction in this pathway, but in different bacterial species. These metal ion-dependent enzymes reportedly catalyze a 1,5-keto-enol tautomerization reaction followed by a Michael addition of water. MhpD, and most likely VPH, are members of the fumarylacetoacetate hydrolase (FAH) superfamily. The crystal structure of MhpD and the sequence of VPH identified four potential active site residues, Lys-60, Leu-72, Asp-78, and Ser-160 (Ser-161 in VPH). The K60A and D78N mutants of VPH and MhpD had the most damaging effects on catalysis. Moreover, the K60A mutant seemingly uncoupled tautomerization from hydration and provided evidence for an α,β–unsaturated ketone in the reaction. The

effects of the L72A and S160A (S161A in VPH) mutants were smaller, suggesting less important roles in the mechanism.

5-(carboxymethyl)-2-Oxo-3-hexene-1,6-dioate decarboxylase (COHED) is a metal ion-dependent enzyme in the homoprotocatechuate (HPC) pathway, a chromosomally encoded meta-fission pathway from *Escherichia coli* C that parallels the catechol meta-fission pathway. COHED is also a member of the FAH superfamily. It is a monomeric protein with two domains. It is postulated that the C-terminal domain catalyzes the decarboxylation reaction and the N-terminal domain carries out the 1,3-keto-enol tautomerization reaction. Site-directed mutagenesis, NMR, and kinetic analysis with different substrates and inhibitors have identified three potential active-site residues Glu-276, Glu-278 (in the C-terminal domain), and Lys-110 (in the N-terminal domain). Replacement of either glutamate with a glutamine eliminated both the decarboxylase and tautomerase activities. The K110A mutant also diminished both activities, but more importantly eliminated the C-3 proton/deuteron exchange reaction observed for substrate analogs. The enzymes of the catechol and homoprotocatechuate pathways provide examples of enzyme optimization toward a specific substrate even among related compounds, as reflected by the FAH superfamily. Hence, the results of these studies add to the growing body of information about how enzymes evolve and how pathways are assembled.

Table of Contents

List of Tables

List of Figures

List of Schemes

Chapter 1: Introduction

Evolution of Metabolic Pathways

The origin and assembly of metabolic pathways and how the enzymes in them evolve have been explored over the past 70 years or so. Two different models for the formation of metabolic pathways were put forth early on, the retro-evolution or retrograde theory by Horowitz in 1945 and the recruitment theory of "borrowed" enzymes proposed by Jensen in 1976 (1-3). The retro-evolution theory suggests that enzymes evolved in a backward manner where the last enzyme in a pathway is the parent of all of the proteins that precede it in the pathway. According to this idea, the first organisms existed in a rich "primordial soup" in which the environment provided all the necessary nutrients (vitamins, sugars, amino acids, etc.) required for life (1). In time these essential nutrients were depleted. There was selective pressure to add steps to metabolic pathways to utilize available precursors, and organisms capable of synthesizing their own nutrients developed a selective advantage. Initially, the biosynthetic pathways involved a single step in which an abundant precursor was consumed to generate the required nutrient (Figure 1.1).

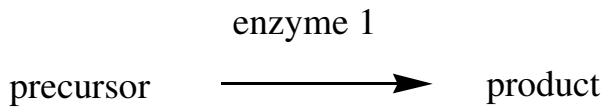

Figure 1.1. Depiction of Horowitz's retrograde theory, where enzyme 1 converts an abundant precursor into a desired product.

In this manner, the substrate of one reaction becomes the product for the reaction immediately preceding it. The expansion of pathways by this model assumes that a new enzyme evolves to supply the depleted substrate from a more abundant precursor by evolution of the enzyme that uses the substrate. If this were the case, the two consecutive enzymes would share some active-site architecture. This similarity in structure would result by the duplication of the existing gene encoding the protein and modification through mutation to generate a new protein to catalyze a preceding step. In Horowitz's view, enzyme 2 (Figure 1.2) arises as a result of the duplication and modification of the gene encoding for enzyme 1. These are homologous enzymes, meaning they are derived from a common ancestor and are therefore structurally related and often times show a

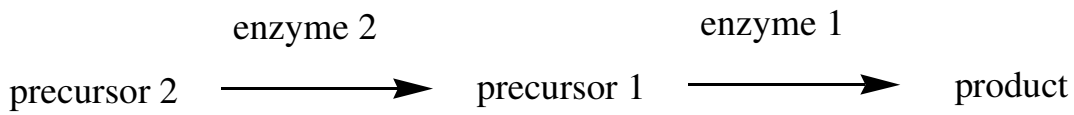

Figure 1.2. Depiction of Horowitz's retrograde theory, where enzyme 2 results from a gene duplication of enzyme 1 followed by mutation.

high degree of sequence similarity (4). Thus, as pathways grew in size and complexity, they expanded in a retrograde or backward manner. The "last" enzyme in the pathway

(enzyme 1, Figure 1.2) is the ancestral parent for all the other preceding proteins in the series. Each additional new enzyme would confer an evolutionary advantage to the host organism allowing it to synthesize a supplementary nutrient requirement.

According to Horowitz, the mechanisms of the reactions catalyzed by the ancestral enzyme and the newly evolved enzyme are not necessarily related, but they may share the ability to bind the same substrate and/or product (4). This theory suggests that substrate binding is the primary evolutionary constraint. The retro-evolution model has vulnerable points. For example, many metabolic intermediates are too unstable for an enzyme to evolve to utilize them as substrates (3). As these metabolic intermediates are removed from the environment, their availability would continue to decline, creating another obstacle for the retrograde theory (5). In addition, if the retrograde model were always applicable, many pathways would consist of homologous proteins catalyzing successive reactions. Although there are examples of homologous proteins being sequentially encoded within an operon, they are the exception not the rule. The consecutive enzymes in the tryptophan biosynthetic pathway exemplify substrate-constrained evolution (6).

(Potential) Retrograde Evolution: PRAI and InGPS

In tryptophan biosynthesis, phosphoribosylanthranilate isomerase (PRAI or TrpF) and indoleglycerol phosphate synthase (InGPS or TrpC) catalyze sequential reactions (Figure 1.3). These two proteins are generally expressed separately in most organisms,

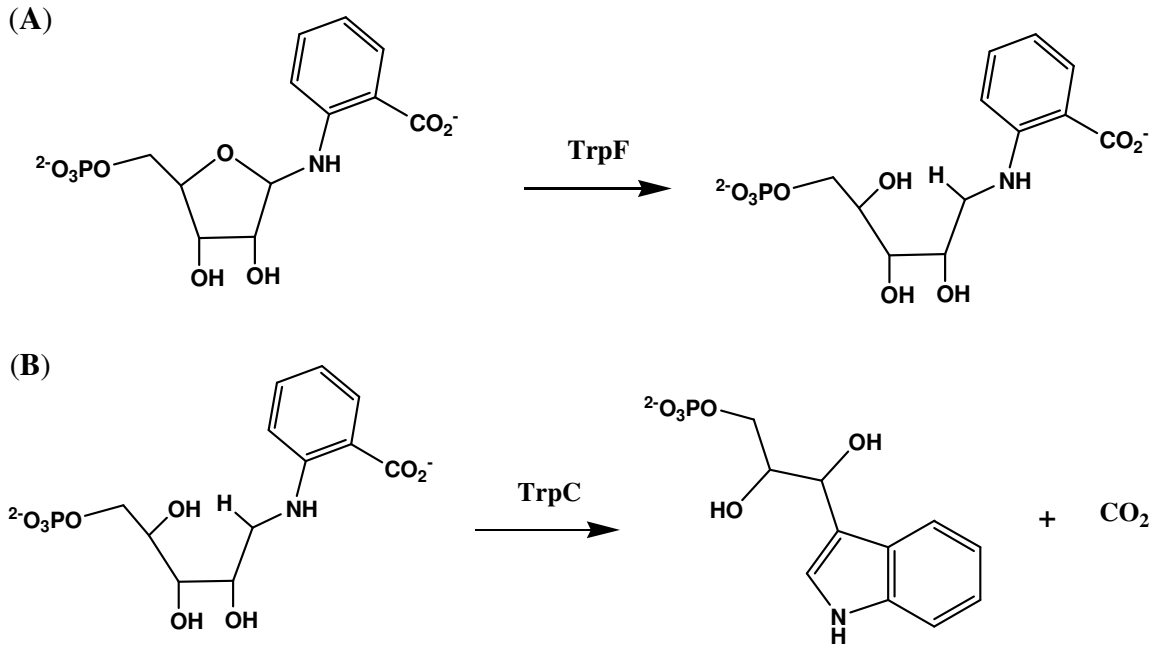

Figure 1.3. Reactions catalyzed by (A) phosphoribosylanthranilate isomerase (PRAI or TrpF) and (B) indoleglycerol phosphate synthase (InGPS or TrpC) in the tryptophan biosynthesis pathway.

but in *E. coli* the two proteins are fused to form a monomeric bifunctional enzyme. PRAI and InGPS share a common $(\beta/\alpha)_8$ structural motif and a 22% sequence identity (7). The major sequence and structural similarities between the two enzymes are found in their phosphate-binding site and hydrophobic pocket, both formed by residues of the same loops. Although the positions of the active sites in the tertiary structures are similar, most of the catalytic residues, as opposed to those residues involved in binding, deviate significantly when the two structures are superimposed. The conservation of the parts of the tertiary structures of PRAI and InGPS that presumably fulfill equivalent functions provides strong evidence that the two domains of the bifunctional enzyme result from a

gene duplication event (7). The structural, sequence, and mechanistic evidence indicate the retrograde evolution theory applies to this pair of enzymes.

The Patchwork Assembly of Metabolic Pathways and Catalytic Promiscuity

A second strategy for the evolution of enzymes (or pathways), proposed by Jensen, is known as the "patchwork evolution" model (3). Jensen suggested that primitive enzymes had broad catalytic specificity, permitting them to react with a wide range of chemically-related substrates. This capability would enable early organisms to obtain the most catalytic versatility with their limited enzyme resources. Over time, genes for these enzymes would be duplicated, allowing mutations to occur that conferred increased specialization and catalytic efficiency, and generated a larger number of specific proteins. The patchwork theory of metabolic pathways involves the recruitment of pre-existing enzymes, which are "borrowed" and "retooled" to make new enzymes that are assembled into new pathways. The primary choice of which enzyme to borrow is based on the enzyme's substrate specificity or its chemical mechanism. Some enzymes have the ability to use active site features to catalyze not only their own primary and physiological activity, but also several alternative, low level activities, allowing the enzyme to behave in a catalytically promiscuous way (8). Duplication of the gene followed by a series of mutations to amplify the desired activity generates a new enzyme, now having the progenitor's low-level activity as the primary activity. These

promiscuous enzymes can be selected to provide new functions when the secondary catalytic reactions provide a selective advantage to the organism.

Patchwork Evolution Model: The Pentachlorophenol Degradation Pathway

The pentachlorophenol degradative pathway is a recently discovered example of a pathway that may have been assembled through a 'patchwork' combination of enzymes from two different existing pathways. Pentachlorophenol (PCP), a pesticide introduced about 70 years ago, is degraded by a three-step pathway (Figure 1.4) in the soil bacterium *Sphingobium chlorophenolicum* ATCC 39723 (9).

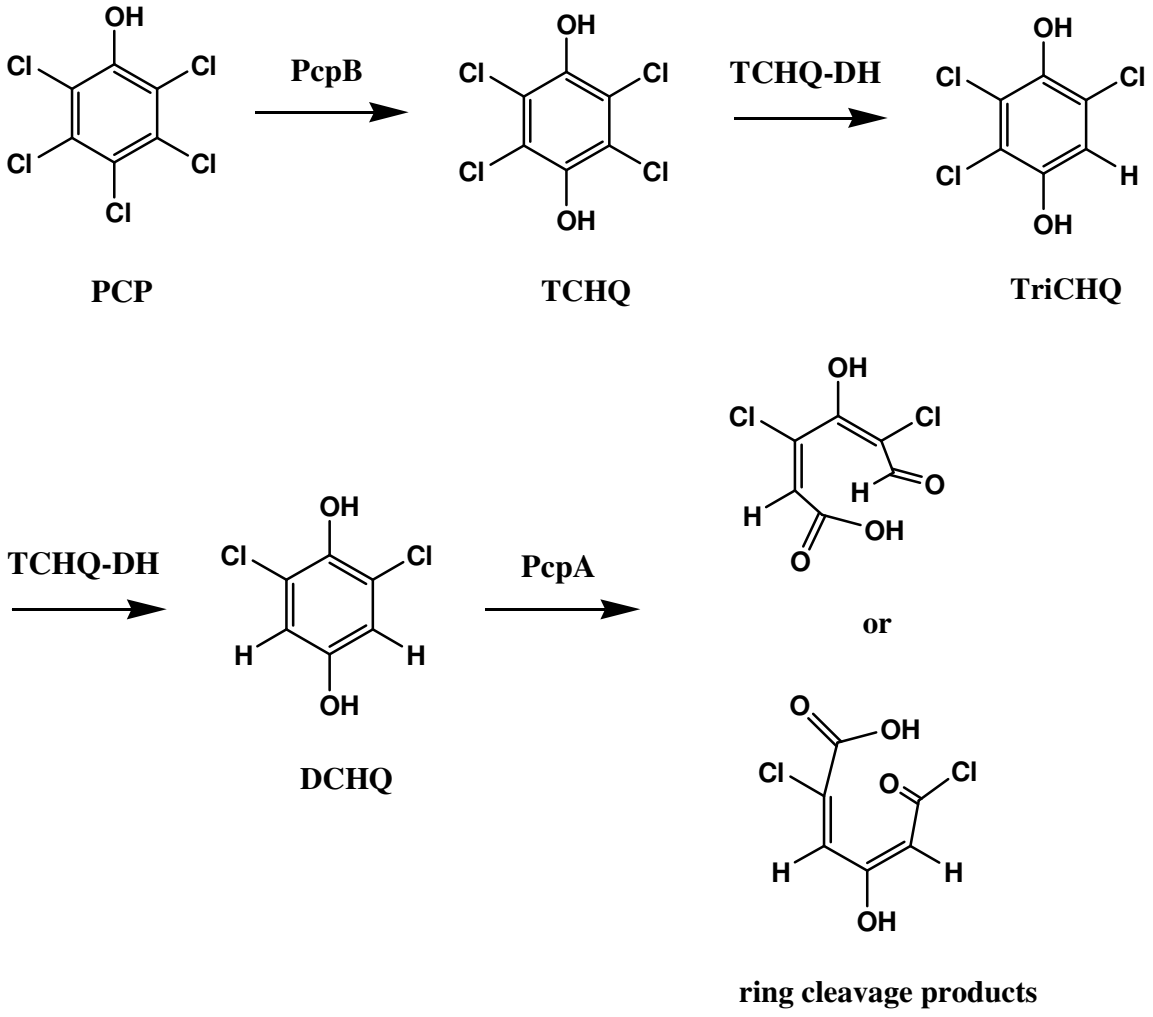

Figure 1.4. Pathway for degradation of pentachlorophenol. Abbreviations: PCP, pentachlorophenol; TCHQ, tetrachlorohydroquinone; TriCHQ, trichlorohydroquinone; DCHQ, 2,6-dichlorohydroquinone; PcpB, PCP hydroxylase; TCHQ-DH, TCHQ dehalogenase; PcpA, DCHQ dioxygenase.

The first step in the pathway is catalyzed by PCP hydroxylase (PcpB) which converts PCP to tetrachlorohydroquinone (TCHQ) (10). The subsequent two reductive

dehalogenation reactions are both carried out by TCHQ dehalogenase to first form trichlorohydroquinone (TriCHQ) followed by 2,6-dichlorohydroquinone (DCHQ) (11). The third step involves the Fe^{2+}–dependent ring cleavage of the aromatic ring by DCHQ dioxygenase, PcpA (12).

PcpB, the first enzyme in the pathway, is a flavin monooxygenase that utilizes molecular oxygen and two equivalents of NADPH to convert PCP to TCHQ (10). This reaction appears to be the rate-limiting step in the biodegradation of PCP (9). Unlike most flavin monooxygenases, PCP hydroxylase is a broad-specificity enzyme capable of hydroxylating a variety of substituted phenols. It is possible that the poor catalytic efficiency is a result of the nonspecificity of the enzyme, or because it has been recently recruited to utilize PCP as a new substrate and has not yet evolved to optimize this function.

The second enzyme in the pathway is TCHQ dehalogenase, a member of the zeta class of the glutathione S-transferase (GST) superfamily (13, 14). The enzyme performs two consecutive reductive dehalogenation steps using TCHQ and then TriCHQ. Typically, GSTs catalyze the necleophilic attack of glutathione upon an electrophilic substrate to form a glutathione conjugate, which is important in detoxification of alkylating agents (15). TCHQ dehalogenase appears to be distantly related to one of these GSTs, a maleylacetoacetate (MAA) isomerase (16). Although these enzymes share an insignificant overall sequence identity, the active site regions are highly conserved. Remarkably, TCHQ dehalogenase was found to catalyze the glutathione-dependent isomerization of maleylacetone, a substrate related to maleylacetoacetate, nearly as well

as MAA isomerase (16). These observations suggest that an MAA isomerase with a promiscuous activity was recruited to play a role in the dehalogenation reaction of this pathway.

Copley suggests that the original function of this set of enzymes might have been to carry out the ring cleavage of naturally occurring compounds. This assumption is supported by two observations: the dioxygenase (PcpA) preferentially cleaves DCHQ and PCP hydroxylase hydroxylates the naturally occurring 2,6-dichlorophenol. Certain fungi and insects naturally produce chlorophenols (17, 18) so it is conceivable that many soil bacteria are capable of degrading these compounds. A model of the PCP degradation pathway as a patchwork assembly is shown in Figure 1.5. PcpB, which accepts chlorophenols as substrates, would be recruited to hydroxylate PCP to TCHQ. Next, an MAA isomerase was selected from an existing metabolic pathway to convert TCHQ to TriCHQ and then to DCHQ. Finally, the PcpA dioxygenase would perform its normal role by cleaving DCHQ.

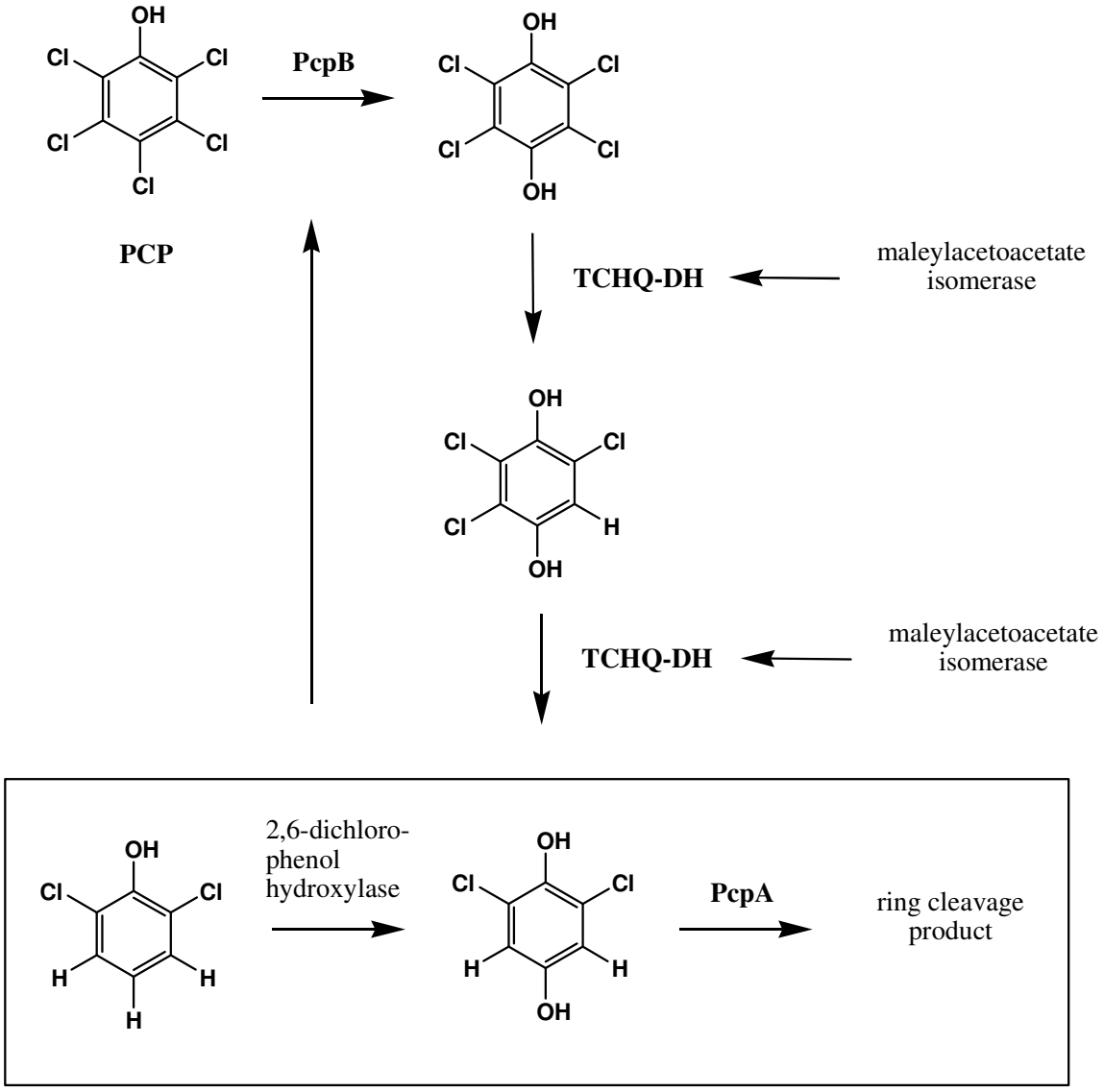

Figure 1.5. Patchwork model for the assembly of the pentachlorophenol degradation pathway. Abbreviations: PCP, pentachlorophenol; PcpB, PCP hydroxylase; TCHQ-DH, TCHQ dehalogenase; PcpA, DCHQ dioxygenase.

Recruitment of Homologous Enzymes: The Case of Enoyl CoA Hydratase and 4-Chlorobenzoyl CoA Dehalogenase

The assembly of certain metabolic pathways can be explained by the recruitment model, as exemplified in the PCP degradation pathway. This model can be used to explain the origins of other pathways based on one of two lines of evidence. First, there is evidence that a given enzyme exhibits catalytic promiscuity (8). Second, homologous enzymes are capable of catalyzing different reactions, suggesting the existence of a common ancestor. This second strategy may have been employed in the evolution of rat mitochondrial crotonase (enoyl CoA hydratase) and 4-chlorobenzoyl- CoA dehalogenase, enzymes found in the fatty acid β-oxidation (19) and 4-chlorobenzoate degrading pathways, respectively (Figure 1.6) (20-21).

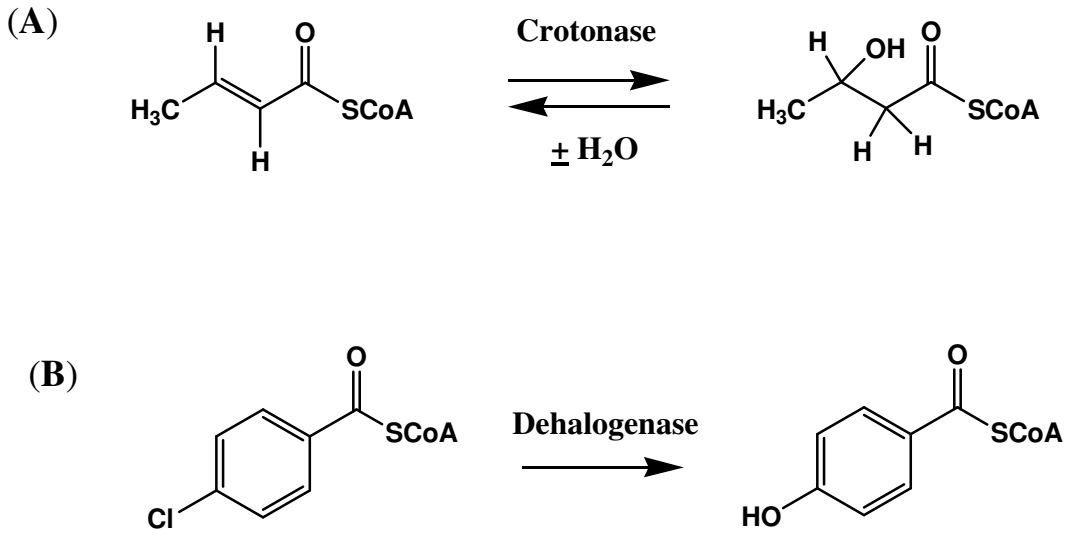

Figure 1.6. (A), Reaction catalyzed by crotonase. (B), Reaction catalyzed by 4-chlorobenzoyl-CoA dehalogenase.

Enoyl CoA hydratase (crotonase) is the second enzyme in the fatty acid β-oxidation pathway and catalyzes the *syn* addition of water to α,β-unsaturated fatty acid CoA thiolesters. Crotonase is extremely efficient with rates for the substrate approaching diffusion control (22). The quaternary structure of crotonase is characterized as a dimer of trimers with each subunit containing 261 amino acid residues (23). The catalytic mechanism involves two important glutamate residues: Glu-144 and Glu-164. During catalysis, Glu-144 acts as the catalytic base activating a water molecule for nucleophilic attack at C-3, and Glu-164, as the general acid, delivers a proton to C-2 (Figure 1.7). The carbonyl group of the thioester lies within hydrogen-bonding distance to the structurally

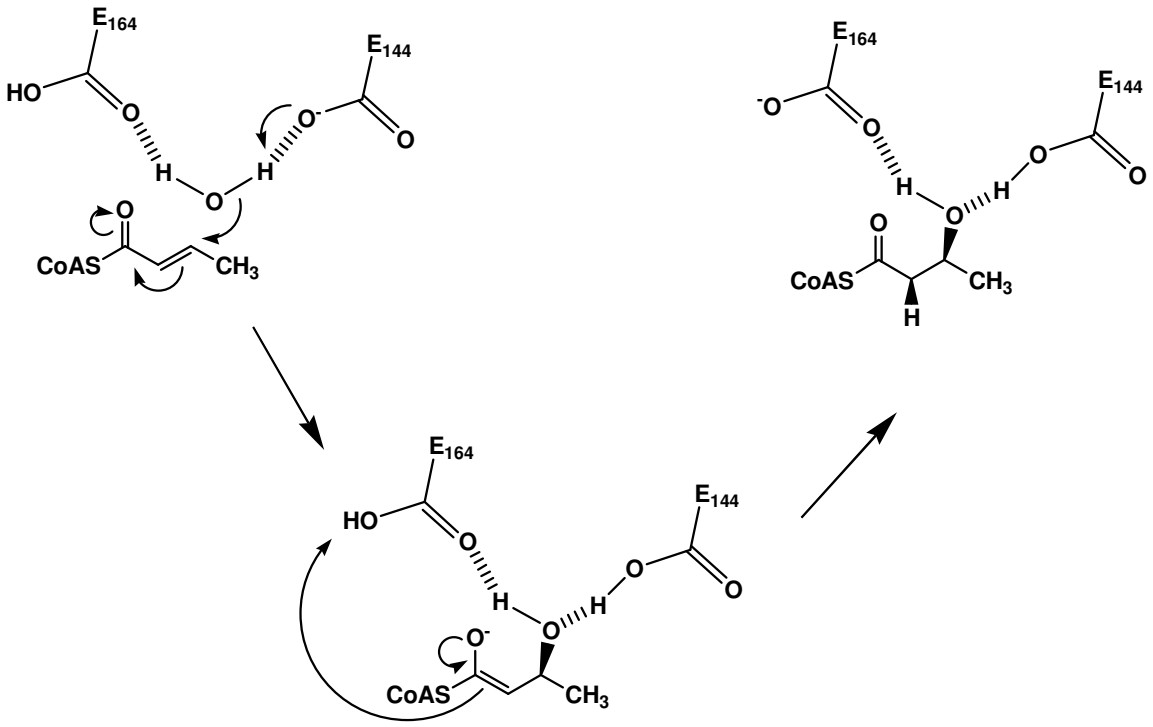

Figure 1.7. Proposed mechanism of crotonase, as adapted from Hofstein, H.A., et al. (19).

conserved backbone amide groups of Ala-98 and Gly-141, which is positioned at the N-terminal end of an α-helix. These hydrogen bonds and the positive end of the helix dipole moment create a "pocket" of positive charge, a so-called oxyanion hole, to stabilize the enolate anion intermediate (19, 22).

4-Chlorobenzoyl-CoA dehalogenase, from *Pseudomonas sp.* strain CBS-3 is part of the 4-chlorobenzoate degrading pathway (20, 21). This dehalogenase catalyzes the hydrolysis of 4-chlorobenzoyl-CoA to 4-hydroxybenzoyl-CoA. The crystal structure of the dehalogenase shows that it is a trimer, with each subunit containing 269 amino acid residues (24). The dehalogenase proceeds via a nucleophilic aromatic substitution reaction in which the side-chain carboxylate group of Asp-145 attacks the benzoyl ring of

the substrate at C-4 to displace a chloride ion from the ring and results in the formation of a Meisenheimer complex (a structural analog of an enolate anion) (Figure 1.8). Based on

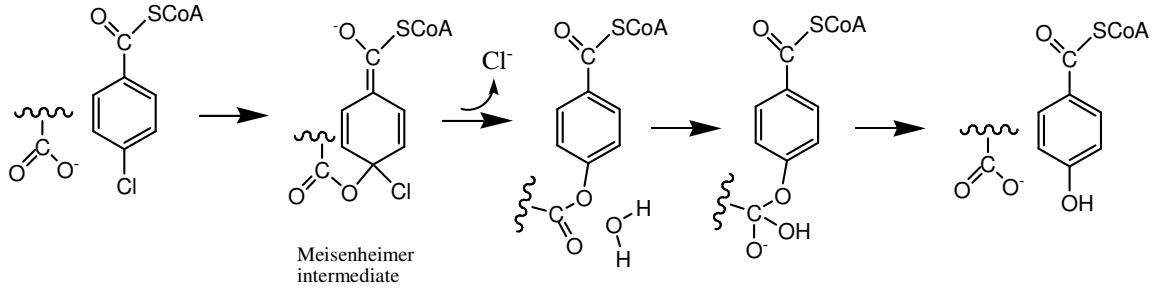

Figure 1.8. Mechanism of 4-chlorobenzoyl-CoA dehalogenase.

the crystal structure, His-90 most likely activates the water molecule for nucleophilic attack at the carboxylate group of the enzyme intermediate. The thioester carbonyl group also lies within an oxyanion hole, created by the peptide NH groups of Phe-64 and Gly-114, which is located at the N-terminal end of an α-helix (25-29).

An examination of the crystal structures of crotonase and 4-chlorobenzoyl-CoA dehalogenase revealed they were nearly superimposable. Both enzymes share 30% sequence identity and 60% sequence similarity, which provides additional evidence for a common ancestor. These two enzymes share a fold that forms the oxyanion hole. The fold consists of two layers of β-sheets that are perpendicular to one another and surrounded by α-helices. Other than the oxyanion hole, no active site groups or features are conserved between the two proteins (24). However, both mechanisms involve the generation and stabilization of an enolate intermediate. It is likely that nature used a precursor with a similar global fold and evolved it to catalyze each of the individual

reactions catalyzed by crotonase and 4-chlorobenzoyl-CoA dehalogenase. Crotonase, which is part of a critical metabolic pathway, was perhaps the ancestral enzyme recruited to carry out the dehalogenation. Another possibility is that an unknown ancestor served as the progenitor for both enzymes because of its catalytic promiscuity (8).

Enzyme Superfamilies

The concept of an enzyme superfamily stemmed from the discovery that two enzymes, mandelate racemase and muconate lactonizing enzyme, are structurally homologous proteins although they catalyze different reactions. This finding suggests that enzymes capable of performing distinct chemical reactions can be related by divergent evolution (4). Enzyme superfamilies have been an area of much recent study and are a topic of interest in this dissertation. However, two terms need to be defined for this discussion.

A superfamily is a group of structurally homologous enzymes that catalyze the same chemical reaction with differing substrate specificities, or they catalyze different overall reactions with differing substrate specificities but share a common mechanistic feature (partial reaction, intermediate, or transition state). The latter is facilitated by conserved active site residues that perform the same functions in all members of the superfamily. Typically, superfamily members share less than 50% sequence identity, and frequently share less than 20% sequence identity (30).

A subset of the superfamily classification is an enzyme family. A family is a group of homologous enzymes that share more than 30% sequence identity, often these

are orthologs (the same enzyme found in different species) but not always (30). Family members may also share specific structural features (i.e. quaternary structure) as well as other additional conserved active site residues specific for the overall mechanism of that family. One example of a family of enzymes includes the members of the muconate lactonizing enzyme (MLE) family in the enolase superfamily (31).

The Enolase Superfamily

The discovery that mandelate racemase (MR) and muconate lactonizing enzyme (MLE) are structurally homologous led to the initial characterization of relationships within an enzyme superfamily. Shortly thereafter, a yeast enolase (for which the enolase superfamily is named) was found to share the same structure and partial reaction as that of MR and MLE (31). Enolase catalyzes the metal-ion dependent elimination of water from 2-phosphoglycerate to yield phosphoenolpyruvate and is only one of many different reactions catalyzed by this mechanistically diverse superfamily (Figure 1.9) (31,32).

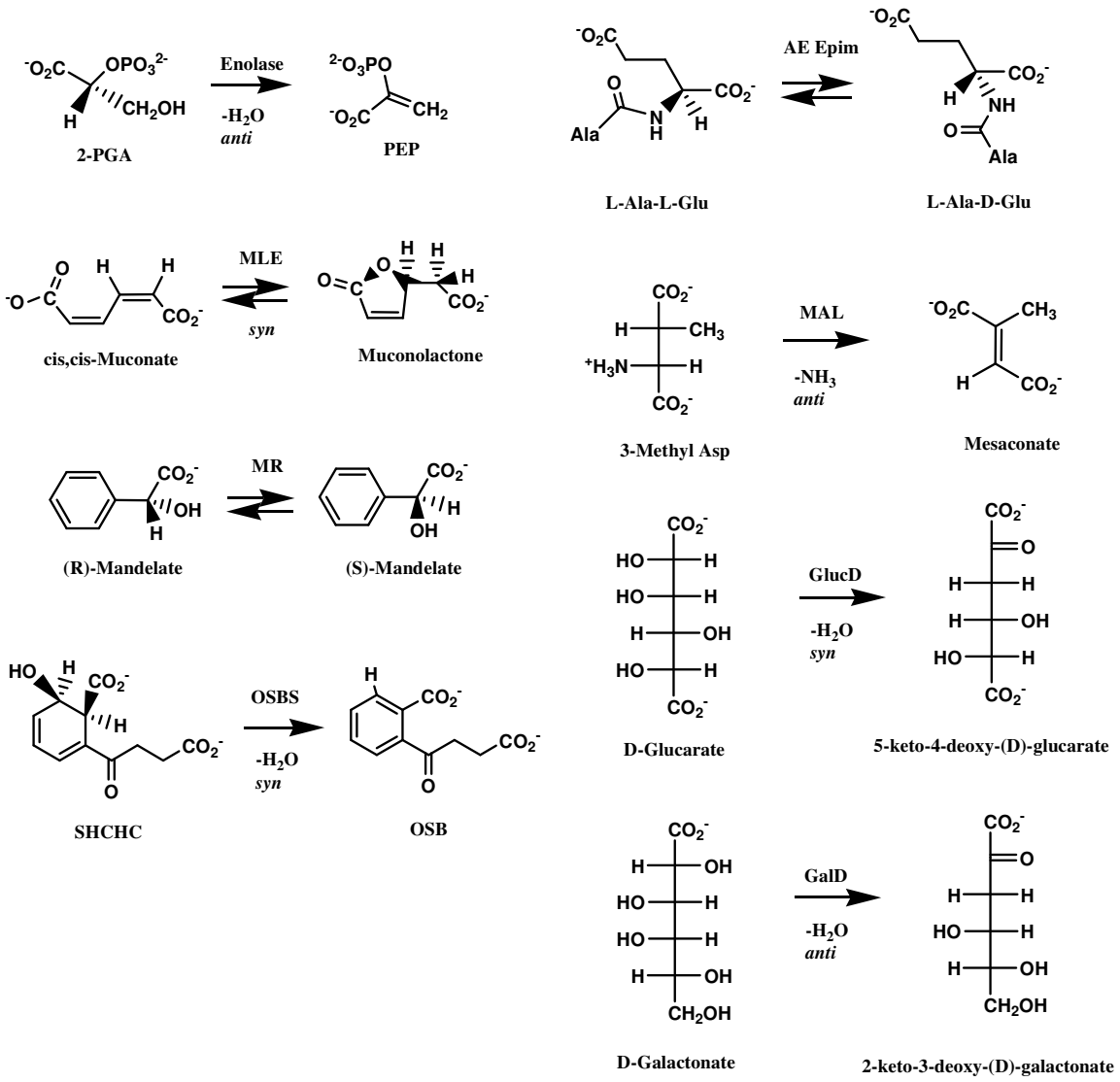

Figure 1.9. Reactions catalyzed by members of the enolase superfamily (4). Abbreviations: 2-PGA, 2-phosphoglycerate; PEP, phosphoenolpyruvate; MLE, muconate-lactonizing enzyme; MR, mandelate racemase; OSBS, o-succinylbenzoate synthase; SHCHC, 2-succinyl-6-hydroxy-2,4-cyclohexadiene-1-carboxylic acid; OSB, o-succinylbenzoic acid; AE, L-Ala-D/L-Glu epimerase; MAL, 3-methylaspartate ammonia lyase; GlucD, (D)-glucarate dehydratase; GalD, (D)-galactonate dehydratase.

Enolase superfamily members share two conserved domains, an N-terminal domain that governs substrate specificity and a TIM-barrel domain [$(\beta/\alpha)_8$] that contains the catalytic groups. Superfamily members share a partial reaction in which an active site base abstracts the α-proton of the carboxylate substrate to generate an enolate anion intermediate that is stabilized by coordination to an essential Mg^{2+} ion. Depending on the identity of the reaction, the intermediates are channeled to different products in the various active sites. The conserved architecture of the two domains provides compelling evidence that the enolase superfamily represents divergent evolution from a common progenitor (4, 33).

The Crotonase Superfamily – Stabilization of Enolate Ions

Crotonase (enoyl CoA hydratase) and 4-chlorobenzoyl CoA dehalogenase are members of the crotonase superfamily. Crotonase catalyzes the reversible addition of water to α,β-unsaturated enoyl-CoA thioesters. Many members of this superfamily use coenzyme A (CoA) thioesters as substrates. Reactions catalyzed by members of this superfamily are exemplified in Figure 1.10 (4, 22). The feature common to all the

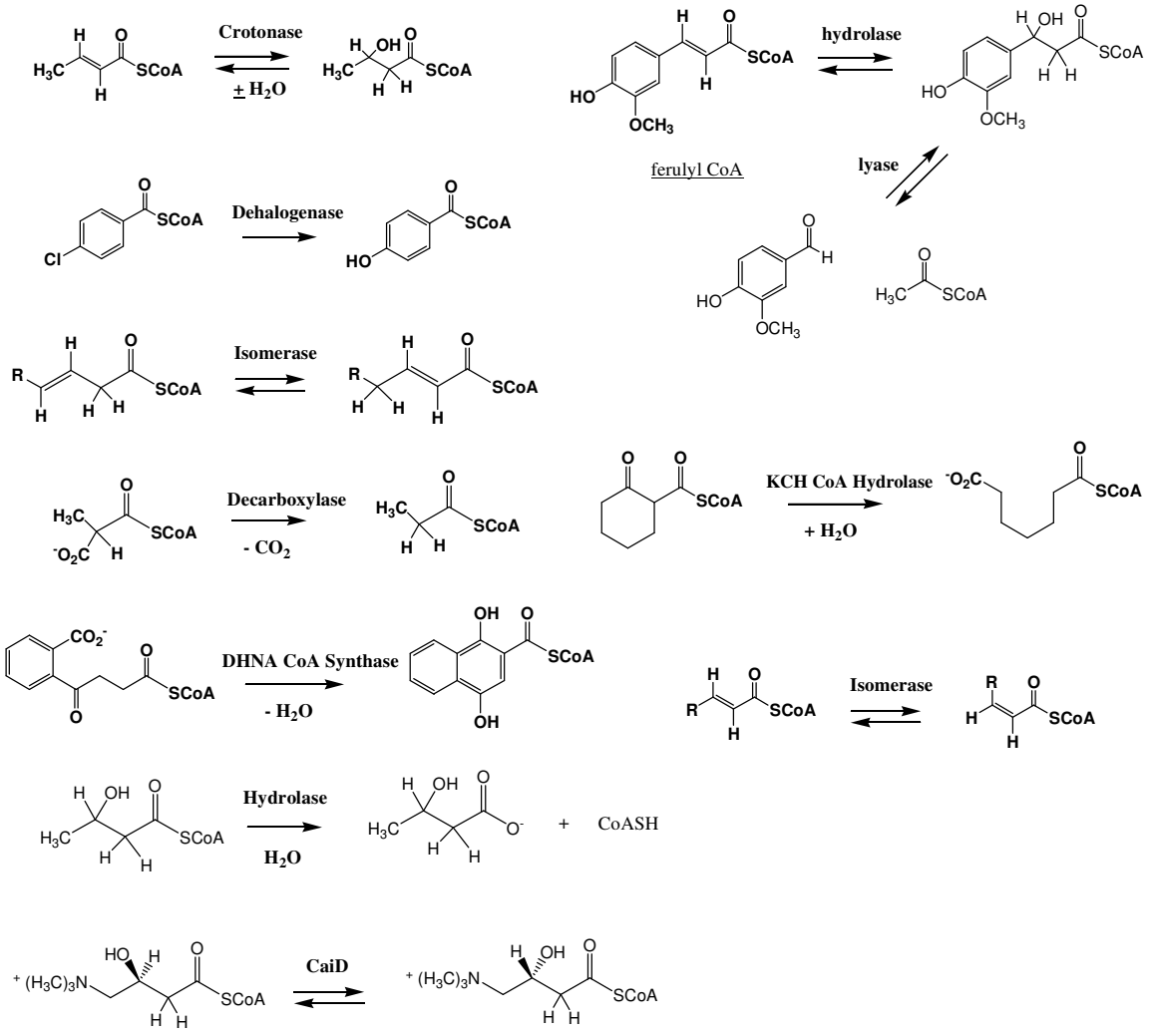

Figure 1.10. Reactions catalyzed by members of the crotonase superfamily (4, 22). Abbreviations: DHNA, dihydroxynaphthoate; CaiD, carnitinyl CoA epimerase; KCH, 2-ketocychlohexyl.

reactions catalyzed within this superfamily is the stabilization of negative charge localized on the oxygen of the thioester carbonyl of an acyl-CoA substrate or tetrahedral intermediate formed in the hydrolysis of peptide bonds. Stabilization of the enolate anion is accomplished through hydrogen bonding to two structurally conserved backbone NH

groups that form an "oxyanion hole". Other than the functional groups conserved in the oxyanion hole, no other active site catalytic groups are conserved within this superfamily (22, 34, 35). This conserved structural feature provides evidence for the premise that a requirement for the stabilization of an otherwise unstable intermediate has been the dominant force in the evolution of this superfamily. The similarities of structure-function among the crotonase superfamily members suggest that divergent evolution may have generated these various activities. For instance, experiments have shown that 4-chlorobenzoyl CoA dehalogenase can be used as a template for the rational design of a new enzyme that has a low level crotonase activity (36). This observation indicates that these two enzymes may have evolved from a common ancestral protein.

Overview of Microbial Degradation of Aromatic Compounds

The benzene ring is one of the most abundant units of chemical structure in the natural world. The ring is stabilized by resonance and its degradation, a process critical for the functioning of the earth's carbon cycle, is carried out almost entirely by microorganisms (37). Some of these microorganisms are able to use aromatic hydrocarbons as their sole sources of carbon and energy for growth. This capability results from metabolic pathways that convert the aromatic hydrocarbon into Krebs cycle intermediates. Initially, the aromatic hydrocarbon undergoes hydroxylation generating catechol (Figure 1.11) or a substituted catechol. Subsequently, the catecholic compound undergoes ring fission by one of two metabolic pathways: the so-called ortho- or meta-

cleavage pathways (37). The ortho-cleavage pathway involves ring cleavage between the two hydroxyl groups followed by a series of reactions resulting in the production of β-ketoadipate. The meta-cleavage pathway involves ring cleavage between the carbon bound to the hydroxyl group and the adjacent hydrogen bound carbon, followed by degradation of the ring cleavage product to pyruvate and a short chain aldehyde (37). The pathway choice is dependent upon the microbial species and/or the characterization of the growth substrate (38). The enzymes of this pathway raise numerous mechanistic, structural, and evolutionary questions. Moreover, the degradative potential of these pathways present an attractive strategy for the degradation of aromatic hydrocarbons in the environment.

The Catechol meta-Fission Pathway

The catechol meta-fission pathway is a plasmid-encoded set of enzymes that allows organisms to degrade various aromatic compounds as their sole sources of carbon and energy. The enzymes coded by the TOL plasmid pWW0 from *Pseudomonas putida* mt-2, a soil bacterium, convert catechol and 3-substituted catechols to acetaldehyde and pyruvate (37). This set of catabolic enzymes plays a key role in the complete degradation of toluene, *m*- and *p*-xylene, 3-ethyltoluene, and 1,2,4-trimethylbenzene (39). This group of reactions exemplifies the general strategy found in meta-fission pathways (37).

The genes for the meta-fission pathway enzymes are clustered into a single operon comprised of 13 structural genes, of which two, *xylT* and *xylQ*, have no known

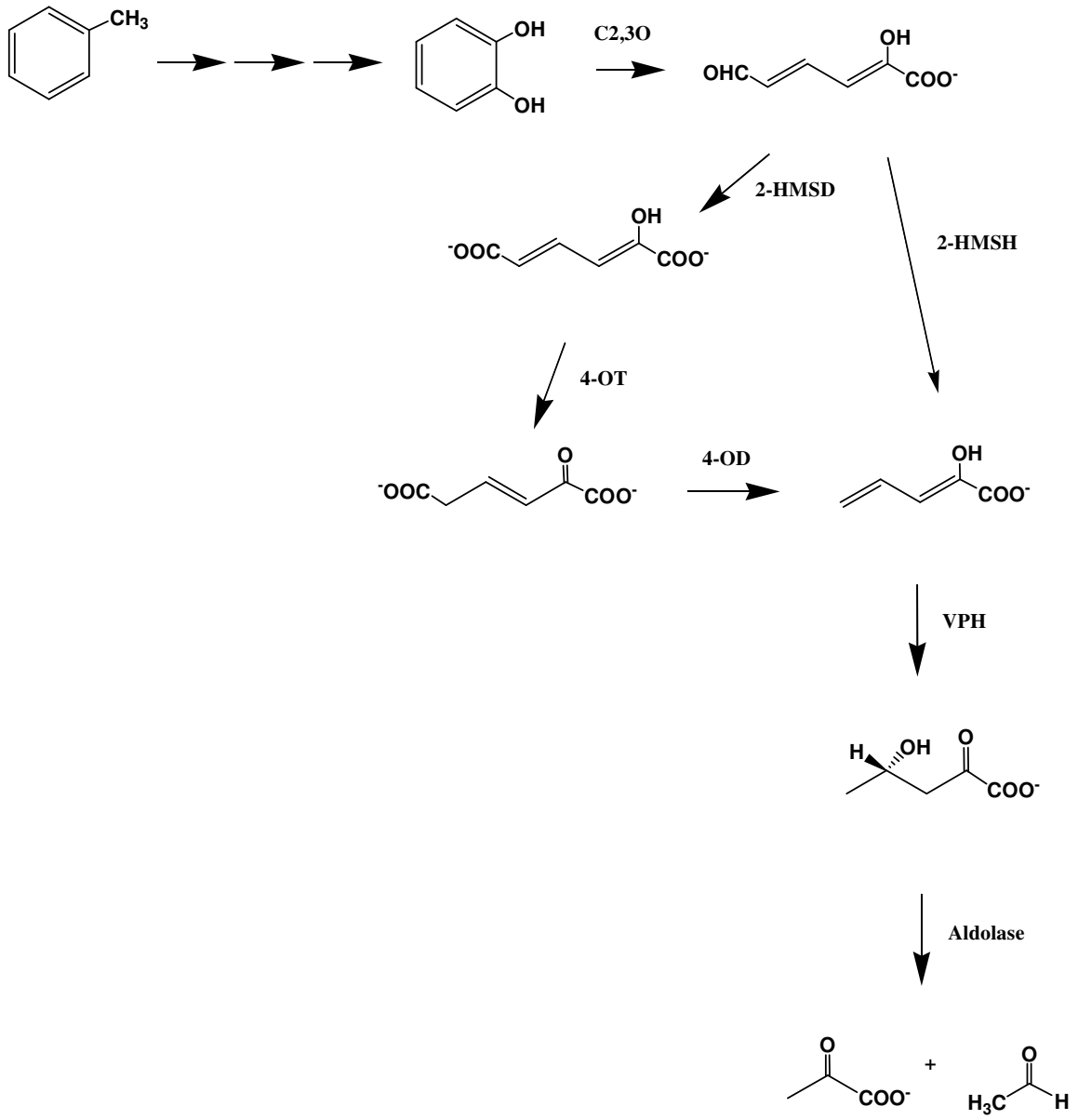

Figure 1.11. The catechol meta-fission pathway. Abbreviations: C2,3O, catechol 2,3-dioxygenase; 2-HMSD, 2-hydroxymuconate semialdehyde dehydrogenase ; 4-OT, 4-oxalocrotonate tautomerase; 4-OD, 4-oxalocrotonate decarboxylase; VPH, vinylpyruvate hydratase; 2-HMSH, 2-hydroxymuconate semialdehyde hydrolase.

function. The remaining genes encode the enzymes required for the conversion of the aromatic hydrocarbon to catechol and then to pyruvate and acetaldehyde (38).

The intermediates and reactions that convert catechol to Krebs cycle intermediates are shown in Figure 1.11. Catechol 2,3-dioxygenase (C2,3O) is the first enzyme in the pathway, and converts catechol to 2-hydroxymuconate semialdehyde (2-HMS) (37, 40). In some pathways, the aldehyde portion of 2-HMS is oxidized by 2-hydroxymuconate semialdehyde dehydrogenase (2-HMSD), an NAD^+–dependent reaction, to produce 2-hydroxymuconate (37). Subsequent ketonization to the α,β–unsaturated ketone is catalyzed by 4-oxalocrotonate tautomerase (4OT) (39, 41). The metal ion-dependent 4-oxalocrotonate decarboxylase (4-OD) is responsible for catalyzing the decarboxylation of the conjugated ketone to generate 2-hydroxy-2,4-pentadienoate (HPD) (39). In other pathways, 2-hydroxymuconate semialdehyde hydrolase (2-HMSH) directly hydrolyzes 2-HMS (and other ketones, Figure 1.12) to HPD and the corresponding acid (either formate or acetate) (42). Subsequently, vinylpyruvate hydratase (VPH), which exists as a complex with 4-OD and is also metal ion-dependent, catalyzes the addition of water to HPD producing 2-oxo-4*S*-hydroxypentanoate (KHP) (37, 39). The action of KHP aldolase cleaves 2,4-HP and generates pyruvate and acetaldehyde, which are channeled to the Krebs cycle (37).

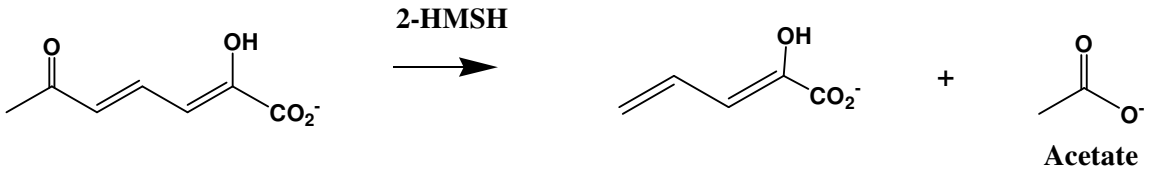

Figure 1.12. Conversion of 2-hydroxy-6-oxo-2,4-heptadienoate to 2-hydroxy-2,4-pentadienoate and acetate by 2-HMSH.

The Homoprotocatechuate Pathway

The homoprotocatechuate (HPC) pathway (another meta-fission pathway) is an inducible set of enzymes from *Escherichia coli* C that converts 3,4-dihydroxyphenylacetate to succinic semialdehyde and pyruvate (Figure 1.13).

The enzymes of this pathway are chromosomally encoded and may be part of a degradative route for phenylalanine and tyrosine (43).

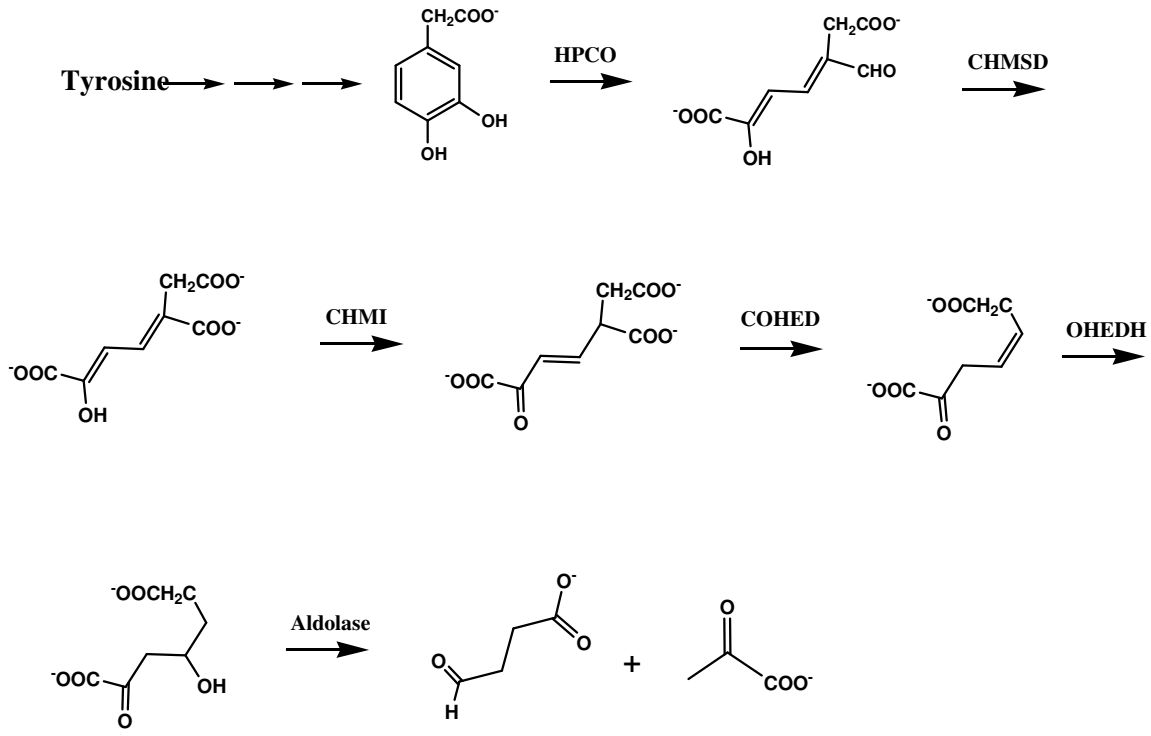

Figure 1.13. The homoprotocatechuate pathway. Abbreviations: HPCO, homoprotocatechuate dioxygenase; CHMSD, 5-(carboxymethyl)-2-hydroxymuconate semialdehyde dehydrogenase; CHMI, 5-(carboxymethyl)-2-hydroxymuconate isomerase; COHED, 5-(carboxymethyl)-2-oxo-3-hexene-1,6-dioate decarboxylase; OHEDH, 2-oxo-4-heptene-1,7-dioate hydratase.

The intermediates and reactions that convert homoprotocatechuate to Krebs cycle intermediates are shown in Figure 1.13. Homoprotocatechuate dioxygenase (HPCO) is responsible for the ring opening of homoprotocatechuate to generate 5-(carboxymethyl)-2-hydroxymuconate semialdehyde (CHMS). The aldehyde portion of CHMS is oxidized to 5-(carboxymethyl)-2-hydroxymuconate by the NAD^+-dependent CMHS dehydrogenase (43). Subsequent ketonization to 5-(carboxymethyl)-2-oxo-3-hexene-1,6-

dioate is catalyzed by 5-(carboxymethyl)-2-hydroxymuconate isomerase (CHMI) (44, 45). The magnesium-dependent 5-(carboxymethyl)-2-oxo-3-hexene-1,6-dioate decarboxylase (COHED) catalyzes the decarboxylation of the conjugated ketone to generate 2-oxo-4-heptene-1,7-dioate (OHED) (46, 47). Subsequently, 2-oxo-4-heptene-1,7-dioate hydratase (OHEDH), also magnesium dependent, is responsible for catalyzing the hydration across the double bond of OHED producing 2-oxo-*4S*-hydroxyheptanoate (47-49). The final step in the pathway involves an aldolase-catalyzed reaction to cleave 2-oxo-*4S*-hydroxyheptanoate into pyruvate and succinic semialdehyde (43).

Evolutionary Trends

The related catechol and homoprotocatechuate pathways present a particularly interesting set of parallel enzymatic reactions. A comparative analysis of the enzymes of the catechol meta-fission pathway (*P. putida* mt-2) with those of the HPC meta-fission pathway (*E. coli* C) has been explained by Whitman et al. (41, 44, 49-50). One interesting feature of these pathways is that the same chemical reactions are carried out on slightly different substrates by enzymes that are not obviously related. Although the structural similarities between intermediates (i.e., the intermediates in the catechol meta-fission pathway have a hydrogen at C-5 while those in the HPC meta-fission pathway have a carboxymethyl group) suggested that the corresponding enzymes might be evolutionarily related, the results of sequence analyses did not suggest obvious links. For example, there is little sequence identity between 4-OT and CHMI as well as between 4-

OD and COHED. VPH and OHED hydratase (OHEDH) share ~36% identity. Despite the wide range of compounds metabolized by the different meta-fission pathways, the same general pattern is observed. Identical reactions are carried out on similar substrates by enzymes that in some cases share significant sequence identity and in other cases do not. The parallelism among these pathways raises questions about how these enzymes originated and evolved and how they acquired their individual specificities.

The meta-fission pathway is an ideal model for the study of enzyme evolution for several reasons. Because the pathway is plasmid-encoded, it might have been generated due to an environmental pressure. It is probable that the enzymes of the TOL plasmid were recruited from existing metabolic pathways, in agreement with Jensen's hypothesis (3). Evolutionary aspects of the meta-fission pathway may be similar to those proposed by Copley in pentachlorophenol degradation (9). However, the meta-fission pathway is optimized for degradation, as opposed to that of pentachlorophenol catabolism. Due to the differences in sizes, structures (of the enzymes for which structures are available), substrate requirements, and the instability of some pathway intermediates, it is not likely that this pathway evolved in the manner suggested by Horowitz's retro-evolution theory. The one exception might be 4-OD and VPH, which share ~37% sequence identity.

Fumarylacetoacetate Hydrolase (FAH) Superfamily

Recent structural work revealed a relationship between 5-(carboxymethyl)-2-oxo-3-hexene-1,6-dioate decarboxylase (COHED), which catalyzes the Mg^{2+}-dependent

decarboxylation of 5-(carboxymethyl)-2-oxo-3-hexene-1,6-dioate (**1**) to 2-oxo-4-heptene-1,7-dioate (**2**) (Figure 1.14), and another enzyme, the mouse fumarylacetoacetate hydrolase (FAH) (51). FAH is a member of a eukaryotic pathway responsible for the degradation of tyrosine and phenylalanine. (The HPC pathway has also been proposed to be a prokaryotic catabolic route for these same amino acids.) A deficiency of the human FAH causes the fatal metabolic disease, tyrosinemia type I (52). FAH catalyzes the last step in the pathway, which is the hydrolytic cleavage of fumarylacetoacetate (**3**, Figure 1.14) to produce fumarate (**4**) and acetoacetate (**5**) (52). A third member of the family, MhpD, is a hydratase enzyme located in the chromosome of *E. coli*. MhpD catalyzes the Mg^{2+}-dependent hydration of 2-hydroxy-2,4-pentadienoate (**6**) to produce 2-oxo-4-hydroxypentanoate (**7**) (Figure 1.14) (53, 54). These three enzymes along with another *E. coli* homologue designated YcgM (physiological function unknown) are the four known members of the fumarylacetoacetate hydrolase-like superfamily.

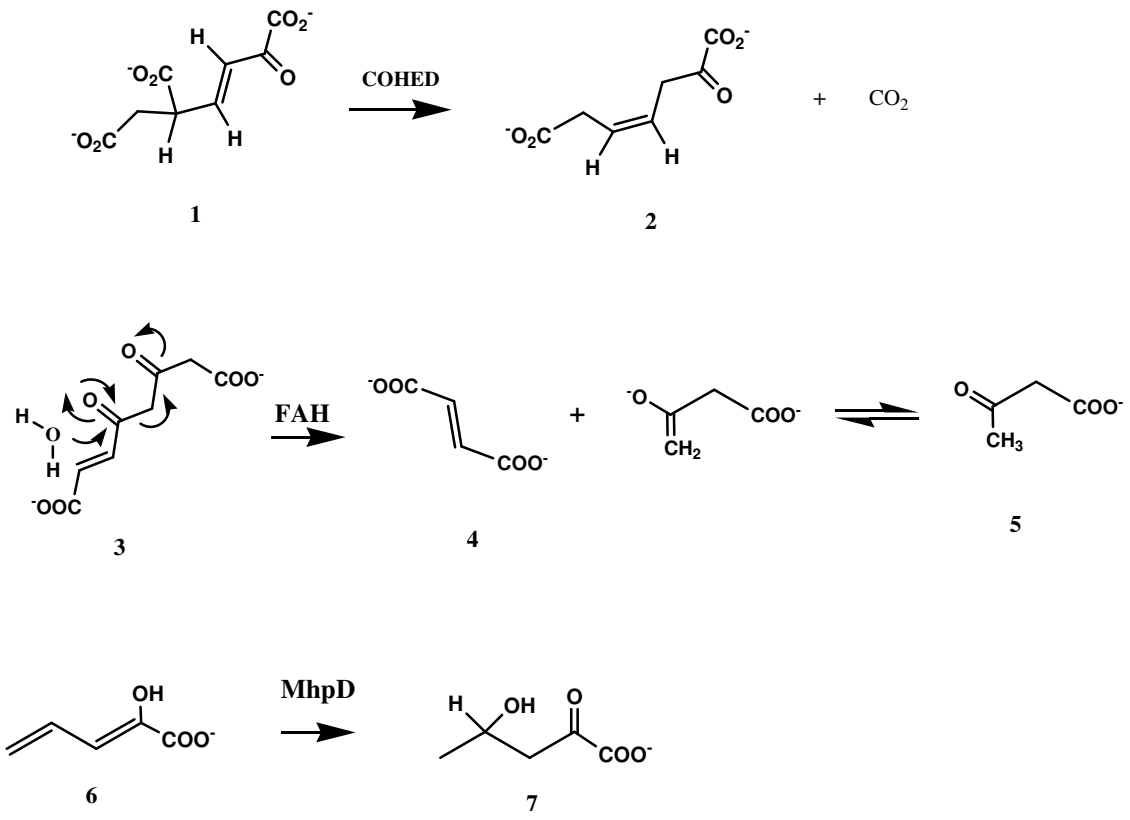

Figure 1.14. Reactions catalyzed by the known members of the FAH superfamily.

The monomeric COHED (solved as a 45-kDa complex with Ca^{2+}) consists of two domains, the N-terminal domain (residues 1-200) and the C-terminal domain (residues 221-429), which share 34% sequence identity. The two domains form a structure that is structurally homologous with the C-terminal domain of the dimeric FAH (which consists of 300 residues) (51), despite the lack of significant sequence identity (~15%). The C-terminal domain of COHED is also structurally homologous with YcgM (solved as a complex with Mg^{2+}). The dimeric YcgM consists of 219 residues and is found in an unidentified gene cluster. The annotated activity for YcgM is that of a putative

isomerase. The pentameric MhpD is made up of 269 residues per subunit and is part of the phenylpropionic acid catabolic pathway (54). MhpD was crystallized without a bound metal ion or ligand to assist in identifying the active site. The four proteins share an EXE motif, which has been implicated in divalent metal ion binding [in COHED (E276 and E278) (51), in FAH (E199 and E201) (52), MhpD (E105 and E107), and in YcgM (E70 and E72)] based on the observation that these residues bind a metal in COHED and FAH.

4-Oxalocrotonate decarboxylase (4-OD) and vinylpyruvate hydratase (VPH, which exist as a complex with 4-OD) may also be members of the FAH superfamily. 4-OD has a 23% sequence identity with YcgM and displays the EXE motif (E109 and E111). In addition, VPH, which shares ~37% sequence identity with 4-OD, has an EXE motif (E106 and E108). Mutation of the two glutamates in 4-OD (E109Q and E111Q) resulted in the corresponding complexes with greatly reduced 4-OD activity and fully active VPH. Mutation of glutamate-106 (E106Q) in VPH led to a loss of VPH activity while 4-OD remained fully active (55). Hence, both sets of mutations demonstrate the significant role of these glutamate residues in the catalytic activity of 4-OD and VPH.

The 4-Oxalocrotonate Decarboxylase (4-OD) and Vinylpyruvate Hydratase (VPH) Complex

Two sequential enzymes in the meta-fission pathway of *Pseudomonas putida* mt-2 are 4-oxalocrotonate decarboxylase (4-OD) and vinylpyruvate hydratase (VPH). 4-OD and VPH are encoded by separate genes and form a complex that converts 2-oxo-3-

hexenedioate (**8**) to 2-oxo-*4S*-hydroxypentanoate (**7**) using Mn^{2+} or Mg^{2+} (Scheme 1). The independent expression of each enzyme results in an unstable 4-OD (rapidly loses activity upon purification) and the precipitation of VPH in the early stages of purification (55). Consequently, an expression system was constructed that co-expresses the two enzymes allowing the formation of an active soluble complex. Sequence analysis

Scheme 1

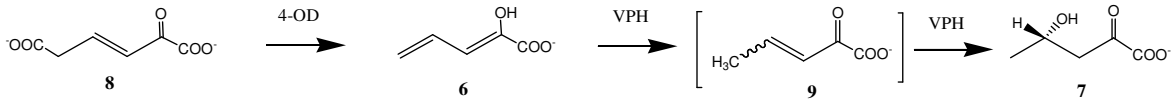

identified potential catalytic residues in both enzymes, which have been mutated (separately), and the mutants expressed as complexes having either active 4-OD or VPH (55). The availability of these complexes provides significant quantities of enzyme and works well for addressing the mechanistic questions.

Stereochemical and isotope labeling experiments were carried out using 4-OD and **8**. In these experiments, 4OD/VPH and 4-OD/E106Q-VPH (which has full 4-OD activity but no VPH activity), in separate reactions, were incubated with **8** in ^2H_2O and stereochemistry of deuterium incorporation at the C-3 position of **10** was determined. The study revealed that the 4-OD/E106Q-VPH complex generated a racemic mixture of [3-^{2}H]**10**, indicating that **10** results from a nonenzymatic process. Based on these

Scheme 2

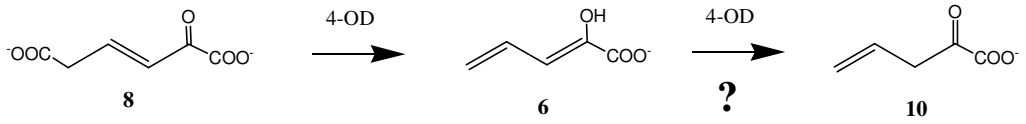

findings, it has been proposed that 4-OD converts **8** to **6** (Scheme 2) (55, 56). Subsequently, VPH converts **6** to **7** through **9** (Scheme 1) (49, 57). A VPH-catalyzed ketonization of **6** to **9** followed by the Michael addition of water to C-4 of **9** gives the *4S* isomer of **7**. This mechanism is based on the observation that VPH converts **11**, an alternate substrate for VPH, (Scheme 3) to *4S*-**13**, in $^{2}H_2O$, where deuterium has been stereoselectively incorporated at C-3 and C-5. VPH initially catalyzes the ketonization of **11** to **12** resulting in the incorporation of deuterium at C-5, producing the *5R* isomer. The Michael addition of $^{2}H_2O$ to C-4 generates the *4S*, *3S* isomeric product. The overall stereochemical course of the reaction with **8** (in Scheme 1) and **11** (in Scheme 3) cannot be assigned because the configuration of **9** (and **12**) remains unknown.

Scheme 3

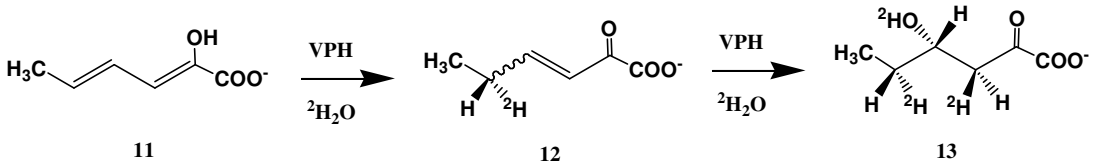

Incubation of the *trans*-**9** (with 4-OD/VPH) does not lead to product formation, but acts as a competitive inhibitor with a $K_I = 335 \pm 60\mu M$, suggesting that there is active

site binding. This result does not rule out the working hypothesis for two reasons. First, the other isomer, *cis*-**9** has not been incubated with the enzyme. Second, the enzyme may initially exist in a protonation state that allows it to catalyze the ketonization of **6** to **9**, so that if the enzyme is in the wrong protonation state, it would be unable to catalyze the hydration of **9** from solution.

MhpD: Vinylpyruvate Hydratase Homologue

MhpD, a homolog of VPH, is a metal ion-dependent monofunctional enzyme located in the chromosome of *Escherichia coli* and is part of a meta-cleavage pathway that metabolizes phenylpropionic acid (54). Like VPH, MhpD converts **6** to **7** using Mn^{2+} or Mg^{2+} (Scheme 4). Both enzymes share ~42% sequence identity and the characteristic EXE motif. Although extensive stereochemical experiments have not been carried out on MhpD, the stereochemistry at the C-4 position of **7** has been determined. Thus, it has been proposed that MhpD converts **6** to **7** through **9** (49, 57). A MhpD-catalyzed ketonization of **6** to **9** followed by the Michael addition of water to C-4 of **9** gives the *4S* isomer of **7** (Scheme 4).

Scheme 4

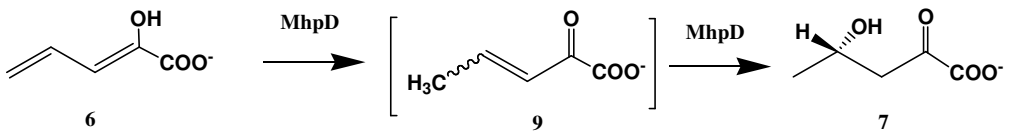

6 9 7

Recently the crystal structure of MhpD has been determined and is available in the Protein Data Bank (PDB code 1sv6). The pentameric MhpD has been solved to 2.90Å resolution in the absence of a bound metal ion or a ligand to assist in identifying the active site (Figure 1.15) (Fedorov, A.A., et al., Crystal structure of 2-hydroxypentadienoic acid hydratase from *Escherichia coli*, To be published). Based on its structural resemblance to other superfamily members, MhpD is classified as a member of the fumarylacetoacetate hydrolase (FAH)-like superfamily. Because a crystal structure of the 4OD/VPH complex is not available, the crystal structure of MhpD could act as a template to identify conserved active site residues in both MhpD and VPH as discussed in Chapter 2.

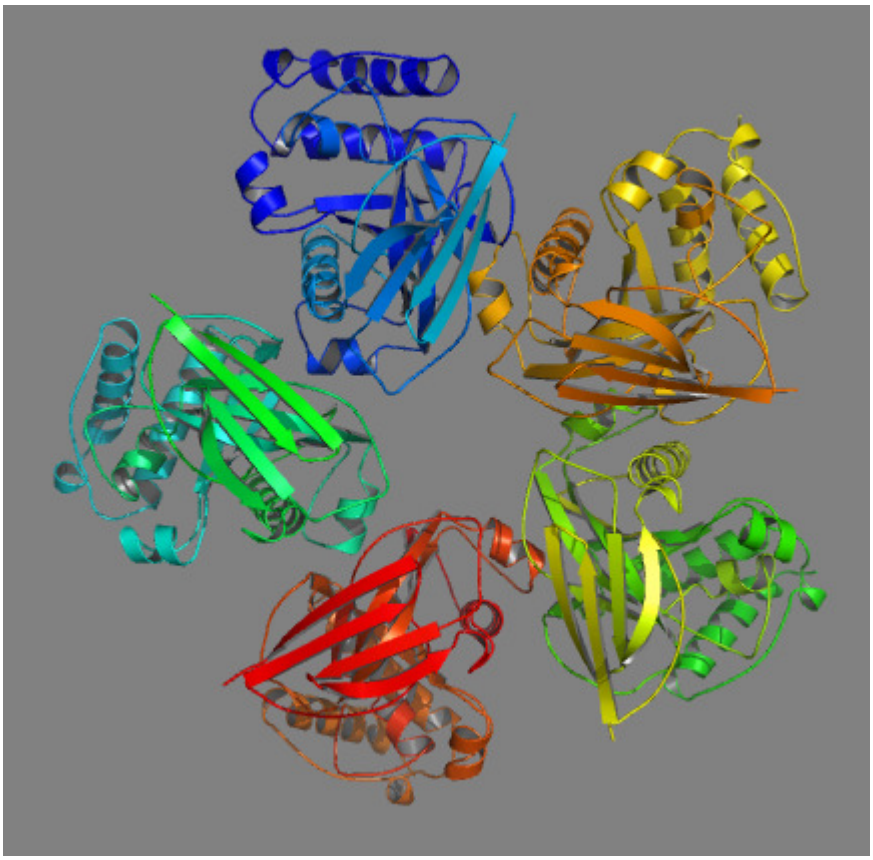

Figure 1.15. The five monomers that form the overall MhpD structure (PDB code 1sv6)

5-(carboxymethyl)-2-Oxo-3-hexene-1,6-dioate Decarboxylase (COHED)

COHED is part of the homoprotocatechuate (HPC) pathway in *E. coli* C and converts 5-(carboxymethyl)-2-oxo-3-hexene-1,6-dioate (**1**) to 2-oxo-4-heptene-1,7-dioate (**2**) using Mg^{2+} (Scheme 5) (46). The stereochemical course of the reaction catalyzed by COHED has been determined. The decarboxylation reaction initially catalyzed by COHED was investigated using (*5R*)-**1** to generate 2-hydroxy-2,4-heptadiene-1,7-dioate (**14**). A comparison of the ^{1}H NMR spectrum of **14** generated by COHED (one isomer,

4*E* or 4*Z*) to the ^{1}H NMR spectrum of **14** generated by the thermal decarboxylation of **1** (presumably both isomers) in combination with their relative coupling constants indicate that the 4*Z* isomer is produced (Scheme 5). The second part of the investigation determined the configuration of [3-^{2}H]**2**, resulting from the 1,3-keto-enol tautomerization of (*4Z*)-**14** in $^{2}H_2O$. COHED was incubated with **14** in $^{2}H_2O$. The resulting [3-^{2}H]**2** product was degraded to (*2R*)-[3-^{2}H]malate, which was analyzed by ^{1}H NMR spectroscopy. A comparision of the ^{1}H NMR spectrum of (*2R*)-[3-^{2}H]malate derived from the COHED reaction with that of (*2R,3R*)-[3-^{2}H]malate indicated that COHED ketonizes **14** to (3*S*)-[3-^{2}H]**2** (Scheme 5) (47).

Scheme 5

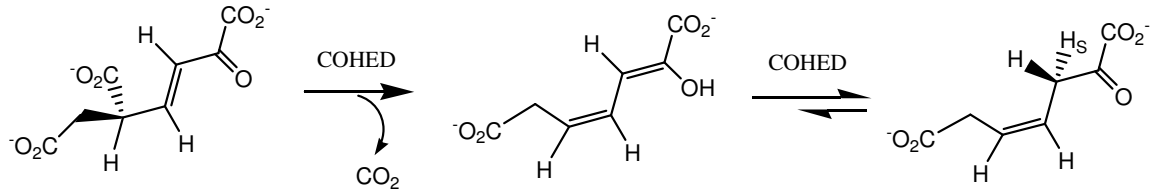

The crystal structure of COHED (with Ca^{2+}) has been solved and identified as a member of the FAH (fumarylacetoacetate hydrolase) superfamily (Figure 1.16) (51). However, since COHED was crystallized only in the presence of a bound metal ion, the location of the active site remains somewhat speculative. Thus, the structure of COHED was superimposed with that of FAH, which has a defined active site. The combination of

the Ca^{2+} ion position in COHED coupled with the FAH structural similarities led to the identification of three potential active site residues as discussed in Chapter 3.

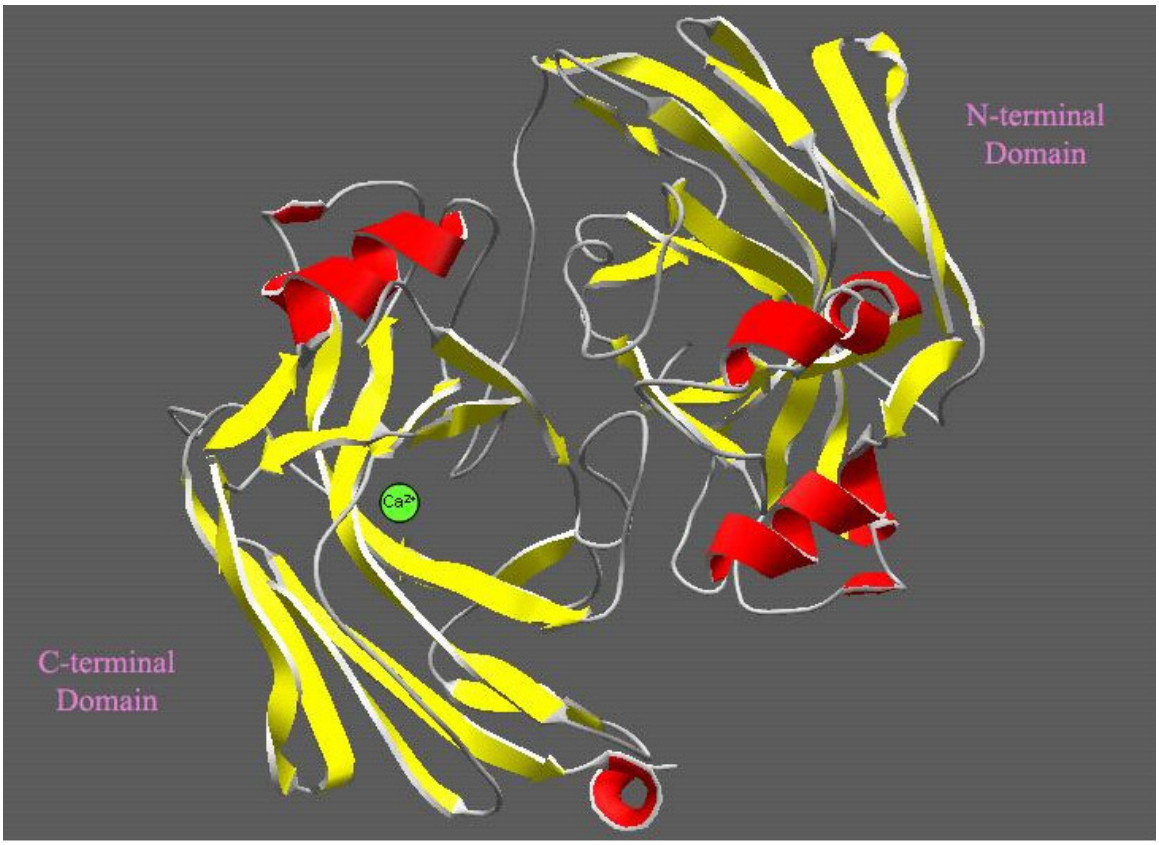

Figure 1.16. Ribbon diagram of COHED monomer (PDB code 1gtt) (51).

REFERENCES - INTRODUCTION

1. Horowitz, N.H. (1945) On the evolution of biochemical syntheses. *Proc. Natl. Acad. Sci. USA 31*, 153-157.

2. Horowitz, N.H. (1965) The evolution of biochemical synthesis – retrospect and prospect, in *Evolving Genes and Proteins* (V. Bryson and H.J. Vogel, Eds.) pp 15-23, Academic Press, New York.

3. Jensen, R.A. (1976) Enzyme recruitment in evolution of new function. *Ann. Rev. Microbiol. 30*, 409-425.

4. Gerlt, J.A. and Babbitt, P.C. (2001) Divergent evolution of enzymatic function: mechanistically diverse superfamilies and functionally distinct suprafamilies. *Ann. Rev. Biochem. 70*, 209-246.

5. Lazcano, A. and Miller, S.L. (1999) On the origin of metabolic pathways. *J. Mol. Evol. 49*, 424-431.

6. Kirschner, K., Szadkowski, H., Jardetzky, T.S., and Hager, V. (1987) Phosphoribosylanthranilate isomerase-indoleglycerol-phosphate synthase from *Escherichia coli*. *Methods Enzymol. 142*, 386-397.

7. Wilmanns, M., Priestle, J.P., Niermann, T., and Jansonius, J.N. (1992) Three-dimensional structure of the bifunctional enzyme phosphoribosylanthranilate isomerase: indoleglycerolphosphate synthase from *Escherichia coli* refined at 2.0Å resolution. *J. Mol. Biol. 223*, 477-507.

8. O'Brien, P.J. and Herschlag, D. (1999) Catalytic promiscuity and the evolution of new enzymatic activities. *Chem. Biol. 6*, R91-R105.

9. Copley, S.D. (2000) Evolution of a metabolic pathway for degradation of a toxic xenobiotic; the patchwork approach. *Trends. Biochem. Sci. 25*, 261-265.

10. Xun, L. and Orser, C.S. (1991) Purification and properties of pentachlorophenol hydroxylase: a flavoprotein from *Flavobacterium* sp. Strain ATCC 39723. *J. Bacteriol. 173*, 4447-4453.

11. Xun, L., Topp, E., and Orser, C.S. (1992) Purification and characterization of a tetrachloro-*p*-hydroquinone reductive dehalogenase from a *Flavobacterium* sp. *J. Bacteriol. 174*, 8003-8007.

12. Xun, L., Resing, K., Lawson, S.L., Babbitt, P.C., and Copley, S.D. (1999) Evidence that pcpA encodes 2,6-dichlorohydroquinone dioxygenase, the ring-cleavage enzyme required for pentachlorophenol degradation in *Sphingomonas chlorophenolica* Strain ATCC 39723. *Biochemistry 38*, 7659-7669.

13. McCarthy, D.L., Navarrete, S., Willett, W.S., Babbit, P.C., and Copley, S.D. (1996) Exploration of the relationship between tetrachlorohydroquinone dehalogenase and the glutathione *S*-transferase superfamily. *Biochemistry 35*, 14634-14642.

14. Board, P.G., Baker, R.T., Chelvanayagam, G., and Jermiin, L.S. (1997) Zeta, a novel class of glutathione transferases in a range of species from plants to humans. *Biochem. J. 328*, 929-935.

15. Armstrong, R.N. (1997) Structure, catalytic mechanism, and evolution of the glutathione transferase. *Chem. Res. Toxicol. 10*, 2-18.

16. Anandarajah, K., Kiefer, P.M., Jr., Donohoe, B.S., and Copley, S.D. (2000) Recruitment of a double bond isomerase to serve as a reductive dehalogenase during biodegradation of pentachlorophenol. *Biochemistry 39*, 5303-5311.

17. Gribble, G.W. (1994) The natural production of chlorinated compounds. *Environ. Sci. Technol. 28*, 311A-319A.

18. Siuda, J.F. and DeBernardis, J.F. (1973) Naturally occurring halogenated organic compounds. *Lloydia 36*, 107-143.

19. Hofstein, H.A., Feng, Y., Anderson, V.E., and Tonge, P.J. (1999) Role of glutamate 144 and glutamate 164 in the catalytic mechanism of enoyl-CoA hydratase. *Biochemistry 38*, 9508-16.

20. Scholten, J.D., Chang, K.H., Babbitt, P.C., Charest, H., Sylvestre, M., and Dunaway-Mariano, D. (1991) Novel enzymic hydrolytic dehalogenation of a chlorinated aromatic. *Science 253*, 182-185.

21. Chang, K.H., Liang, P.H., Beck, W., Scholten, J.D., and Dunaway-Mariano, D. (1992) Isolation and characterization of the three polypeptide components of 4-chlorobenzoate dehalogenase from *Pseudomonas* sp. Strain CBS-3. *Biochemistry 31*, 5605-5610.

22. Holden, H.M., Benning, M.M., Haller, T., and Gerlt, J.A. (2001) The crotonase superfamily: divergently related enzymes that catalyze different reactions involving acyl coenzyme A thioesters. *Acc. Chem. Res. 34*, 145-157.

23. Engel, C.K., Mathieu, M., Zeelen, J.P., Hiltunen, J.K., and Wierenga, R.K. (1996) Crystal structure of enoyl-coenzyme A (CoA) hydratase at 2.5Å resolution: a spiral fold defines the CoA-binding pocket. *EMBO J. 19*, 5135-5145.

24. Benning, M.M., Taylor, K.L., Liu, R. Q., Yang, G., Xiang, H., Wesenberg, G., Dunaway-Mariano, D., and Holden, H.M. (1996) Structure of 4-chlorobenzoyl coenzyme A dehalogenase determined to 1.8Å resolution: an enzyme catalyst generated via adaptive mutation. *Biochemistry 35*, 8103-8109.

25. Yang, G., Liang, P.H., and Dunaway-Mariano, D. (1994) Evidence for nucleophilic catalysis in the aromatic substitution reaction catalyzed by (4-chlorobenzoyl)coenzyme A dehalogenase. *Biochemistry 33*, 8527-8531.

26. Taylor, K.L., Liu, R.Q., Liang, P.H., Price, J, Dunaway-Mariano, D., Tonge P.J., Clarkson, J., and Carey, P.R. (1995) Evidence for electrophilic catalysis in the 4-chlorobenzoyl-CoA dehalogenase reaction: UV, Raman, and ^{13}C-NMR spectral studies of dehalogenase complexes of benzoyl-CoA adducts. *Biochemistry 34*, 13881-13888.

27. Yang, G., Liu R.Q., Taylor, K.L., Xiang, H., Price, J., and Dunaway-Mariano, D. (1996) Identification of active site residues essential to 4-chlorobenzoyl-coenzyme A dehalogenase catalysis by chemical modification and site directed mutagenesis. *Biochemistry 35*, 10879-10885.

28. Taylor, K.L., Xiang, H., Liu, R.Q., Yang, G., and Dunaway-Mariano, D. (1997) Investigation of substrate activation by 4-chlorobenzoyl-coenzyme A dehalogenase. *Biochemistry 36*, 1349-1361.

29. Xiang, H., Dong, J., Carey, P.R., and Dunaway-Mariano, D. (1999) Product catalyzes the deamidation of D145N dehalogenase to produce the wild-type enzyme. *Biochemistry 38*, 4207-4213.

30. Glasner, M.E., Gerlt, J.A., and Babbitt, P.C. (2007) *Mechanisms of protein evolution and their application to protein engineering, in Advances in Enzymology and Related Areas of Molecular Biology, Volume 75: Protein Evolution* (Toone, E.J., Ed.) pp 193-239, John Wiley and Sons, Inc., Hoboken, New Jersey.

31. Gerlt, J.A., Babbitt, P.C., and Rayment, I. (2005) Divergent evolution in the enolase superfamily: the interplay of mechanism and specificity. *Arch. Biochem. Biophys. 433*, 59-70.

32. Babbitt, P.C., Hasson, M.S., Wedekind, J.E., Palmer, D.R.J., Barrett, W.C., Reed, G.H., Rayment, I., Ringe, D., Kenyon, G.L., and Gerlt, J.A. (1996) The enolase superfamily: a general strategy for enzyme-catalyzed abstraction of the α-protons of carboxylic acids. *Biochemistry 35*, 16489-16501.

33. Gerlt, J.A. and Raushel, F.M. (2003) Evolution of function in $(\beta/\alpha)_8$-barrel enzymes. *Curr. Opin. Chem. Biol. 7*, 252-264.

34. Babbitt, P.C. and Gerlt, J.A. (1997) Understanding enzyme superfamilies. chemistry as the fundamental determinant in the evolution of new catalytic activities. *J. Biol. Chem. 272*, 30591-30594.

35. Gerlt, J.A. and Babbitt, P.C. (1998) Mechanistically diverse enzyme superfamilies: the importance of chemistry in the evolution of catalysis. *Curr. Opin. Chem. Biol. 2*, 607-612.

36. Xiang, H., Luo, L., Taylor, K.L., and Dunaway-Mariano, D. (1999) Interchange of catalytic activity within the 2-enoyl-coenzyme A hydratase/isomerase superfamily based on a common active site template. *Biochemistry 38*, 7638-7652.

37. (a) Bayly, R.C. and Barbour, M.G. (1984) The Degradation of Aromatic Compounds by the Meta and Genisate Pathways, in *Microbiological Degradation of Organic Compounds* (Gibson, D.T., Ed.) pp 253-294, Marcel Dekker, New York. (b) Dagley, S. (1986) Biochemistry of Aromatic Hydrocarbon Degradation in *Pseudomonads*, in *The Bacteria: A Treatise on Structure and Function* (Ornston, L. Nicholas and Sokatch, J.R., Eds.) pp 527-555, Academic Press, New York. (c) Dagley, S. (1975) A Biochemical Approach to Some Problems of Environmental Pollution, in *Essays in Biochemistry Vol. 11* (Campbell, P.N., Aldridge, W.N., Eds.) pp 81-138, Academic Press, New York.

38. Shingler, V., Powlowski, J., and Marklund, U. (1992) Nucleotide sequence and functional analysis of the complete phenol/3,4-dimethylphenol catabolic pathway of Pseudomonas sp. strain CF600. *J. Bacteriol. 174*, 711-724.

39. (a) Harayama, S., Lehrbach, P.R., and Timmis, K.N. (1984) Transposon mutagenesis analysis of meta-cleavage pathway operon genes of the TOL plasmid of *Pseudomonas putida mt-2*. *J. Bacteriol 160,* 251-255. (b) Harayama, S., Rekik, M., Ngai, K.L., and Ornston, L.N. (1989) Physically associated enzymes produce and metabolize 2-hydroxy-2,4-dienoate, a chemically unstable intermediate formed in catechol metabolism via meta cleavage in *Pseudomonas putida*. *J. Bacteriol. 171*, 6251-6258.

40. Sanvoisin, J., Langley, G.J., and Bugg, T.D.H. (1995) Mechanism of Extradiol Catechol Dioxygenases: Evidence for a Lactone Intermediate in the 2,3-Dihydroxyphenylpropionate 1,2-Dioxygenase Reaction. *J. Am. Chem. Soc. 117,* 7836-7837.

41. Whitman, C.P., Aird, B.A., Gillespie, W.R., and Stolowich, N.J. (1991) Chemical and enzymic ketonization of 2-hydroxymuconate, a conjugated enol. *J. Am. Chem. Soc. 113*, 3154-3162.

42. Diaz, E. and Timmis, K.N. (1995) Identification of functional residues in a 2-hydroxymuconic semialdehyde hydrolase. A new member of the alpha/beta hydrolase-fold family of enzymes which cleaves carbon-carbon bonds. *J. Biol. Chem. 270*, 6403-6411.

43. (a) Sparnins, V.L., Chapman, P.J., and Dagley, S. (1974) Bacterial degradation of 4-hydroxyphenylacetic acid and homoprotocatechuic acid. *J. Bacteriol. 120*, 159-167. (b) Jenkins, J.R. and Cooper, R.A. (1988) Molecular cloning, expression, and analysis of the genes of the homoprotocatechuate catabolic pathway of Escherichia coli C. *J. Bacteriol. 170*, 5317-5324.

44. Hajipour, G., Johnson, W.H., Jr., Dauben, P.D., Stolowich, N.J., and Whitman, C.P. (1993) Chemical and enzymatic ketonization of 5-(carboxymethyl)-2-hydroxymuconate. *J. Am. Chem. Soc. 115*, 3533-3542.

45. (a) Garrido-Pertierra, A. and Cooper, R.A. (1981) Identification and purification of distinct isomerase and decarboxylase enzymes involved in the 4-hydroxyphenylacetate catabolic pathway of *Escherichia coli*. *Eur. J. Biochem. 117*, 581-584. (b) Roper, D.I. and Cooper, R.A. (1990) Purification, properties, and nucleotide sequence of 5-(carboxymethyl)-2-hydroxymuconate isomerase of *Escherichia coli C*. *FEBS Lett 266*, 63-66.

46. Johnson, W.H., Jr., Hajipour, G., and Whitman, C.P. (1992) Characterization of a dienol intermediate in the 5-(carboxymethyl)-2-oxo-3-hexene-1,6-dioate decarboxylase reaction. *J. Am. Chem. Soc. 114*, 11001-11003.

47. Johnson, W.H., Jr., Hajipour, G., and Whitman, C.P. (1995) The stereochemical course of 5-(carboxymethyl)-2-oxo-3-hexene-1,6-dioate decarboxylase from *Escherichia coli C*. *J. Am. Chem. Soc. 117*, 8719-8726.

48. Roper, D.I., Stringfellow, J.M., and Cooper, R.A. (1995) Sequence of the hpcC and hpcG genes of the meta-fission homoprotocatechuic acid pathway of *Escherichia coli C*: nearly 40% amino-acid identity with the analogous enzymes of the catechol pathway. *Gene 156*, 47-51.

49. Burks, E. A., Johnson, W. H., Jr., and Whitman, C. P. (1998) Stereochemical and Isotopic Labeling Studies of 2-Oxo-hept-4-ene-1,7-dioate Hydratase: Evidence for an Enzyme-Catalyzed Ketonization Step in the Hydration Reaction. *J. Am. Chem. Soc. 120*, 7665-7675.

50. Whitman, C.P., Hajipour, G., Watson, R.J., Johnson, W.H., Jr., Bembenek, M.E., and Stolowich, N.J. (1992) Stereospecific ketonization of 2-hydroxymuconate by 4-oxalocrotonate tautomerase and 5-(carboxymethyl)-2-hydroxymuconate isomerase. *J. Am. Chem. Soc. 114*, 10104-10110.

51. Tame, J.R., Namba, K., Dodson, E.J., and Roper D.I. (2002) The crystal structure of HpcE, a bifunctional decarboxylase/isomerase with a multifunctional fold. *Biochemistry 41*, 2982-2989.

52. Timm, D.E., Mueller, H.A., Bhanumoorthy, P., Harp, J.M., and Bunick, G.J. (1999) Crystal structure and mechanism of a carbon-carbon bond hydrolase. *Structure 7*, 1023-1033.

53. Pollard, J.R., Rialland, D., and Bugg, T.D. (1998) Substrate selectivity and biochemical properties of 4-hydroxy-2-keto-pentanoic acid aldolase from *Escherichia coli*. *Appl. Environ. Microbiol. 64*, 4093-4094.

54. Pollard, J.R. and Bugg, T.D. (1998) Purification, characterisation and reaction mechanism of monofunctional 2-hydroxypentadienoic acid hydratase from *Escherichia coli*. *Eur. J. Biochem. 251*, 98-106.

55. Stanley, T.M., Johnson Jr., W.H., Burks, E.A., Hwang, C-C, Cook, P.F., and Whitman, C.P. (2000) Expression and stereochemical and isotope effect studies of active 4-oxalocrotonate decarboxylase. *Biochemistry 39*, 718-726.

56. Lian, H. and Whitman, C.P. (1994) Stereochemical and Isotopic Labeling Studies of 4-Oxalocrotonate Decarboxylase and Vinylpyruvate Hydratase: Analysis and Mechanistic Implications. *J. Amer. Chem. Soc. 116*, 10403-10411.

57. Schwab, J.M. and Henderson, B.S. (1990) Enzyme-catalyzed allylic rearrangements. *Chem. Rev. 90*, 1203-1245.

Chapter 2: Expression and Characterization of Active site Mutants of Vinylpyruvate Hydratase and its homologue MhpD from *Escherichia coli*: Analysis and Implications

INTRODUCTION:

Several bacterial *meta*-cleavage pathways involved in the degradation of aromatic compounds proceed through a common intermediate, 2-hydroxy-2,4-pentadienoate (**2**, HPD, Scheme 1) (1,2). The reaction producing this intermediate is catalyzed by a number of homologous hydratase enzymes, including vinylpyruvate hydratase (EC 4.2.1.80; VPH) from *Pseudomonas putida mt-2* (1-3) and 2-hydroxypentadienoic acid hydratase (EC 4.2.1.80; MhpD) from *Escherichia coli* (4), both of which convert HPD to 2-oxo-*4S*-hydroxypentanoate (**4**, Scheme 1). VPH exists as a complex with another enzyme, 4-oxalocrotonate decarboxylase (4-OD), with both enzymes utilizing either

Scheme 1

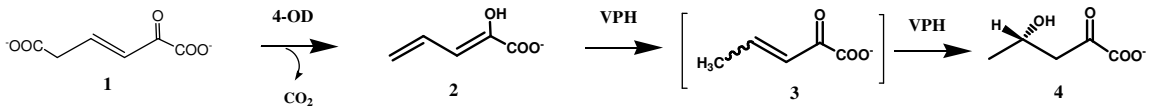

manganese or magnesium as a cofactor (2,3). 4-OD catalyzes the previous step in the pathway converting 2-oxo-3-hexenedioate (**1**, Scheme 1) to **2**. 4-OD and VPH are expressed by separate genes and are part of an inducible pathway encoded by the TOL plasmid pWW0 (2). MhpD is a metal-dependent monofunctional enzyme, the gene is located in the chromosome of *E. coli* (4). Previous work suggests that VPH and MhpD

catalyze the hydration of **2** to **4** through the intermediate 2-oxo-3-pentenoate (**3**, Scheme 1) (3,5). In such a mechanism, it can be reasonably argued that VPH catalyzes the ketonization of **2** to **3** followed by the Michael addition of water to **3** to yield **4**.

Recently, the crystal structure of MhpD became available in the Protein Data Bank (PDB code 1sv6). Based on structural similarities, MhpD is classified as a member of the fumarylacetoacetate hydrolase (FAH)-like superfamily. The three proteins that represent the FAH superfamily are FAH (fumarylacetoacetate hydrolase) (6), COHED (5-(carboxymethyl)-2-oxo-3-hexene-1,6-dioate decarboxylase, a decarboxylase from *E. coli* C) (7), and YcgM (an *E. coli* homologue, with unknown physiological function). Both FAH and COHED are metal ion-dependent enzymes involved in C-C bond cleavage. One of the characteristics of the superfamily is an EXE motif, which has been implicated in the binding of a divalent metal [in COHED (E276 and E278) (7), in FAH (E199 and E201) (6), and in YcgM (E70 and E72)]. VPH and MhpD may also be members of the FAH superfamily. VPH has an EXE motif (E106 and E108). Mutation of glutamate-106 (E106Q) in VPH resulted in a loss of catalytic activity (3). The loss of activity is not likely due to a structural defect since past results have shown that a structurally damaged VPH produces insoluble protein. Hence, this mutation demonstrates the significant role of the glutamate residue in maintaining the catalytic activity of VPH. MhpD shares ~42% sequence identity with VPH and has the characteristic EXE motif (E105 and E107). Because a crystal structure of the 4OD/VPH complex is not available, the crystal structure of MhpD could be used to identify conserved active site residues in both MhpD and VPH.

The pentameric MhpD was crystallized without a bound metal ion or ligand that could identify active site residues (Figure 2.1). However, the EXE motif (E105 and E107) is likely to be part of the metal binding site and can be used as a starting point in the identification of active site residues. Examining the positions of these two glutamates led to identification of a neighboring third glutamate residue (Glu-138). Based on their proximity to each other and similar function in other FAH superfamily members, it is reasonable to assume that this glutamate triad is part of the metal binding site of MhpD. Other residues within the immediate area of the glutamate triad were examined and four residues, Lys-60, Leu-72, Asp-78, and Ser-161 (Ser-160 in MhpD), were chosen for further investigation. These four residues are conserved within VPH and MhpD and are targets for a series of site-directed mutations to examine their roles as potential catalytic residues in VPH and MhpD.

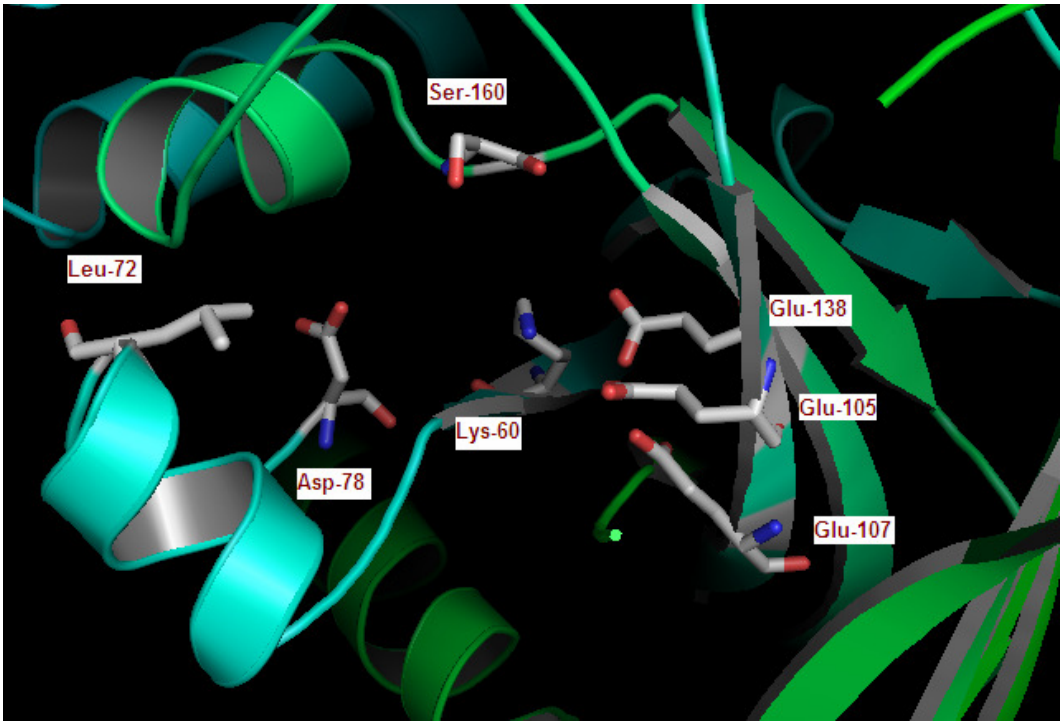

Figure 2.1. Close-up view of the proposed key residues in the active-site of MhpD (PDB code 1sv6).

MATERIALS AND METHODS

Materials. All reagents, buffers, media components, and solvents were obtained from Sigma-Aldrich Chemical Co. (St. Louis, MO), Fisher Scientific Inc. (Fair Lawn, New Jersey), or Becton Dickinson Microbiology Systems (Sparks, MD) with the following exceptions. Literature procedures were used for the syntheses of 2-hydroxy-2,4-pentadienoate (**2**) (8), 2-hydroxy-2,4-hexadienoate (**6**) (9), 2-oxo-3-pentynoate (**10**) (10), 3-bromopropiolic acid (**11**) (11), and oxirane-2-carboxylate (**12**) (12). The YM-10 ultrafiltration membranes and the Amicon stirred cells were obtained from Millipore Corp. (Billerica, MA). Restriction enzymes, PCR reagents, the Expanded High Fidelity PCR System, and the Rapid DNA Ligation Kit were obtained from Roche Diagnostics Corp. (Indianapolis, IN). The QIAprep Spin Miniprep Kit and MinElute Kit were obtained from Qiagen, Inc. (Valencia, CA). The QuikChange II Site-Directed Mutagenesis Kit was acquired from Stratagene (La Jolla, CA). Oligonucleotides for DNA amplification or mutant construction were synthesized by either Sigma-Genosys (The Woodlands, TX) or Integrated DNA Technologies (Coralville, IA). The pLC20-30 plasmid, encoding the gene for MhpD, was obtained from the *E. coli* Genetic Stock Center at Yale University (New Haven, CT). The *mhpD* gene was amplified from the plasmid pLC20-30, a member of the Clarke and Carbon Library of Plasmids.

Bacterial Strains and Plasmids. *Escherichia coli* strain DH5α (Invitrogen, Carlsbad, CA) was used for cloning and isolation of plasmids. *E. coli* strain BL21-Gold(DE3) from Stratagene was used for recombinant protein expression. The expression vector pET24a-(+) was obtained from Novagen, Inc. (Madison, WI). The

construct pET24a-(4OD/VPH) (3) and pET24a-(E109Q4OD/VPH) [Wang, S.C. and Whitman, C.P. (2008) unpublished results] were used as templates for the construction of the VPH mutants.

General Methods. Techniques for cloning and DNA manipulation were based on methods described elsewhere (13), or as suggested by the manufacturer. The PCR was carried out in a Perkin-Elmer DNA thermocycler (Model 480) obtained from Perkin Elmer Inc. (Wellesley, MA). DNA sequencing was performed by the DNA Core Facility in the Institute for Cellular and Molecular Biology (ICMB) at the University of Texas at Austin. Plasmid DNA was introduced into cells by electroporation using a Cell-Porator Electroporation System (Whatman Biometra, Göttingen, Germany). HPLC was performed on a Waters (Milford, MA) 501/510 system or a Beckman System Gold HPLC (Fullerton,CA) using either a TSKgel DEAE-5PW anion-exchange (150 × 21.5 mm) or a TSKgel Phenyl-5PW hydrophobic interaction (150 × 21.5 mm) column (Tosoh Bioscience, Montgomeryville, PA). Gel filtration chromatography was carried out on a Spectra/Chrom Aqueous column (2.5 × 100 cm) obtained from Spectrum Chromatography (Houston, TX) using Sephadex G-75 resin. Protein was analyzed by SDS-PAGE under denaturing conditions on gels containing 15% polyacrylamide. Protein concentrations were determined by the method of Waddell (14). Absorbance data were obtained on an Agilent 8453 Diode Array spectrophotometer (Agilent Technologies, Palo Alto, CA). The kinetic data were fitted by nonlinear regression using the Grafit program (Erithacus Software Ltd., Horley, U.K.) obtained from Sigma Chemical Co. ^{1}H-Nuclear magnetic resonance (NMR) spectra were recorded in 100%

H_2O on a Varian Unity INOVA-500 spectrometer using selective presaturation of the water signal with a 2 s presaturation interval. The lock signal is dimethyl-d_6 sufoxide (DMSO- d_6). Chemical shifts are standardized to the DMSO- d_6 signal at 2.49 ppm.

Construction of the 4OD/L72A-VPH and 4OD/S161A-VPH Mutants. Two single mutants of VPH (L72A and S161A) were prepared using the gene for VPH (*xylJ*) in plasmid pET24a-(4OD/VPH) as the template. Mutations were made using the overlap extension polymerase chain reaction as described elsewhere (15). The external primers were oligonucleotides 5´-TAATACGACTCACTATAGG-3´ (designated primer A) and 5´-CTCAGCTTCCTTTCGGGCTT-3´ (designated primer D). Primer A corresponds to the coding sequence of the T7 promotor region of the pET24a vector and primer D corresponds to the complementary sequence of the region upstream from the T7 terminator region of the vector. The L72A mutant of VPH was generated by the PCR using the oligonucleotides 5´-GTGCAGAACATGGCCGGCGTGCACCAG-3´ (primer B) and 5´-CTGGTGCACGCCGGCCATGTTCTGCAC-3´ (primer C), as the internal primers. In each primer, the mutation is underlined and the remaining bases correspond to the coding sequence (primer B) or the complementary sequence (primer C) for the VPH gene. The AC and BD fragments were amplified using pET24a-(4OD/VPH) as template, the appropriate synthetic primers, and the PCR reagents supplied in the Expanded High Fidelity PCR system following the protocol supplied with this system. The PCR reaction mixture (total volume 50µL) contained dNTP (200 µM), primers (50 ng each), plasmid (50 ng), a mixture of *Taq* DNA polymerase and *Tgo* DNA polymerase (3 units), and the accompanying 10X buffer (diluted to 1X). The amplification protocol

consisted of a 5-min denaturation step at 94 ºC, followed by 30 cycles of 94 ºC for 60 s, 58 ºC for 60 s, and 72 ºC for 90 s, with a final 10-min elongation step at 72 ºC.

The AC and BD fragments along with primers A and D were combined into one PCR mixture to generate the AD segment (~1800 base pairs) using the PCR amplification procedure described above. The purified AD segment and the pET24a vector were digested with *Xba*I and *Hind*III restriction enzymes, purified (via the MinElute Kit), and ligated using T4 DNA ligase. Aliquots of the ligation mixture were introduced into competent *E. coli* DH5α cells by electroporation. Transformants were selected at 37ºC on LB/Kn (50 µg/mL) plates and plasmid DNA was isolated from several single colonies. The 4OD/ L72AVPH gene was sequenced in order to verify that only the desired mutations had been introduced during the PCR.

The S161A mutant was constructed in the same manner, but different internal primers were used. For the S161A mutant Primers B and C were oligonucleotides 5´-GCGGACAACGCCGCCTGCGGGCTGTTC-3´ and 5´-GAACAGCCCGCAGGCGGCGTTGTCCGC-3´, respectively.

Construction of the E109Q-4OD/K60A-VPH and E109Q-4OD/D78N-VPH Mutants. The two single mutants E109Q-4OD/K60A-VPH and E109Q-4OD/D78N-VPH were prepared using the dicistronic gene in plasmid pET24a-(E109Q-4OD/VPH) as the template. These two point mutations were generated by mutagenic primer-directed replication using the QuikChange II Site-Directed Mutagenesis Kit. Following the protocol supplied by the manufacturer, the E109Q-4OD/K60A-VPH mutant was generated by the PCR using oligonucleotides 5´-

GTGATCGGCAAGGCGATCGGCGTCACC-3´ (Primer-1) and 5´-GGTGACGCCGATCGCCTTGCCGATCAC-3´ (Primer-2). In each primer, the mutation is underlined and the remaining bases correspond to the coding sequence (Primer-1) or the complementary sequence (Primer-2) for the VPH gene. The E109Q-4OD/D78N-VPH mutant was constructed in the same manner, using the oligonucleotides 5´-GTGCACCAGCCGAACTTCGGCTACCTC-3´ (Primer-3) and 5´-GAGGTAGCCGAAGTTCGGCTGGTGCAC-3´ (Primer-4), as primers.

Construction of MhpD Expression Vector. Using the Expanded High Fidelity PCR system, the *mhpD* gene was synthesized using oligonucleotides 5´-GCACATATGGTCATGACGAAGCAT-3´ and 5´-AAGGTCGACTCATGACAGACTTCC -3´ (Primer-5 and 6, respectively). Primer-5 has three non-specific bases, a *Nde*I site (underlined), and 15 bases corresponding to the first 15 bases of *mhpD*. Primer-6 has three non-specific bases, a *Sal*I site (underlined), and 15 bases corresponding to the last 15 bases of *mhpD*. The purified *mhpD* gene (~800 base pairs) and the pET24a vector were digested with *Nde*I and *Sal*I restriction enzymes, purified (via the MinElute Kit), and ligated using T4 DNA ligase. Aliquots of the ligation mixture were introduced into competent *E. coli* DH5α cells by electroporation. Transformants were selected at 37ºC on LB/Kn (50µg/mL) plates and plasmid DNA (designated pET24a-MhpD) was isolated from several single colonies. The cloned mhpD gene was sequenced in order to verify that no mutations had been introduced during the PCR.

Construction of the MhpD Mutants. The four single mutants of MhpD (K60A, D78N, L72A, and S160A) were prepared using the plasmid pET24a-MhpD as the template. Site-directed mutations were introduced using the QuikChange II Site-Directed Mutagenesis Kit. Accordingly, the K60A mutant of MhpD was generated by the PCR using oligonucleotides 5´- GTGGTAGGGCGTGCAGTGGGCCTGACACATCCG-3´ and 5´-CGGATGTGTCAGGCCCACTGCACGCCCTACCAC-3´ (Primer-7 and 8, respectively). Primer-7 has 12 coding sequence bases, three bases corresponding to the alanine mutation (underlined), and another 18 bases of coding sequence. Primer-8 has 18 complementary sequence bases, three bases corresponding to the alanine mutation (underlined), and another 12 bases of complementary sequence.

The D78N mutant of MhpD was constructed using the oligonucleotides 5´-GTTGATCAACCGAATTTTGGGACGTTA-3´ and 5´-TAACGTCCCAAAATTCGGTTGATCAAC-3´ (Primer-9 and 10, respectively). Primer-9 has 12 coding sequence bases, three bases corresponding to the asparagine mutation (underlined), and another 12 bases of coding sequence. Primer-10 has 12 complementary sequence bases, three bases corresponding to the asparagine mutation (underlined), and another 12 bases of complementary sequence.

The L72A mutant of VPH was produced using the oligonucleotides 5´-GTGCAACAACAAGCGGGCGTTGATCAACCG-3´ and 5´-CGGTTGATCAACGCCCGCTTGTTGTTGCAC-3´ (Primer-11 and 12, respectively). Primer-11 has 12 coding sequence bases, three bases corresponding to the alanine mutation (underlined), and another 15 bases of coding sequence. Primer-12 has 15

complementary sequence bases, three bases corresponding to the alanine mutation (underlined), and another 12 bases of complementary sequence.

The S160A mutant of VPH was generated using the oligonucleotides 5´-GTGGCAGATAACGCCGCCTGTGGGGTGTATGTC-3´ and 5´-GACATACACCCCACAGGCGGCGTTATCTGCCAC-3´ (Primer-13 and 14). Primer-13 has 15 coding sequence bases, three bases corresponding to the alanine mutation (underlined), and another 15 bases of coding sequence. Primer-14 has 15 complementary sequence bases, three bases corresponding to the alanine mutation (underlined), and another 15 bases of complementary sequence.

Overexpression and Purification of the K60A, L72A, D78N, S161A, and wild-type VPH and K60A, L72A, D78N, S160A, and wild-type MhpD Mutants. Each mutant construct was transformed into competent *E. coli* BL21-Gold(DE3) cells by electroporation. Transformants were grown at 37ºC on LB/Kn (50 µg/mL) plates. A single colony was used to inoculate 50 mL of LB/Kn (50 µg/mL) media in a 125 mL Erlenmeyer flask. After overnight growth at 37ºC, a 30 mL aliquot of overnight culture was used to inoculate 6 – 2L Erlenmeyer flasks containing 500 mL of LB/Kn (50 µg/mL) medium (3 L total). The cells were grown to an OD_{600} of 0.6-0.8 (~ 3 h), induced by the addition of 0.5 mM of IPTG, and allowed to grow for another 5 h. Cells were harvested by centrifugation (8 min at 7500*g*) and stored at -20ºC. The enzymes were purified by a modification of a published procedure (3). Accordingly, in a typical purification experiment, the cells from 3 L of culture were thawed and suspended in 16 mL of 50 mM triethanolamine buffer, pH 7.3 (Buffer A), containing 5 mM $MgCl_2$, disrupted by

sonication, and centrifuged (1.5 hours at 60,000*g*). The supernatant was filtered through a 0.2 µm-pore diameter filter and applied to a TSKgel DEAE-5PW column (150 × 21.5 mm) that has been pre-equilibrated with Buffer A. The column was washed with 50 mL of Buffer A, and retained proteins were eluted with an increasing linear gradient (0 to 0.5 M NaCl) in Buffer A (300 mL) at a flow rate of 5 mL/min. Fractions (8 mL) that showed the highest VPH activity were pooled and concentrated to ~20 mL using an Amicon stirred cell equipped with a YM10 (10,000 MW cutoff, respectively) ultrafiltration membrane. The protein typically eluted in fractions #21 – 28. During collection, each fraction was made 5 mM $MgCl_2$. Subsequently, the concentrate was made 1.2 M using solid $(NH_4)_2SO_4$ and the resulting solution was stirred for 60 min. at 4 ºC. After centrifugation (30 min at 17,000*g*), the supernatant was loaded onto the TSKgel Phenyl-5PW column (150 × 21.5 mm) that had previously been equilibrated with Buffer B [10 mM HEPES buffer, 1.2 M $(NH_4)_2SO_4$, pH 7.3]. The column was washed with 50 mL of Buffer B, and retained proteins were eluted with a decreasing linear gradient of 1.2 to 0 M $(NH_4)_2SO_4$ in Buffer C (10mM HEPES buffer, pH 7.3, 250mL) at a flow rate of 5mL/min. Fractions (8 mL) with the highest VPH activity were pooled and concentrated to ~3 mL using an Amicon stirred cell equipped with a YM10 ultrafiltration membrane. The protein typically eluted in fractions #32-37. The fractions collected were made 5 mM $MgCl_2$ during collection. The concentrated protein was loaded onto a Sephadex G-75 column (2.5 × 100 cm) equilibrated with 20 mM HEPES buffer, pH 7.3. Fractions (8 mL) were collected and sufficient $MgCl_2$ (from a 1 M stock solution) was added to give a 5 mM concentration in each tube. The MhpD mutants normally eluted between fractions

#17-25, while the VPH mutants eluted around fractions #22-30. These fractions were assayed for activity and the purity (>95%) was determined by SDS-PAGE. The purified enzymes were filtered through a 0.2 µm-pore diameter filter and stored at 4 ºC.

Enzyme Assays and Steady-State Kinetics. The enzyme kinetic assays were performed in 20 mM Na_2HPO_4, 5mM $MgCl_2$ buffer, pH 7.3, following the decrease in absorbance at 267 nm corresponding to the hydration of **2** to **4** (Scheme 1) or the ketonization of **2** to **3** (Scheme 1). The extinction coefficient for **2** is 10,000 $M^{-1}cm^{-1}$. An aliquot of enzyme (5 – 40 µL) was diluted into buffer (40 mL) and incubated for 1 h. Subsequently, a 1 mL-portion of the diluted enzyme was transferred to a cuvette and assayed for activity by the addition of a small quantity of substrate (4-60 µM) from a 2 or 15 mM stock solution made up in ethanol. The amount of enzyme in each 1-mL cuvette ranged from 1.0 nM – 4.1 µM for MhpD and 9 nM – 6.6 µM for VPH. The chemical rate of ketonization (**2** to **5**, Scheme 2) was determined by following the decrease in absorbance at 267 nm for five different concentrations of **2**. The plot of change in absorbance at 267 nm versus substrate concentration gave a linear fit determination that was used to calculate the chemical rate at different substrate concentrations. The chemical rate of ketonization (**2** to **5**) was subtracted from the observed enzymatic rate.

Scheme 2

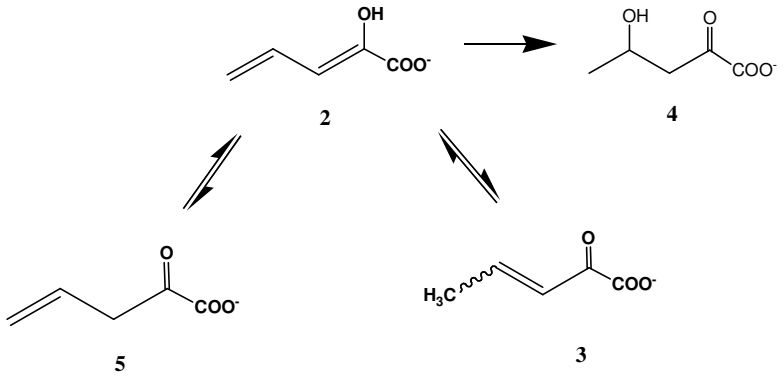

The enzyme kinetic assays for the alternate substrate 2-hydroxy-2,4-hexadienoate (Me-HPD, **6**, Scheme 3) were performed in 20 mM Na_2HPO_4, 5mM $MgCl_2$ buffer, pH 7.3, following the decrease in absorbance at 275 nm corresponding to the hydration of **6** to **8** (Scheme 3) or the ketonization of **6** to **7** (Scheme 3). The extinction coefficient for **6** is 12,000 $M^{-1}cm^{-1}$. An aliquot of enzyme (10 – 60 µL) was diluted into buffer (40 mL) and incubated for 1 h.

Scheme 3

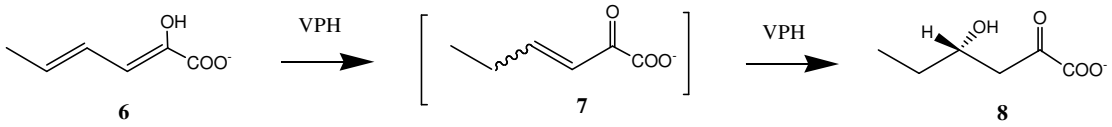

At the end of the incubation period, a 1 mL-portion of the diluted enzyme was transferred to a cuvette and assayed by the addition of a small quantity of substrate (4 - 60 µM) from a 2 or 15 mM stock solution made up in ethanol. The E109Q-4OD/K60A-VPH mutant

required slightly larger amounts of substrate (7 – 125 μM) from a 7 or 25 mM stock solution made up in ethanol. The amount of enzyme in each 1-mL cuvette ranged from 3.8 nM – 4.1 μM for MhpD and 8.9 nM – 6.6 μM for VPH. The chemical rate of ketonization (**6** to **9**, Scheme 4) was determined by following the decrease in absorbance at 275 nm for five different concentrations of **6**. The plot of change in absorbance at 275 nm versus substrate concentration gave a linear fit determination that was used to calculate the chemical rate at different substrate concentrations. The chemical rate of ketonization (**6** to **9**) was subtracted from the observed enzymatic rate.

Scheme 4

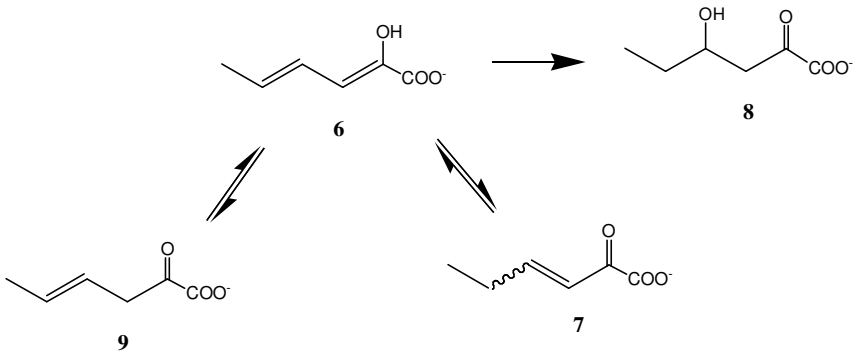

Kinetic parameters were determined by plotting initial rate of formation of **3** or **4** versus substrate concentration. Those data points were then fit by non-linear regression to give the V_{max} and K_m values (Figure 2.2). The V_{max} value was divided by the protein concentration in the cuvette to give the k_{cat} value.

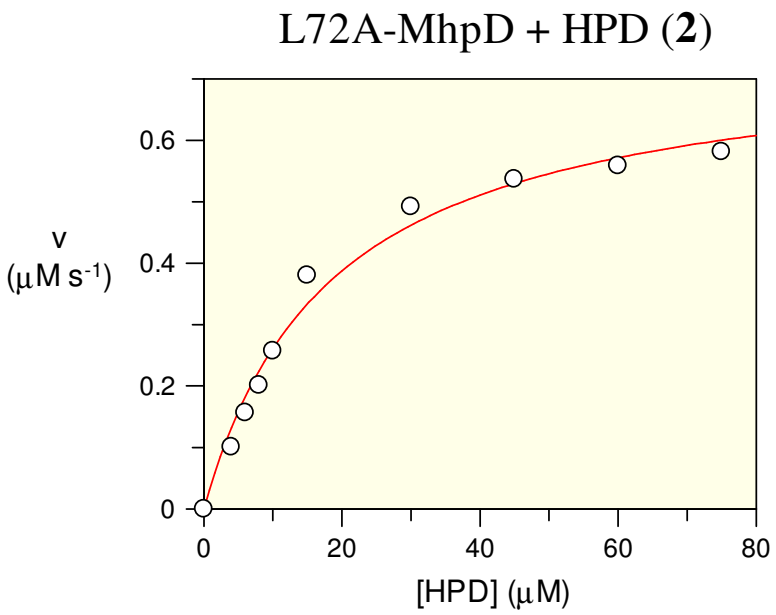

Parameter	Value	Std. Error
Vmax	0.75	0.04
Km	18.74	2.55

Enzyme Concentration – 3.5 nM

$$k_{cat} = \frac{0.75\ \mu M\ s^{-1}}{3.5 \times 10^{-3}\ \mu M} = 214\ s^{-1}$$

Figure 2.2. Michaelis-Menten plot for the L72A-MhpD-catalyzed reaction converting **2** to **4** and sample calculation of kinetic parameters.

Mass Spectral Analysis of VPH and MhpD. The masses of 4OD/VPH, MhpD, E109Q-4OD/K60A-VPH, and K60A-MhpD were determined using an LCQ electrospray ion trap mass spectrometer (ThermoFinnigan, San Jose, CA), housed in the Analytical Instrumentation Facility Core in the College of Pharmacy at the University of Texas at Austin. The proteins (~1 mg/mL) were loaded onto separate PD-10 Sephadex G-25 gel filtration columns, which had previously been equilibrated with 100 mM NH_4HCO_3 buffer (pH 8.0). Using gravity flow, the proteins were eluted in the same buffer. Fractions (0.5 mL) were analyzed for the presence of protein by UV absorbance at 215 nm. The appropriate fractions containing the purified proteins were submitted for analysis by electrospray ionization mass spectrometry (ESI-MS).

Gel Filtration Analysis of VPH and MhpD. The masses of 4OD/VPH, MhpD, E109Q-4OD/K60A-VPH, and K60A-MhpD were determined using a Superose-6 column (Amersham Pharmacia Biotech, Sweden). Using a Gel Filtration Calibration Kit HMW (GE Healthcare, Buckinghamshire, UK) a calibration curve was generated following the protocol provided by the manufacturer and using a mixture of four different proteins: ovalbumin (43 kDa), aldolase (158 kDa), ferritin (440 kDa), and thyroglobulin (669 kDa). The sample proteins (100 µL, ~4 mg/mL) were loaded separately onto the column and the elution time was determined by maximum peak height. The elution time was standardized to a gel-phase distribution coefficient value (K_{av}) and compared to the calibration curve to give the native molecular weight determination.

*^{1}H NMR Spectroscopic Detection of **3** and **4**.* An NMR tube contained an amount of **2** (4 mg, 0.04 mmol) dissolved in DMSO-d_6 (30 µL) and added to 100 mM Na_2HPO_4

buffer (0.6 mL, pH~9.2). The final pH of the solution was 7.2. Subsequently, aliquots of 4OD/VPH (100 µL of a 25 mg/mL solution in 20 mM sodium phosphate buffer, 5 mM magnesium chloride, pH 7.3) were added to the reaction mixture. The concentration of **2** in the NMR tube was 35 mM. The spectrum was recorded after the reaction was allowed to incubate overnight. The same preparation was made for MhpD, all four MhpD mutants (K60A-, L72A-, D78N-, and S160A-MhpD), and all four VPH mutants (E109Q-4OD/K60A-VPH, 4OD/L72A-VPH, E109Q-4OD/D78N-VPH, 4OD/S161A-VPH). **3**: ^{1}H NMR (H_2O, 500 MHz) δ 1.80 (3H, d, H5), 6.02 (1H, d, H3), and 6.89 (1H, m, H4). **4**: ^{1}H NMR (H_2O, 500 MHz) δ 1.03 (3H, d, H5), 2.72 (2H, d, H3), and 4.11 (1H, m, H4).

The relative percentages of **3** and **4** produced after an overnight incubation period containing enzyme and **2** were determined. For **3** and **4**, the signal corresponding to the C-3 proton(s) was identified and integrated. Using 4OD/S161A-VPH as an example, the ratio of the integrals corresponding to C-3 proton(s) indicate that **3** makes up ~ 35% and **4** makes up ~ 65% of the recovered product (Figure 2.3).

3: δ 6.02 (1H, d, H3) Integration - 1.0

4: δ 2.72 (2H, d, H3) Integration - 3.77 $\frac{3.77}{2} = 1.89$ (each proton)

Total = 1.0 + 1.89 = 2.89 $\frac{1.0}{2.89} = 0.346 = 35\%$ (**3**)

$\frac{1.89}{2.89} = 0.654 = 65\%$ (**4**)

Figure 2.3. Sample calculation of the percentages of **3** and **4** produced during ^{1}H NMR analysis. Using the integration values calculated from the ^{1}H NMR spectrum of 4OD/S161A-VPH incubated with **2** to determine the percentage of products **3** and **4** produced after an overnight incubation period.

Inhibition Studies of VPH. Stock solutions of inhibitors were made up in 100 mM Na_2HPO_4 buffer, pH ~9.2. The addition of the inhibitor as a free acid to the buffer adjusted the pH of the aqueous stock solutions to ~7. The concentrations of the stock solutions were 100 mM for 2-oxo-3-pentynoate (**10**), 3-bromopropiolic acid (**11**), and oxirane-2-carboxylate (**12**) (Figure 2.4). A quantity of VPH (30 µL of a 20 mg/mL solution) was diluted into 30 mL of 20 mM Na_2HPO_4 buffer, 5 mM $MgCl_2$ pH 7.3, and allowed to equilibrate at 22 ºC for 1 h. The inhibitors were added to the enzyme stock solutions to give the desired final concentrations. After a 5-min incubation period, 1-mL aliquots were removed and assayed in the presence of varying concentrations of **2** (4 – 60

μM). The final concentrations of inhibitors in the incubation mixtures ranged from 0 – 1 mM.

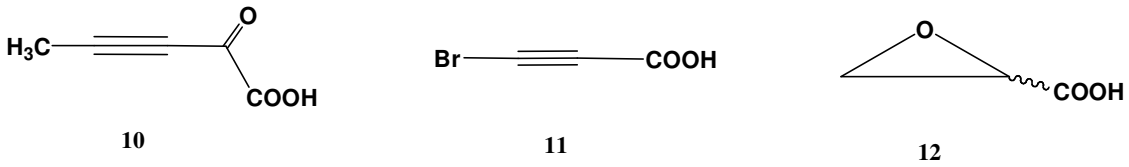

10 **11** **12**

Figure 2.4. Potential Inhibitors for VPH and MhpD as described in the text.

RESULTS

Construction, Expression, and Purification of MhpD. The gene for MhpD was amplified from the plasmid, pLC20-30. The gene was cloned into the expression vector pET24a, and sequenced to verify that no mutations had been introduced during the amplification and cloning processes. The MhpD construct was expressed in *E.coli* strain BL21-Gold(DE3) producing a soluble and active form of the protein. Purification of the recombinant protein involved a four-step protocol (using three columns), which typically provides 15-20 mg of homogeneous enzyme per liter of culture. Analysis by SDS-PAGE gave a single band at 28 kDa. MhpD was analyzed by ESI-MS and the spectrum showed a single peak corresponding to a mass of 28983 ± 2 Da (calculated 28890 Da). Gel filtration of MhpD on a Superose-6 column gave a single peak corresponding to a molecular mass of 150 kDa. This value corresponds to the native mass of MhpD and is indicative of a pentameric structure, consistent with the crystal structure (PDB code 1sv6).

Construction, Expression, and Purification of MhpD Mutants. The K60A, D78N, L72A, and S160A mutants of MhpD were constructed by mutagenic primer-directed replication using the commercial mutagenesis QuikChange II Site-Directed Mutagenesis Kit. Each mutation was generated by the PCR using the plasmid pET24a-MhpD as the template, the appropriate primers, and PCR reagents. The subsequent constructs were sequenced to confirm that only the desired mutation had been introduced. The resulting plasmid containing the mutant gene was transformed into the *E. coli* strain BL21-Gold(DE3) where the mutant proteins were expressed and purified following the same

protocol developed for the wild-type enzyme. The expression system typically yielded 10-15 mg of purified protein (per liter of culture) for each of the four mutants. Analysis by SDS-PAGE gave a single band at 28 kDa. The K60A mutant of MhpD was analyzed by ESI-MS and the spectrum showed a single peak corresponding to a mass of 28923 ± 2 Da (calculated 28833 Da). Gel filtration analysis of the K60A mutant of MhpD on a Superose-6 column gave a single peak relating to a molecular mass of 150 kDa. This value corresponds to the native mass of MhpD and is indicative of a pentameric structure.

Construction, Expression, and Purification of 4OD/L72A-VPH and 4OD/S161A-VPH Mutants. It is not possible to purify 4-OD and VPH separately so a single pET24a plasmid was constructed which contains both the 4-OD and VPH genes (3). Hence, 4-OD and VPH are co-expressed to generate the enzyme complex, 4OD/VPH. Two single mutants, 4OD/L72A-VPH and 4OD/S161A-VPH, were generated by the overlap extension PCR (15) using the plasmid pET24a-(4OD/VPH) as the template, the appropriate synthetic primers, and the PCR reagents. Both the 4-OD gene and the mutated VPH gene were sequenced in each of the new constructs to ensure that only the desired mutation had been incorporated into VPH. The mutated plasmid was transformed into the *E. coli* strain BL21-Gold(DE3) where the mutant complex was expressed and purified. Purification of each of the recombinant enzymes typically produced 10-15 mg of homogeneous protein per liter of culture. Analysis by SDS-PAGE resulted in two single bands around 28 kDa, corresponding to 4OD and VPH.

Construction, Expression, and Purification of the E109Q-4OD/K60A-VPH and E109Q-4OD/D78N-VPH Mutants. Single mutants of VPH (4OD/K60A-VPH and

4OD/D78N-VPH) were generated initially. Each single mutant showed 1,5-keto-enol tautomerase activity (converting **2** to **3**) as determined by UV and NMR analysis. To ensure that the observed activities are not due to 4OD, the double mutants (E109Q-4OD/K60A-VPH and E109Q-4OD/D78N-VPH) were constructed and examined. The E109Q-4OD/VPH complex has little decarboxylase activity (essentially inactivating 4OD), while still allowing VPH to process **2** to **4**. The E109Q-4OD/K60A-VPH and E109Q-4OD/D78N-VPH mutants were created by mutagenic primer-directed replication using the commercial mutagenesis QuikChange II Site-Directed Mutagenesis Kit. Each mutation was generated by the PCR using the plasmid pET24a-(E109Q-4OD/VPH) as the template, the appropriate primers, and PCR reagents. Both the E109Q-4OD gene and the mutated (K60A and D78N) VPH genes were sequenced in each of the new constructs to ensure that only the desired mutations had been introduced. The mutated plasmid (either E109Q-4OD/K60A-VPH or E109Q-4OD/D78N-VPH) was transformed into the *E. coli* strain BL21-Gold(DE3) where the mutant complex was expressed and purified. Purification of each of the recombinant enzymes typically produced 10-15 mg of homogeneous protein per liter of culture. Analysis by SDS-PAGE resulted in two single bands at ~28 kDa. E109Q-4OD/K60A-VPH was analyzed by ESI-MS and the spectrum showed two peaks corresponding to a combined mass of 56323 ± 2 Da (calculated 56326 Da) [ESI-MS of 4OD/VPH wild-type had a combined mass of 56384 ± 2 Da (calculated 56384 Da)]. Gel filtration analysis of E109Q-4OD/K60A-VPH on a Superose-6 column gave a single peak relating to a molecular mass of 316 kDa, indicative of either a pentameric or hexameric structure.

Kinetic Properties of VPH and Mutants with HPD and Me-HPD. VPH and the corresponding mutants were assayed using **2** (Figures 2.5-2.10). The loss of absorbance can correspond to the 1,5-keto-enol tautomerization of **2** to produce **3** or the hydration of **2** to yield **4**. All the enzyme constructs show activity using **2** (generating either **3** or **4**) and the kinetic parameters are shown in Table 2.1. For the native 4OD/VPH complex, the K_m value is 13 ± 2 μM and the k_{cat} value is 240 ± 24 s^{-1}. This results in a k_{cat}/K_m = 2.0 × 10^7 $M^{-1}s^{-1}$. The E109Q-4OD/K60A-VPH mutant shows a 1600-fold decrease in k_{cat}, a 3-fold increase in K_m, and k_{cat}/K_m is reduced 5,000-fold. The E109Q-4OD/D78N-VPH mutant shows a 2300-fold decrease in k_{cat}, a 2-fold increase in K_m, and a 4200-fold decrease in k_{cat}/K_m. The 4OD/L72A-VPH mutant shows a 7-fold decrease in k_{cat}, a comparable K_m value to that of wild-type, and a 10-fold decrease in the k_{cat}/K_m value. The 4OD/S161A-VPH mutant shows a 20-fold decrease in k_{cat}, a similar K_m value to that of wild-type, and a 10-fold decrease in k_{cat}/K_m. The active site mutants of VPH have resulted in comparable K_m values (7-35 μM) to that of wild type (13 μM), whereas the k_{cat} values are 10-2300 fold (0.1-33 s^{-1}, respectively) lower from that of wild-type (240 s^{-1}).

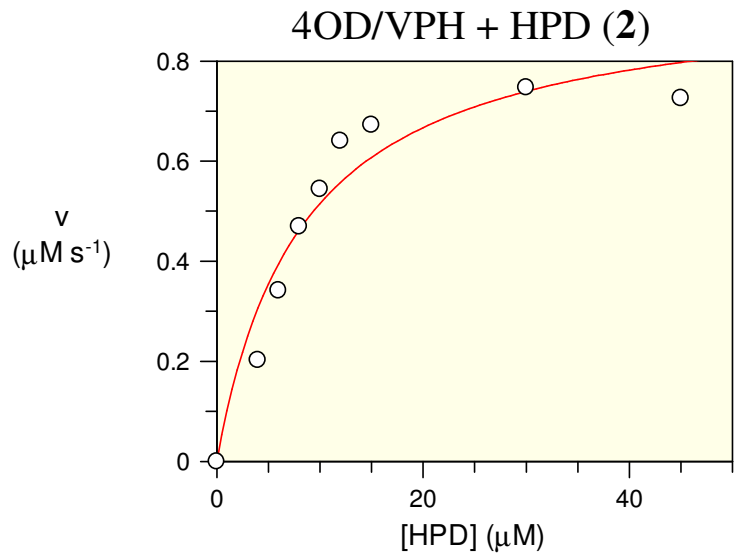

Figure 2.5. Michaelis-Menten plot for the initial rate of formation of **4** versus substrate concentration for the 4OD/VPH-catalyzed reaction converting **2** to **4**.

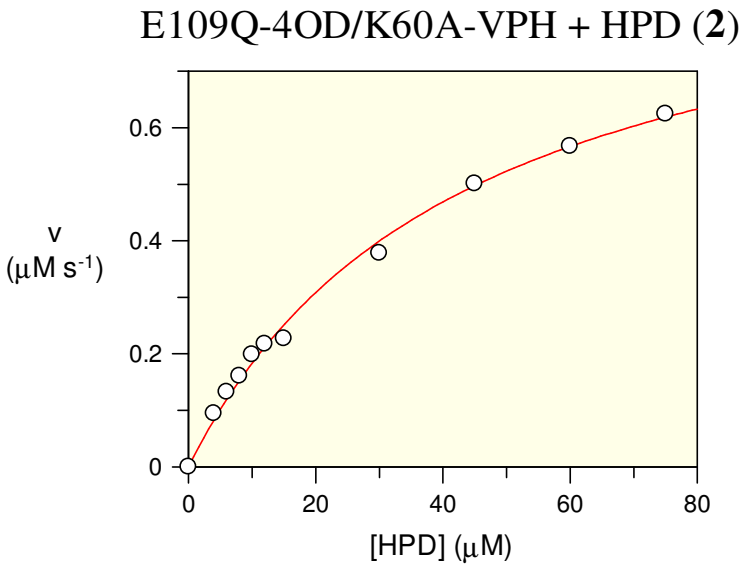

Figure 2.6. Michaelis-Menten plot for the initial rate of formation of **3** versus substrate concentration for the E109Q-4OD/K60A-VPH-catalyzed reaction converting **2** to **3**.

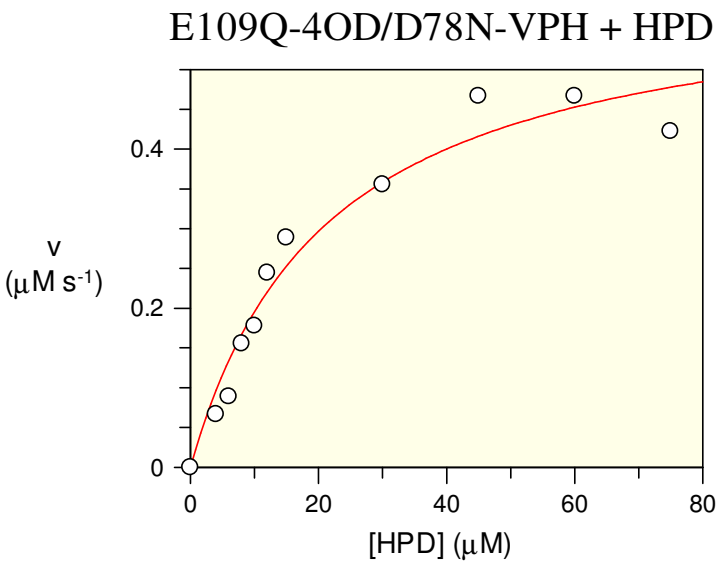

Figure 2.7. Michaelis-Menten plot for the initial rate of formation of **4** versus substrate concentration for the E109Q-4OD/D78N-VPH-catalyzed reaction converting **2** to **4**.

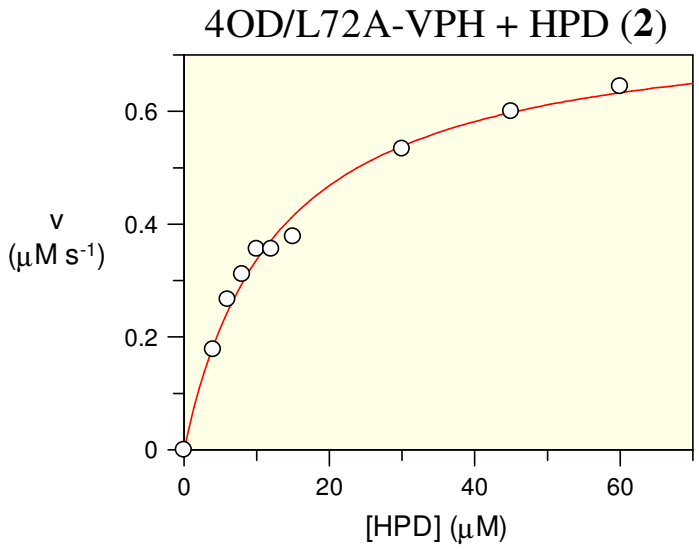

Figure 2.8. Michaelis-Menten plot for the initial rate of formation of **4** versus substrate concentration for the 4OD/L72A-VPH-catalyzed reaction converting **2** to **4**.

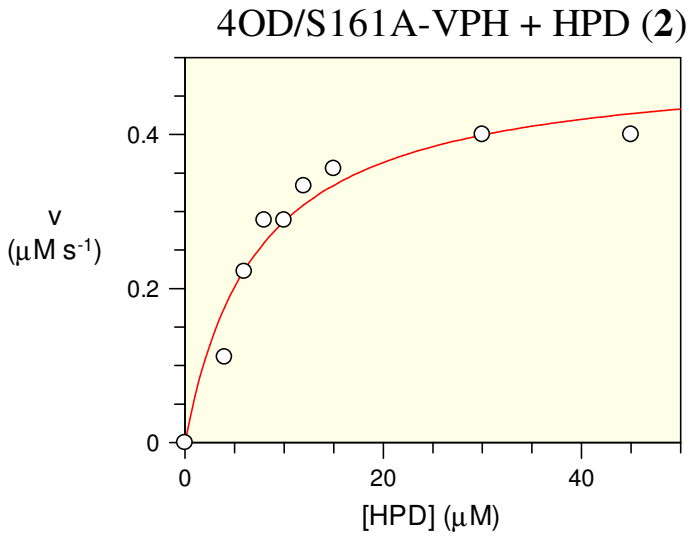

Figure 2.9. Michaelis-Menten plot for the initial rate of formation of **4** versus substrate concentration for the 4OD/S161A-VPH-catalyzed reaction converting **2** to **4**.

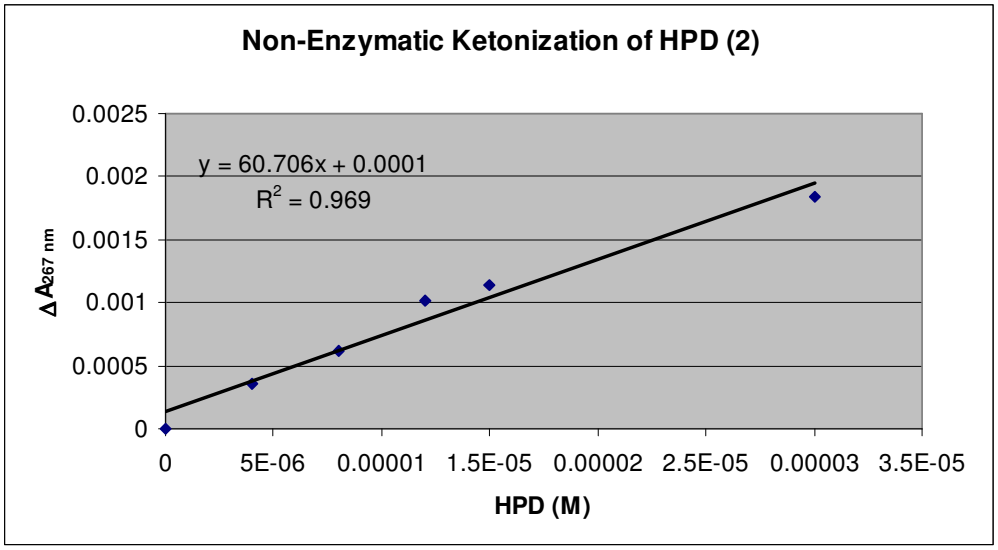

Figure 2.10. Plot of the non-enzymatic change in absorbance at 267 nm versus substrate concentration with a linear fit determination for the 1,3-keto-enol tautomerization of HPD (**2**) to **5**.

Table 2.1: Kinetic Parameters for VPH and corresponding mutants with HPD (2) generating 3 or 4

Enzyme	k_{cat} (s^{-1})	K_m (μM)	k_{cat}/K_m ($M^{-1}s^{-1}$)
4OD/VPH (wt)	240 ± 23	13 ± 3	$2.0\times10^{7} \pm 5.3\times10^{6}$
E109Q-4OD/K60A-VPH	0.14 ± 0.007	35 ± 4	$4.0\times10^{3} \pm 521$
E109Q-4OD/ D78N-VPH	0.094 ± 0.01	20 ± 6	$4.8\times10^{3} \pm 2.0\times10^{3}$
4OD/S161A-VPH	11 ± 0.9	7.0 ± 2	$1.7\times10^{6} \pm 7.0\times10^{5}$
4OD/L72A-VPH	33 ± 1	13 ± 2	$2.4\times10^{6} \pm 6.3\times10^{5}$

The E109Q-4OD/K60A-VPH mutant produced the α,β-unsaturated ketone (**3**) from HPD (**2**). The presence of this compound (**3**) was determined by observing an increase in UV absorbance at 233 nm with a rate of 0.05 s^{-1} (Figure 2.11 and 2.12). Incubating E109Q-4OD/K60A-VPH with 40 μM of **2** for 14 min generated 21 μM of **3**, as estimated by UV spectroscopy. The E109Q-4OD/K60A-VPH catalyzed conversion of **2** to **3** reaches equilibrium after ~27 min, whereas the non-enzymatic conversion takes ~22 hrs to reach equilibrium.

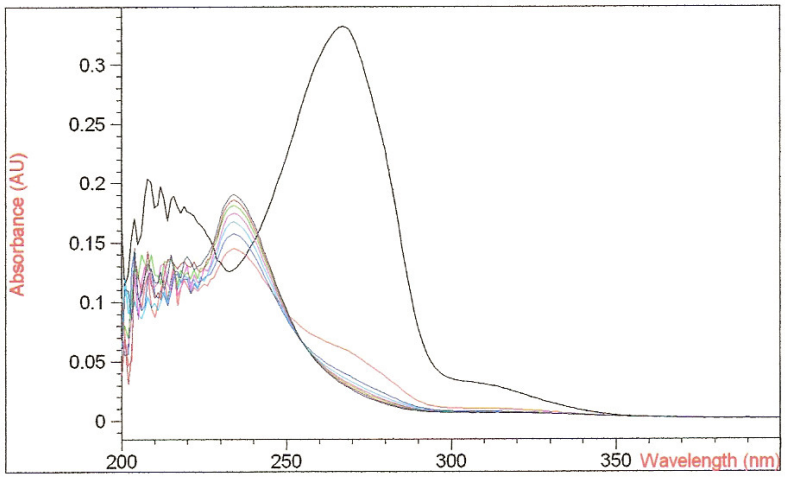

Figure 2.11. UV-Vis spectra of E109Q-4OD/K60A-VPH incubated with **2** following the decrease in absorbance at 267 nm (**2**) and the increase in absorbance at 233 nm corresponding to the production of **3**. Scans taken every 2 min for 16 min.

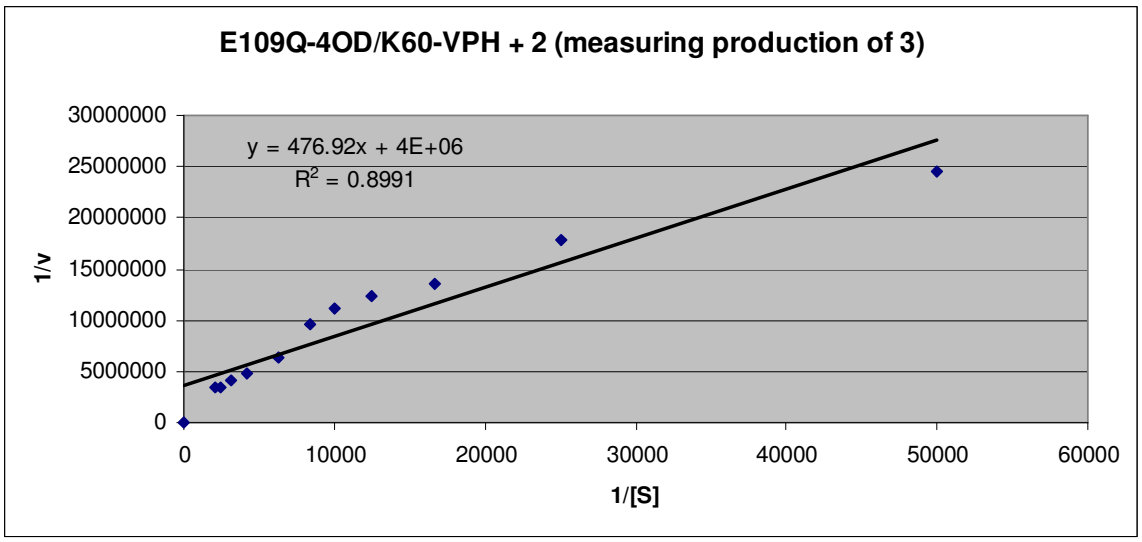

Figure 2.12. Lineweaver-Burk plot of E109Q-4OD/K60A-VPH with **2** measuring the production of **3** at 233 nm.

$$\frac{1}{v} = \frac{K_m}{V_{max}}\frac{1}{[S]} + \frac{1}{V_{max}} \qquad \text{Enzyme - } 5.15 \times 10^{-6}\ \text{M}$$

$$y = 476.9\,x + 4.0 \times 10^{6}$$

$$\frac{1}{V_{max}} = 4.0 \times 10^{6} \qquad V_{max} = 2.5 \times 10^{-7}\ \text{M s}^{-1} \qquad \frac{K_m}{V_{max}} = 476.9 \qquad K_m = 119\ \mu\text{M}$$

$$k_{cat} = \frac{0.25\ \mu\text{M s}^{-1}}{5.15\ \mu\text{M}} = 0.049\ \text{s}^{-1}$$

VPH and the corresponding mutants were also assayed using **6** (Figures 2.13-2.18). The loss of absorbance can correspond to the 1,5-keto-enol tautomerization of **6** to produce **7** or the hydration of **6** to yield **8**. All the enzyme constructs show activity using **6** (generating either **7** or **8**) and the kinetic parameters are shown in Table 2.2. The native

4OD/VPH complex has a K_m value of 6.0 ± 0.7 μM and a k_{cat} value of 64 ± 3 s^{-1}. This results in a $k_{cat}/K_m = 1.1 \times 10^7$ $M^{-1}s^{-1}$. The E109Q-4OD/K60A-VPH mutant shows a 350-fold decrease in k_{cat}, a 5-fold increase in the K_m value, and k_{cat}/K_m is reduced by 2000-fold. The E109Q-4OD/D78N-VPH mutant shows a 1300-fold decrease in k_{cat}, a comparable K_m value to that of wild-type, and a 1500-fold decrease in k_{cat}/K_m. The 4OD/L72A-VPH mutant shows a 32-fold decrease in k_{cat}, a comparable K_m value to that of wild-type, and a 40-fold decrease in the k_{cat}/K_m value. The 4OD/S161A-VPH mutant shows a 20-fold decrease in k_{cat}, a similar K_m value to that of wild-type, and a 30-fold decrease in k_{cat}/K_m. The kinetic characterization of these mutants of VPH show similar K_m values (7-9 μM) to that of wild type (6.0 μM), with the exception of the E109Q-4OD/K60A-VPH mutant which had a K_m value of 34 μM. However, the k_{cat} values are 20-1300 fold (0.05-3 s^{-1}, respectively) lower than that of wild-type (64 s^{-1}).

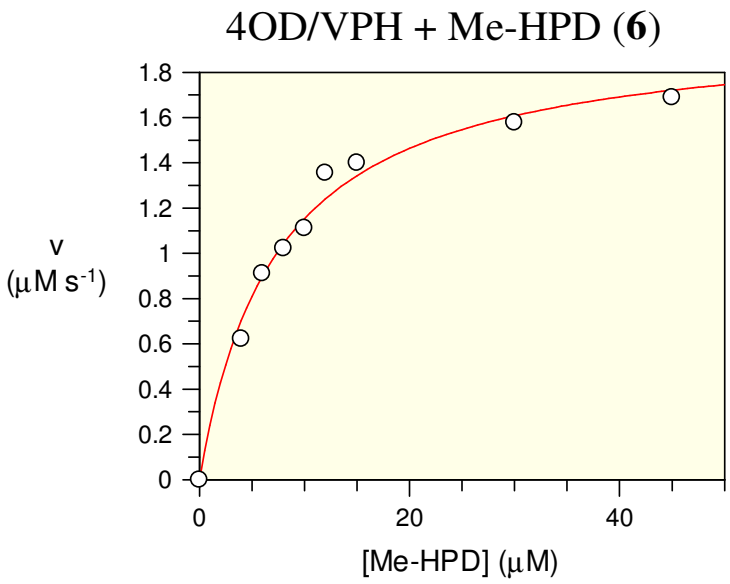

Figure 2.13. Michaelis-Menten plot for the initial rate of formation of **8** versus substrate concentration for the 4OD/VPH-catalyzed reaction converting **6** to **8**.

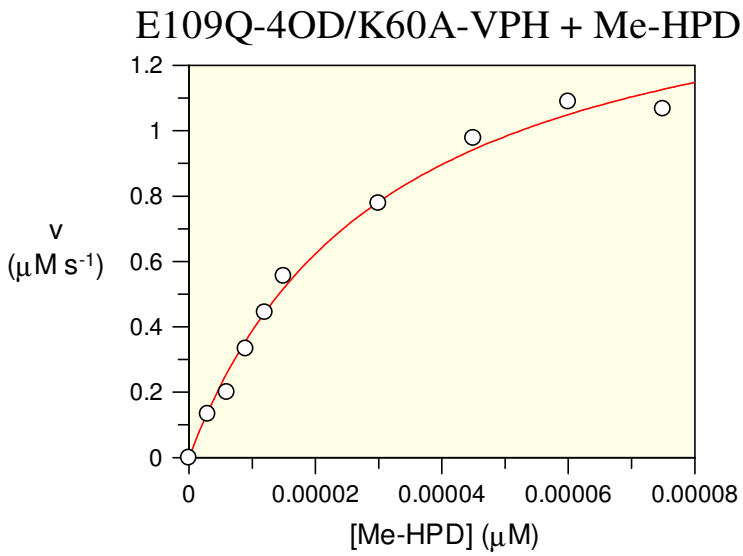

Figure 2.14. Michaelis-Menten plot for the initial rate of formation of **7** versus substrate concentration for the E109Q-4OD/K60A-VPH-catalyzed reaction converting **6** to **7**.

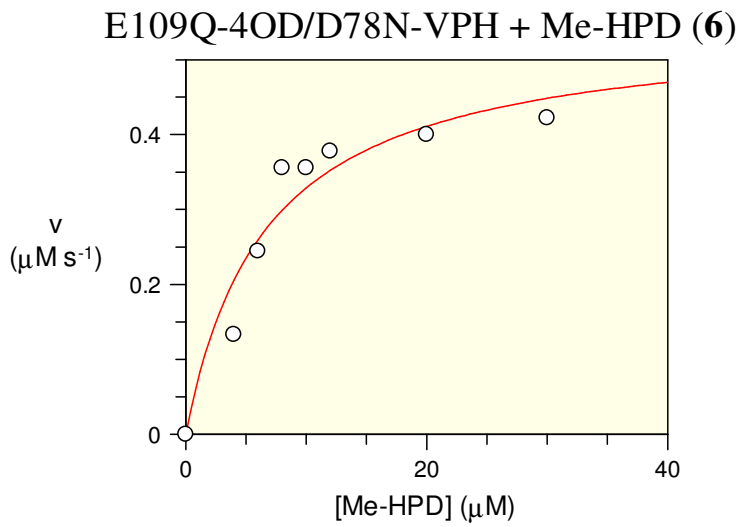

Figure 2.15. Michaelis-Menten plot for the initial rate of formation of **8** versus substrate concentration for the E109Q-4OD/D78N-VPH-catalyzed reaction converting **6** to **8**.

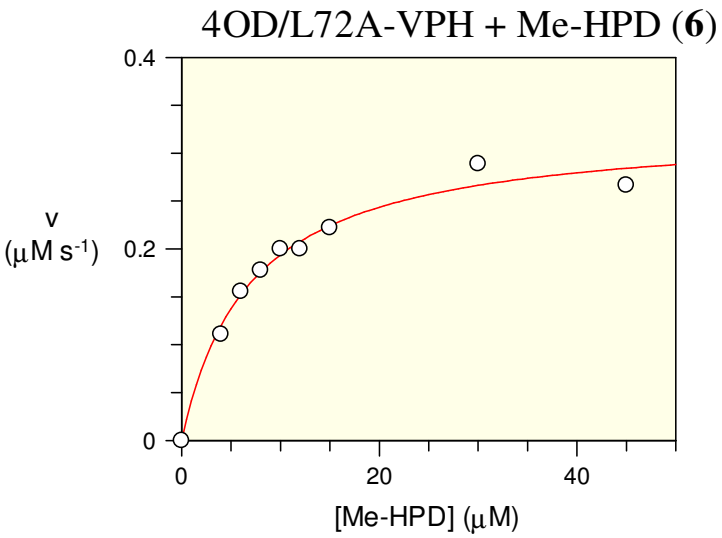

Figure 2.16. Michaelis-Menten plot for the initial rate of formation of **8** versus substrate concentration for the 4OD/L72A-VPH-catalyzed reaction converting **6** to **8**.

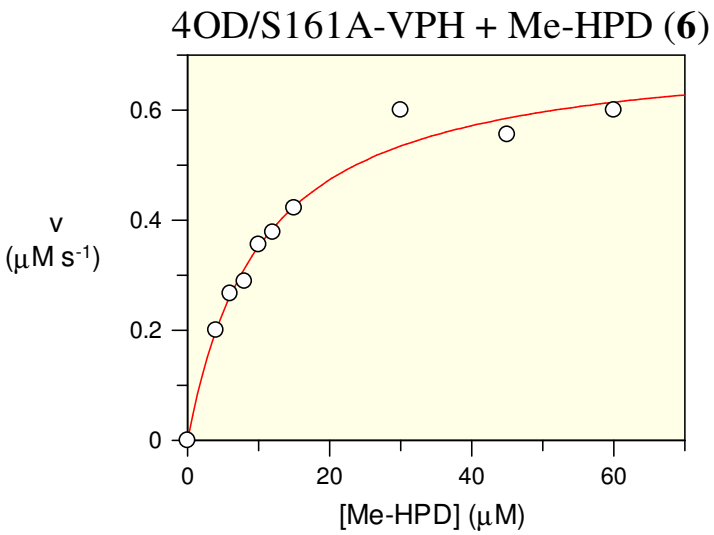

Figure 2.17. Michaelis-Menten plot for the initial rate of formation of **8** versus substrate concentration for the 4OD/S161A-VPH-catalyzed reaction converting **6** to **8**.

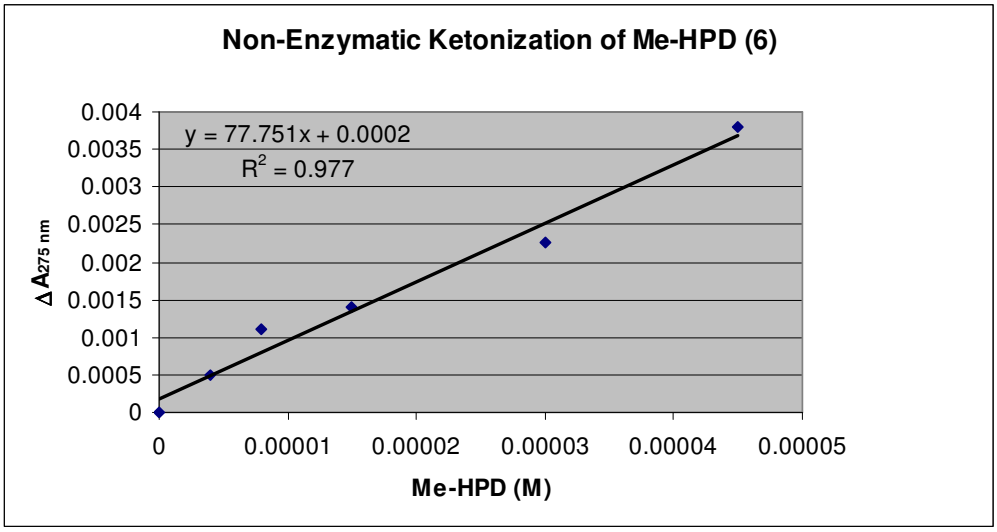

Figure 2.18. Plot of the non-enzymatic change in absorbance at 275 nm versus substrate concentration with a linear fit determination for the 1,3-keto-enol tautomerization of Me-HPD (**6**) to **9**.

Table 2.2: Kinetic Parameters for VPH and corresponding mutants with Me-HPD (6) generating 7 or 8

Enzyme	k_{cat} (s^{-1})	K_m (μM)	k_{cat}/K_m ($M^{-1}s^{-1}$)
4OD/VPH (wt)	64 ± 3	6.0 ± 0.7	$1.1\times10^{7} \pm 1.5\times10^{6}$
E109Q-4OD/K60A-VPH	0.18 ± 0.01	34 ± 6	$5.3\times10^{3} \pm 1.3\times10^{3}$
E109Q-4OD/ D78N-VPH	0.048 ± 0.006	7.0 ± 3	$6.9\times10^{3} \pm 5.0\times10^{3}$
4OD/S161A-VPH	3.0 ± 0.2	9.0 ± 1	$3.3\times10^{5} \pm 3.0\times10^{4}$
4OD/L72A-VPH	2.0 ± 0.1	9.0 ± 1	$2.8\times10^{5} \pm 2.7\times10^{4}$

The E109Q-4OD/K60A-VPH mutant produced the α,β-unsaturated ketone (**7**) from Me-HPD (**6**). The presence of this compound (**7**) was determined by observing an increase in UV absorbance at 236 nm. Incubating E109Q-4OD/K60A-VPH with 60 μM of **6** for 32 min generated 15 μM of (**7**), as estimated by UV spectroscopy. The rate was too slow to determine accurately, but was faster than the non-enzymatic rate (over 30 h to reach equilibrium).

Kinetic Properties of MhpD and Mutants with HPD and Me-HPD. The kinetic parameters for MhpD and the corresponding mutants were assayed using **2** (Figures 2.19-2.23 and 2.10). The loss of absorbance can correspond to the 1,5-keto-enol tautomerization of **2** to **3** or the hydration of **2** to produce **4**. All the enzyme constructs show activity using **2** (generating either **3** or **4**) and the results are listed in Table 2.3. Wild-type MhpD has a K_m value of 9.0 ± 1 μM and a k_{cat} value of 250 ± 17 s^{-1}. This results in a $k_{cat}/K_m = 2.8 \times 10^{7}$ $M^{-1}s^{-1}$. The K60A-MhpD mutant shows an 890-fold decrease in k_{cat}, a 4-fold increase in K_m, and a 3700-fold decrease in k_{cat}/K_m. The D78N-MhpD mutant shows a 1000-fold decrease in k_{cat}, a comparable K_m value to that of wild-

type, and a 1000-fold reduction in k_{cat}/K_m. The L72A-MhpD mutant has the smallest effect on the kinetic parameters with all values being comparable to those for wild-type. The S160A-MhpD mutant shows a 10-fold decrease in k_{cat}, a comparable K_m value to that of wild-type, and a k_{cat}/K_m value that was reduced by 10-fold. The kinetic parameters for the mutants of MhpD show K_m values (8-12 μM) close to that of wild-type (9.0 μM), with the exception of the K60A-MhpD mutant which had a K_m value of 37 μM. The k_{cat} values of the mutants show up to a 1000-fold (0.2 s^{-1}) decrease from that of wild-type (250 s^{-1}).

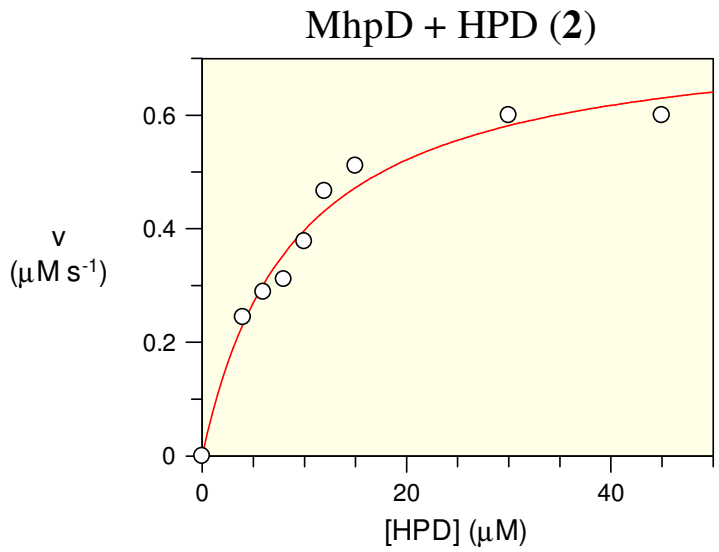

Figure 2.19. Michaelis-Menten plot for the initial rate of formation of **4** versus substrate concentration for the MhpD-catalyzed reaction converting **2** to **4**.

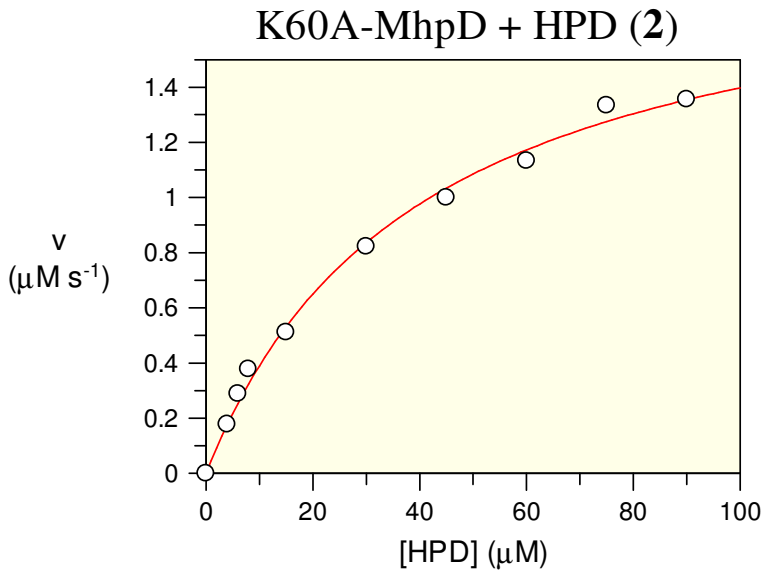

Figure 2.20. Michaelis-Menten plot for the initial rate of formation of **3** versus substrate concentration for the K60A-MhpD-catalyzed reaction converting **2** to **3**.

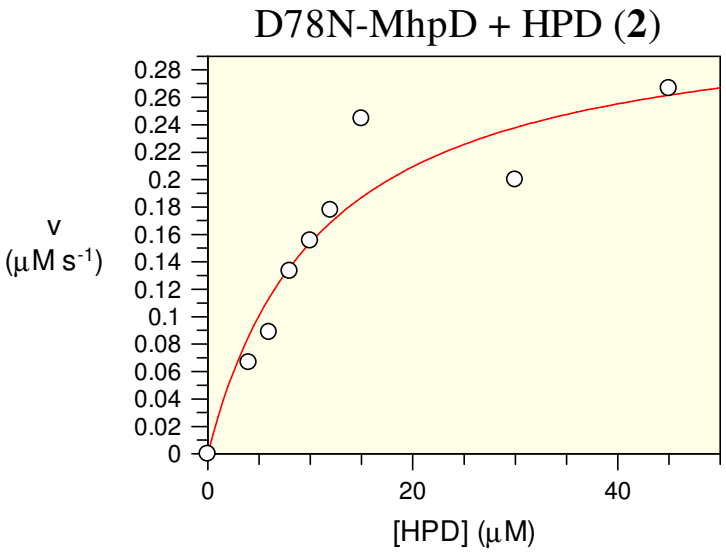

Figure 2.21. Michaelis-Menten plot for the initial rate of formation of **4** versus substrate concentration for the D78N-MhpD-catalyzed reaction converting **2** to **4**.

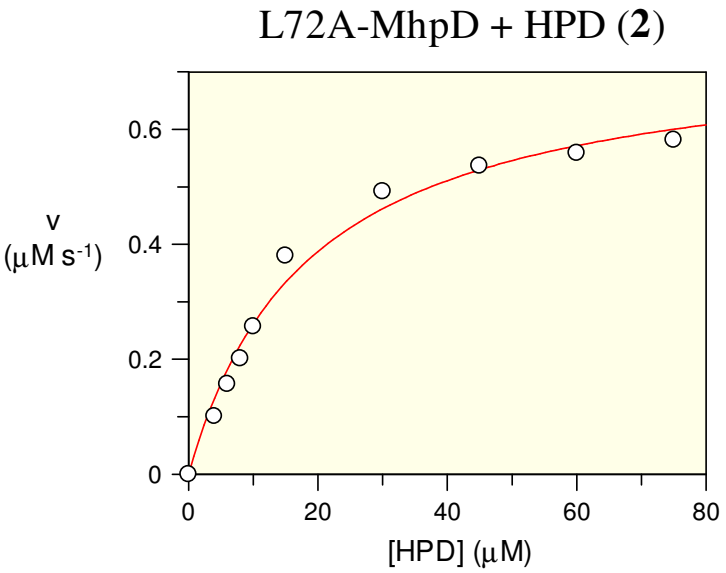

Figure 2.22. Michaelis-Menten plot for the initial rate of formation of **4** versus substrate concentration for the L72A-MhpD-catalyzed reaction converting **2** to **4**.

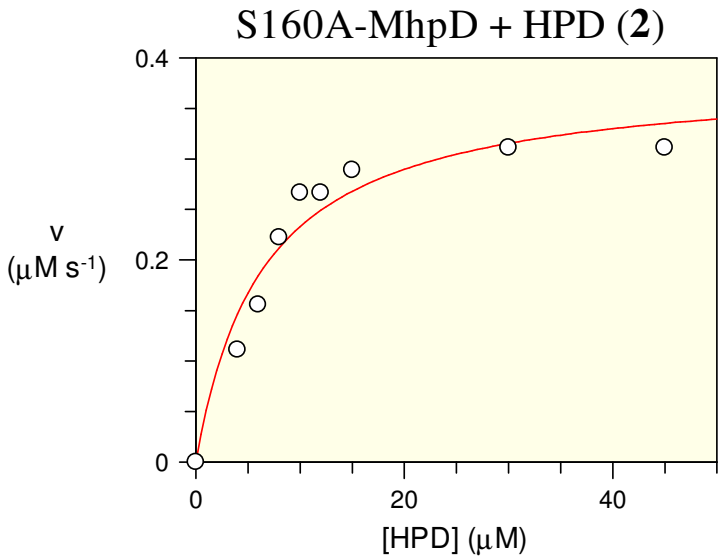

Figure 2.23. Michaelis-Menten plot for the initial rate of formation of **4** versus substrate concentration for the S160A-MhpD-catalyzed reaction converting **2** to **4**.

Table 2.3: Kinetic Parameters for MhpD and corresponding mutants with HPD (2) generating 3 or 4

Enzyme	k_{cat} (s^{-1})	K_m (μM)	k_{cat}/K_m ($M^{-1}s^{-1}$)
MhpD (wt)	250 ± 17	9.0 ± 1	$2.8\times10^{7} \pm 2.4\times10^{6}$
K60A-MhpD	0.28 ± 0.03	37 ± 7	$7.6\times10^{3} \pm 1.3\times10^{3}$
D78N-MhpD	0.24 ± 0.03	8.0 ± 3	$3.1\times10^{4} \pm 1.7\times10^{4}$
S160A-MhpD	23 ± 2	11 ± 2	$2.7\times10^{6} \pm 4.1\times10^{5}$
L72A-MhpD	230 ± 19	12 ± 2	$1.9\times10^{7} \pm 3.3\times10^{6}$

The K60A-MhpD mutant produced the α,β-unsaturated ketone (**3**) from HPD (**2**) (Figure 2.24 and 2.25). The presence of this intermediate was determined by observing an increase in UV absorbance at 233 nm with a rate of 0.36 s^{-1}. Incubating K60A-MhpD

with 40 µM of **2** for 9 min generated 32 µM of **3**, as determined by UV spectroscopy. The K60A-MhpD catalyzed reaction reaches equilibrium after ~10 min, whereas the non-enzymatic reaction takes ~22 hrs to reach equilibrium.

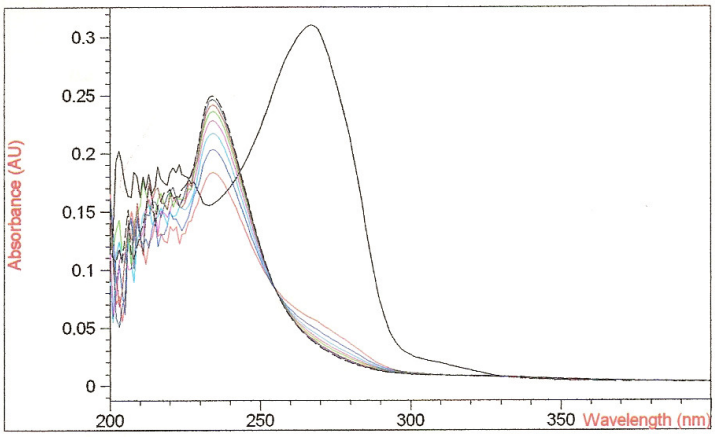

Figure 2.24. UV-Vis spectra of K60A-MhpD incubated with **2** following the decrease in absorbance at 267 nm (**2**) and the increase in absorbance at 233 nm corresponding to the production of **3**. Scan taken every 60 sec for 10 min.

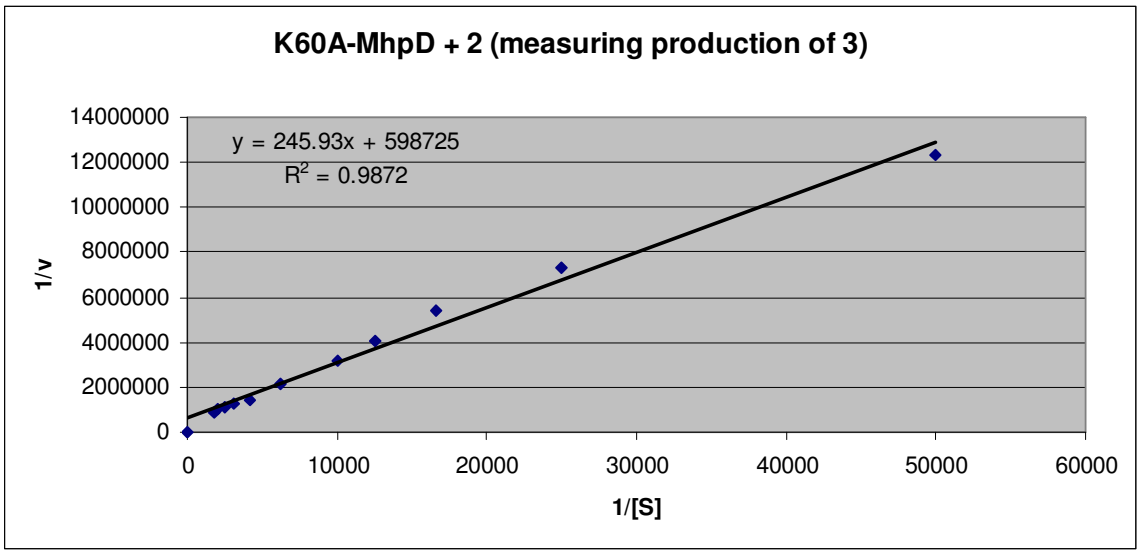

Figure 2.25. Lineweaver-Burk plot of K60A-MhpD with **2** measuring the production of **3** at 233 nm.

$$\frac{1}{v} = \frac{K_m}{V_{max}}\frac{1}{[S]} + \frac{1}{V_{max}} \qquad \text{Enzyme - } 4.66 \times 10^{-6}\ \text{M}$$

$$y = 245.9\,x + 6.0 \times 10^{5}$$

$$\frac{1}{V_{max}} = 6.0 \times 10^{5} \qquad V_{max} = 1.67 \times 10^{-6}\ \text{M s}^{-1} \qquad \frac{K_m}{V_{max}} = 245.9 \qquad K_m = 410\ \mu\text{M}$$

$$k_{cat} = \frac{1.67\ \mu\text{M s}^{-1}}{4.66\ \mu\text{M}} = 0.36\ \text{s}^{-1}$$

MhpD and the corresponding mutants were also assayed using **6** (Figures 2.26-2.30 and 2.18). The loss of absorbance can correspond to the 1,5-keto-enol tautomerization of **6** to **7** or the hydration of **6** to **8**. All the enzyme constructs show

activity using **6** (generating either **7** or **8**) and the kinetic parameters are shown in Table 2.4. Native MhpD has a K_m value of 6.0 ± 1 μM and a k_{cat} value of 54 ± 3 s^{-1} resulting in a k_{cat}/K_m = 9.0 × 10^6 $M^{-1}s^{-1}$. K60A-MhpD shows a 740-fold decrease in k_{cat}, a 2-fold increase in the K_m value, and k_{cat}/K_m is reduced by 1800-fold. The D78N-MhpD mutant shows an 80-fold decrease in k_{cat}, a comparable K_m value to that of wild-type, and a 50-fold decrease in k_{cat}/K_m. The L72A-MhpD mutant gave similar k_{cat} and K_m values to that of the wild-type enzyme. The S160A-MhpD mutant shows a 3-fold decrease in k_{cat}, a 2-fold increase in the K_m value, and a 8-fold decrease in k_{cat}/K_m.

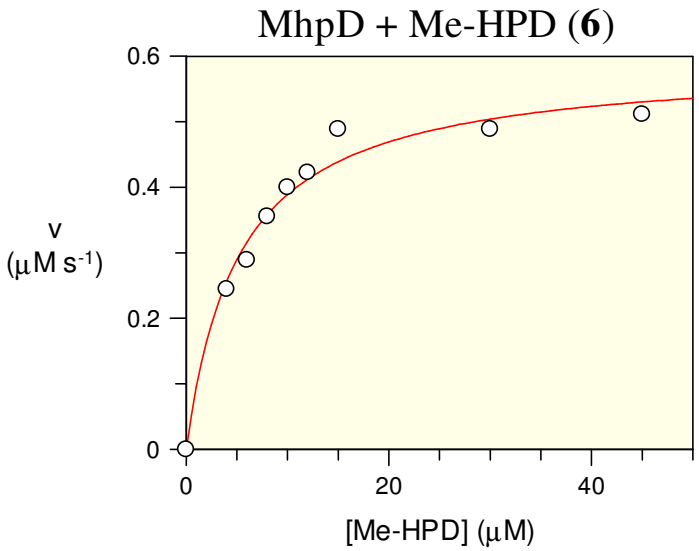

Figure 2.26. Michaelis-Menten plot for the initial rate of formation of **8** versus substrate concentration for the MhpD-catalyzed reaction converting **6** to **8**.

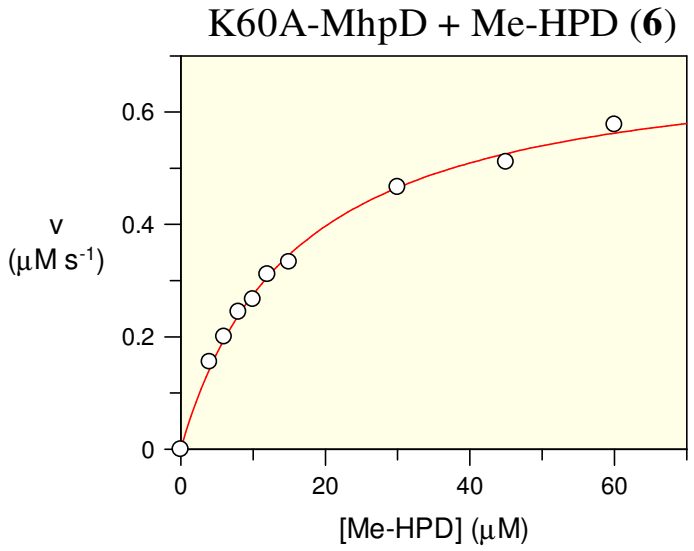

Figure 2.27. Michaelis-Menten plot for the initial rate of formation of **7** versus substrate concentration for the K60A-MhpD-catalyzed reaction converting **6** to **7**.

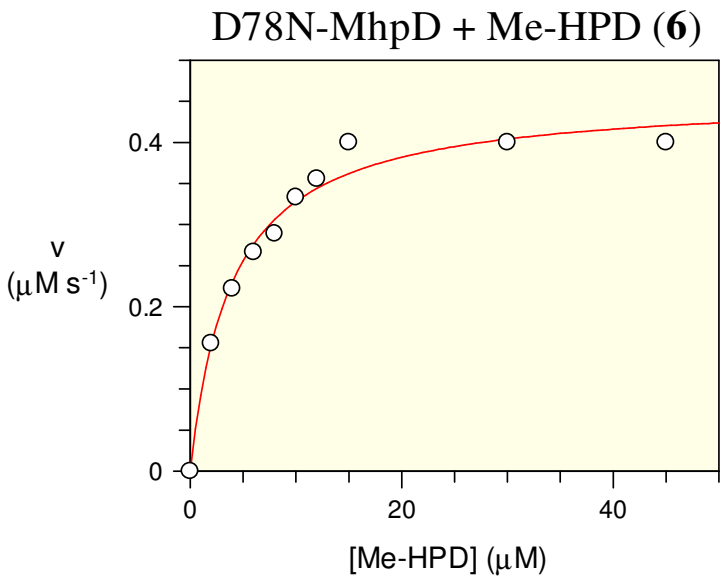

Figure 2.28. Michaelis-Menten plot for the initial rate of formation of **8** versus substrate concentration for the D78N-MhpD-catalyzed reaction converting **6** to **8**.

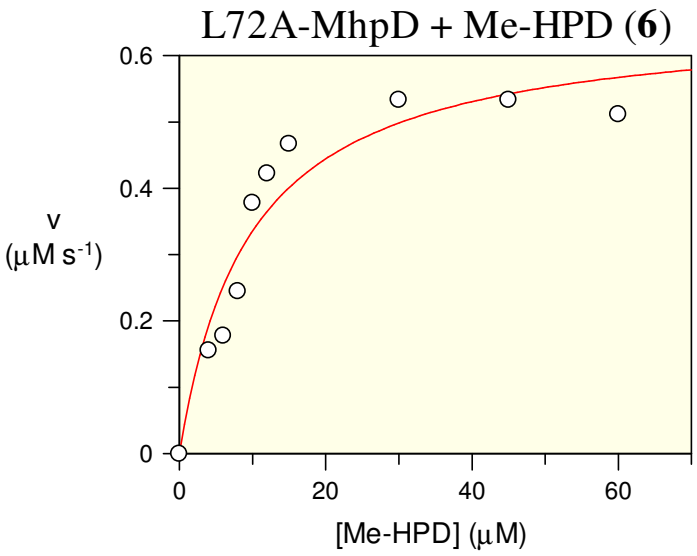

Figure 2.29. Michaelis-Menten plot for the initial rate of formation of **8** versus substrate concentration for the L72A-MhpD-catalyzed reaction converting **6** to **8**.

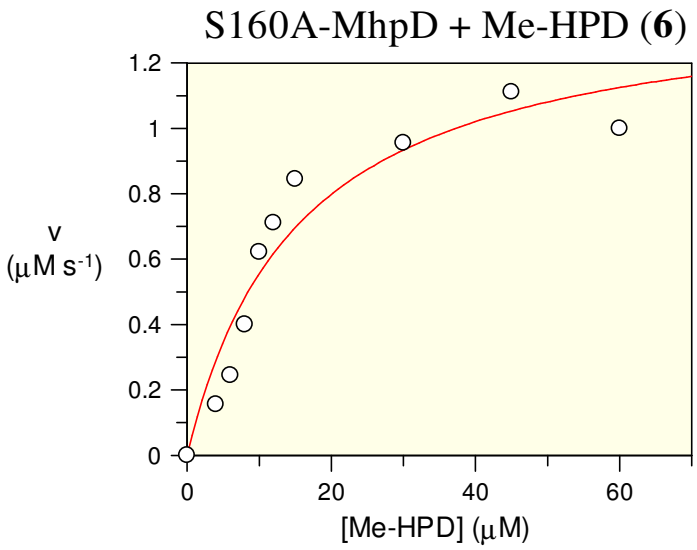

Figure 2.30. Michaelis-Menten plot for the initial rate of formation of **8** versus substrate concentration for the S160A-MhpD-catalyzed reaction converting **6** to **8**.

Table 2.4: Kinetic Parameters for MhpD and corresponding mutants with Me-HPD (6) generating 7 or 8

Enzyme	k_{cat} (s^{-1})	K_m (μM)	k_{cat}/K_m ($M^{-1}s^{-1}$)
MhpD (wt)	54 ± 3	6.0 ± 1	$9.0\times10^{6} \pm 2.1\times10^{6}$
K60A-MhpD	0.073 ± 0.002	15 ± 4	$4.9\times10^{3} \pm 2.5\times10^{3}$
D78N-MhpD	0.69 ± 0.03	4.0 ± 0.6	$1.8\times10^{5} \pm 3.7\times10^{4}$
S160A-MhpD	16 ± 2	13 ± 4	$1.1\times10^{6} \pm 5.0\times10^{5}$
L72A-MhpD	40 ± 4	9.0 ± 2	$4.3\times10^{6} \pm 1.1\times10^{6}$

The characterization of the active site mutants of MhpD shows mixed effects on the kinetic parameters of wild-type MhpD. The D78N mutant has a similar K_m value to that of wild-type, while the K_m values of the K60A-MhpD and S160A-MhpD mutants show a slight increase. However, the k_{cat} values are 3-770-fold (0.07-16 s^{-1}, respectively)

lower than that of wild-type (54 s^{-1}). The L72A-MhpD mutant had the least effect on the kinetic parameters with values comparable to those of the wild-type enzyme.

The K60A-MhpD mutant produced the α,β-unsaturated ketone (**7**) from Me-HPD (**6**). The presence of this intermediate was determined by observing an increase in UV absorbance at 236 nm. Incubating K60A-MhpD with 30 μM of **6** for 30 min generated 12 μM of (**7**), as determined by UV spectroscopy. The rate was too slow to determine accurately, but was faster than the non-enzymatic rate (over 30 h to reach equilibrium).

Summary of Kinetic Studies. Both wild-type VPH and MhpD catalyze a hydration reaction using **2** and **6** with comparable kinetic parameters. The 4OD/L72A-VPH mutant showed a 7-fold decrease in k_{cat} for the conversion of **2** to **4** and a 32-fold decrease in k_{cat} for the conversion of **6** to **8** but had comparable K_m values to that of the wild-type protein. The L72A-MhpD mutant had almost no effect on the kinetic parameters for conversion of **2** to **4** and **6** to **8**. The E109Q-4OD/D78N-VPH mutant and D78N-MhpD showed large decreases (up to 2300-fold) in k_{cat} for catalyzing **2** to **4** and **6** to **8**, but had only a slight increase (up to 2-fold) in K_m. Similar results were found for the E109Q-4OD/K60A-VPH and K60A-MhpD mutants showing large decreases in k_{cat} values (up to 1600-fold) for catalyzing **2** to **3** and **6** to **7**, and increased K_m values (up to 5-fold). The kinetic parameters for 4OD/S161A-VPH- and S160A-MhpD-catalyzed conversion of **2** to **4** and **6** to **8** showed moderate decreases (up to 20-fold) in k_{cat}, but had comparable K_m values to that of the wild-type proteins.

*Inhibition Studies of VPH with **10**, **11** and MhpD with (R)- and (S)-**12**.* VPH and MhpD were examined with three potential inhibitors. The first compound examined was

2-oxo-3-pentynoate (2-OP, **10**) (Figure 2.4), which could be a potent irreversible inhibitor (Scheme 5) (10) or a substrate (Scheme 6) (11). 4-Oxalocrotonate tautomerase (4-OT, the enzyme prior to 4-OD in the catechol meta-fission pathway) is irreversibly inhibited by **13** (an adduct of **10**) through the mechanism shown in Scheme 5, resulting in the formation of a covalent bond to the active site Pro-1 (10). Alternatively, VPH could add H_2O to **10** to form acetopyruvate (**14**) as shown in Scheme 6.

Scheme 5

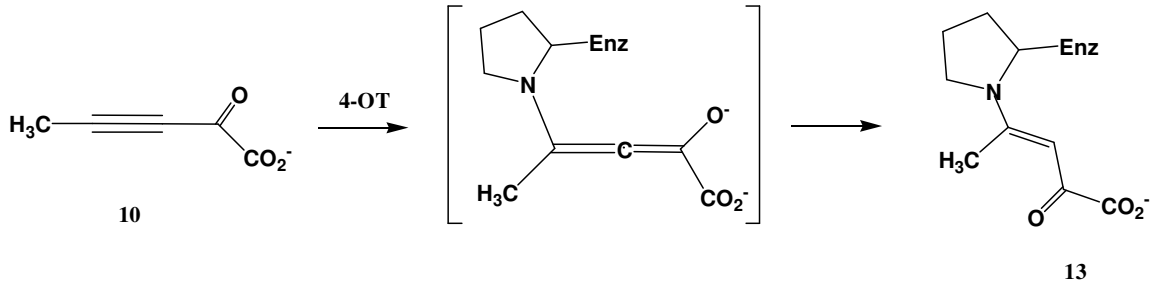

10 **13**

Scheme 6

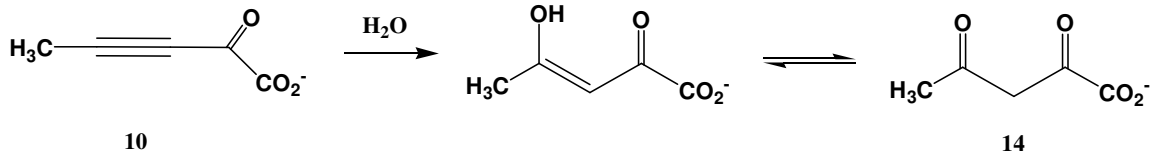

10 **14**

In this experiment 4OD/VPH complex was incubated with a 1970-fold excess of **10**. VPH activity was determined hourly and then after an overnight incubation. VPH was not inhibited by **10** and retained full activity. There was also no evidence for VPH processing **10** through a hydration reaction to generate acetopyruvate (**14**). A second

experiment with VPH and **10** was conducted using 4OD/VPH complex incubated with an excess of **10** for a longer time period (36 hrs). No inhibition of VPH was detected and NMR analysis showed no evidence for hydration of **10** to **14**.

A second experiment examined 3-bromopropiolic acid (**11**, Scheme 7) (11) as a mechanism-based inhibitor of VPH. 3-Bromopropiolic acid (**11**) inactivates *trans*-3-chloroacrylic acid dehalogenase (CaaD, a member of the 4-OT superfamily) through a hydration reaction to generate a potent acylating agent (**15**, Scheme 7) which in turn forms a covalent bond to the active site Pro-1 (Scheme 7) (11).

Scheme 7

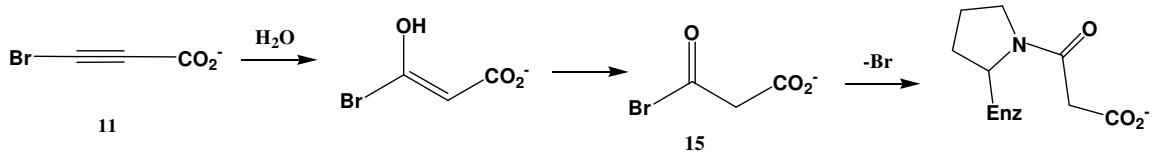

11 15

The 4OD/VPH complex was incubated with a 560-fold excess of **11**. VPH activity was determined hourly and then after an overnight incubation. VPH was not inhibited by **11** and retained full activity.

Two enantiomeric inhibitors, (*R*)- and (*S*)-oxirane-2-carboxylate [(*R*)-**12** and (*S*)-**12**], were also examined as potential affinity labels (Figure 2.4) (12). Like **11**, oxirane-2-carboxylate covalently attaches to the Pro-1 residue in the active site of *cis*-CaaD. In this experiment, only MhpD was incubated with an 8260-fold excess of (*R*)-**12** and (*S*)-**12** as two separate reactions. MhpD activity was determined hourly and then after an overnight incubation. MhpD was not inhibited by (*R*)-**12** or (*S*)-**12** and retained full activity.

DISCUSSION

The two homologous enzymes, VPH and MhpD, catalyze an interesting 1,5-keto-enol tautomerization/hydration reaction with a metal ion cofactor. At first glance, it is not obvious how water adds to C-4 of **2**. However, ketonization of **2** to **3** generates a Michael acceptor. The proximity of the carbonyl group of **3** suggests that VPH and MhpD might utilize this carbonyl group during catalysis. One possible mechanism for the hydration reaction involves the formation of a Schiff base. An example is the dehydration/isomerization reaction catalyzed by arabonate dehydratase in which a Schiff base mechanism is proposed to account for the elimination of water from 2-keto-3-deoxy-L-arabonate (**16**) to generate α-ketoglutarate semialdehyde (**17**, Scheme 8) (16). The dehydratase catalyzes the loss of water α,β to the carbonyl group followed by an allylic isomerization to yield a β,γ-unsaturated α–keto acid which ketonizes to **17**. Based on

Scheme 8

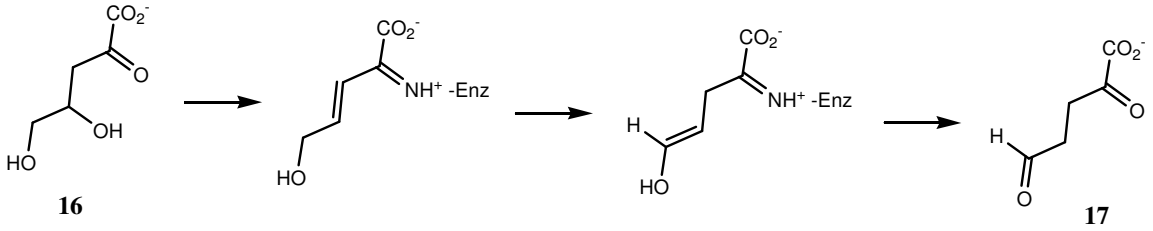

16 **17**

previous work, the possibility of a Schiff base mechanism has been ruled out for the VPH reaction because there is no loss of activity upon incubation with **2** and $NaBH_4$, and no incorporation of ^{18}O in **4** (at C-2) when the reaction is followed in $H_2{}^{18}O$ (Scheme 1) (5).

A second mechanism for the VPH- and MhpD-catalyzed hydration reaction involves the Michael addition of water to the α,β–unsaturated ketone (i.e., **3**) (17, 18). One example of an enzyme that catalyzes a similar reaction is β-hydroxydecanoylthioester dehydrase. This enzyme is a bifunctional enzyme that mediates the interconversion of acyl carrier protein (ACP) thio esters (19). Dehydrase catalyzes two reversible reactions: the dehydration of (*R*)-3-hydroxydecanoyl-ACP (**18**) to (*E*)-2-decenoyl-ACP (**19**) and the isomerization of (*E*)-2-decenoyl-ACP to (*Z*)-3-decenoyl-ACP (**20**) (Scheme 9) (20). The reversible hydration reaction in converting **19** to **18** is very similar to the hydration reaction catalyzed by VPH and MhpD. These two enzymes (VPH and MhpD) may utilize a similar mechanism in which a water molecule attacks the C-4 position of **3** generating a metal ion-stabilized enolate intermediate. Ketonization of the enolate intermediate would yield **4** (Scheme 10).

Scheme 9

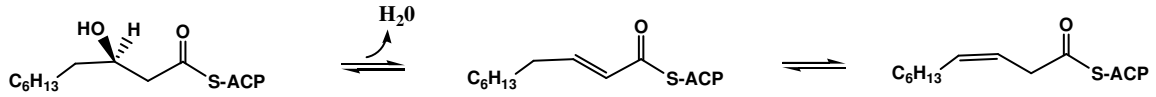

18 **19** **20**

Scheme 10

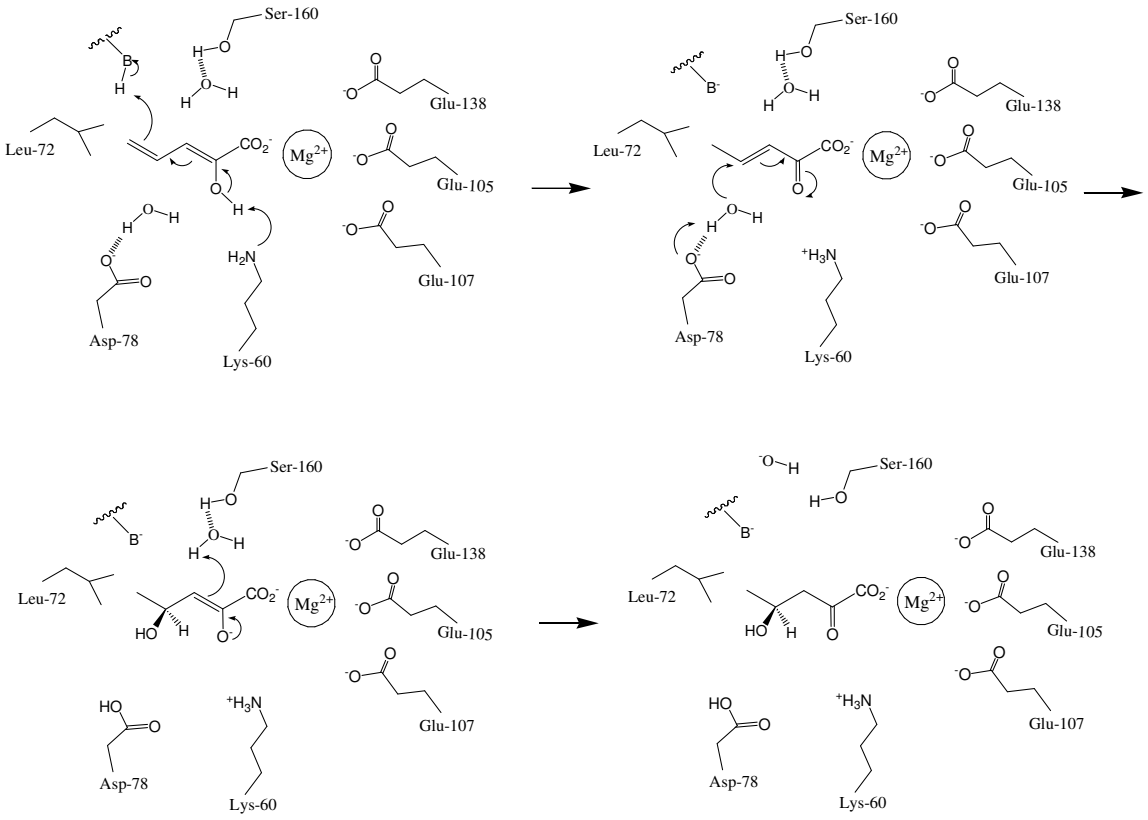

While some of the mechanistic details of the VPH- and MhpD-catalyzed reactions have been elucidated (3-5) the identity of the active-site residues that participate in the chemistry are not known. The availability of a crystal structure for MhpD (Figure 2.1) coupled with sequence analysis (Figure 2.31) helped identify potential active site residues.

From the crystal structure of MhpD, the location of the EXE motif (E105 and E107) and the neighboring Glu-138 residue were identified as the probable metal binding

```
VPH-XylJ -----MDKTLINELGDELYQAMVQRETVTPLTSRGFDISVEDAYHISLRMLERRLAAGE 54
MhpD     ------MTKHTLEQLAADLRRAAEQGEAIAPLRDLIGIDNAEAAYAIQHINVQHDVAQGR 54
4OD-Xyl --MNRTLNREQVLALAEHIENAELQAHDIHKVTNDYPEMTFADAYTIQWEIRRRKEERGN 58
TodJ     MSELDTARTGAVRKAADLLYEATRSGVAVVPVRNLIGETDLEAAYAVQEVNTQRALVAGR 60
BphE     MRKLDPVSTSAASEAADLLYEAARTGVAVAPVRNLIGEKDLEAAYAVQEINTQRALAAGR 60
AmnF     ------MTPQQREEAAQSLYQAMQSGKPIAPLRDTFPDMNVDDAYAIQSINTQRRISLGR 54
DmpE     ------MDKILINELGDELYQAMVNREAVSPLTERGLDISVDDAYHISLRMLERRLAAGE 54
NahL     ------MDKTLIERLGDELYQALVKREVLAPLTERHPDITIADAYRIQQRMNARRLEAGE 54
AtdE     ------MEQAKIQAFADELYEALVNREAVPPLTSRADDITIEDAYHISLRMLERRQQAGA 54
TdnG     ----MTMTPALIEQLGDELYQALTQRQTLEPLTNLHADITIEDAYAIQQKMLARRLAAGE 56
CdoH     ----MAMNSQQIEQLGDELYQALAGCQVVEPLTTRHPDITIADAYAIQQRMLARRLDAGE 56
BphX1    -----MLRDATRDELAADLAQAERSRDPIGQLTAAHPEIDVVDAYEIQLINIRQRVAEGA 55
TesE     -----MSDKQFIETQGQRLYEALRSARTLAPLTDNHPEMTVEDAYHISLHMLRLREASGE 55
HpaH     -----MLSEAIIQQAAQRLNEAEKTGTQISQFSLAYPEITIEDAYEIQKAWVAMKIAEGR 55
BphE2    -----MLDEQTINELAAELYRAEAERVQIEQFSQRFPGMTIDDGYQVSRAWEALKRKDGR 55
                         .  : .*      :  .           .* :.          *

VPH-     RVIGKKIGVTSKAVQNMLGVHQPDFGYLTDAMVYNSGEAMPISEK-LIQPRAEGEIAFIL 113
MhpD     RVVGRKVGLTHPKVQQQLGVDQPDFGTLFADMCYGDNEIIPFSR--VLQPRIEAEIALVL 112
4OD-     KIVGLKMGLTSWAKMAQMGVETPIYGFLADYFSVPDGGVVDCSK--LIHPKIEAEIAVVT 116
TodJ     RLVGRKIGLTSVAVQKQLGVEQPDYGMLFADMARTEGEEIALDD--VLQPKVEAEIAFVL 118
BphE     RLLGRKIGLTSLAVQKQLGVGQPDYGMLFADMARTEGEEISLKD--VLQPKVEAEIAFVF 118
AmnF     RVVGRKIGLTSVVVQQQLGVDEPDFGALFDDMSFGDAETIPLSI--LHQPKVEAEIGFVL 112
DmpE     KVIGKKIGVTSKAVQNMLNVHQPDFGYLTDRMVFNSGEAMPISQL-LMQPKAEGEVAFIL 113
NahL     RVVGKKIGVTSKAVMNMLGVYQPDFGILTDGMLYNEGEAIAADT--LIQPKAEGEIAFVL 112
AtdE     RIIGKKIGVTSKAVMNMLNVHQPDFGYLTDDMVFNSGEEVNISDR-LIAPRAEGEIAFIL 113
TdnG     KVVGKKIGVTSQAVMNMLGVFQPDFGWLTDGMVFNEGEAVPANT--LIQPKAEGEIAFVL 114
CdoH     RVVGKKVGVTSRAVMDMLGVFQPDFGWLTDGMVFNEGQAVAAST--LIQPKAEGEIAFVL 114
BphX1    RVVGHKVGLSSPIMQQMMGVDEPDYGHLLDDMQVFEDTPVQASR--YLSPRVEVEVGFIL 113
TesE     RVIGKKIGVTSKPVQDMLNVHQPDFGFLTDSMEYEDGAAVSLKAAGLIQPRAEGEIAFML 115
HpaH     VLKGHKIGLTSKAMQNSSQINEPDYGALLDDMFFEENSEIPFDR--FIVPRVEVELAFIL 113
BphE2    TVLGHKIGLTSRAMQQAAGIREPDYGTLLDDMFFAEGDDVPFRR--FIAPKVEVELAFVL 113
          : * *:*::          :  * :* *   :   .   :          *: * *:..:

VPH      KKDLMGPGVTNADVLAATECVIPCFEVVDSRIQ------DWKIKIQDTVADNASCGLFVL 167
MhpD     NRDLPATDITFDELYNAIEWVLPALEVVGSRIR------DWSIQFVDTVADNASCGVYVI 166
4OD      KAPLVGPGCHIGDVIAAVDYVIPTVEVIDSRYE------NFKFDLISVVADNASSTRYIT 170
TodJ     GRDLDGDQLTVADLFRAIEFAVPAIEIVGSRIT------NWDIRITDTIADNASSGLYVL 172
BphE     GRDLEGDQLTVADLFRTVEFAVPAIEIVGSRIA------SWDIRITDTIADNASSGLYVL 172
AmnF     GRDLDTEQPTHQEVLQAVDYVVPALEIVGSRIA------DWNIKFVDTVADNASSGVYVL 166
DmpE     KKDLIGPGVTNADVLAATECVMPCFEIVDSRIR------DWKIKIQDTVADNASCGLFVL 167
NahL     KKDLKGPGVTAADVLAATEGVMTCFEIVDSRIR------DWKIKIQDTVADNASCGVFVL 166
AtdE     KKDLTGPGVTNADVLAATECVMPCFEIVDSRIK------DWKIAIQDTIADNASCGLFVL 167
TdnG     KKTLKGPGVTAADVLAATEGVMACFEIVDSRIR------DWKIKIQDTVADNASCGVFVL 168
CdoH     KKTLRGPGVTAADVLAATEGVMACFEIVDSRIR------DWKIKIQDTVADNASCGVFVL 168
BphX1    AADLPGAGCTEDDVLAATEALVPAIELIDTRIK------DWQIKICDTIADNASAAGFVL 167
TesE     KKDLQGPGVTREDVLAATEWVAPCFEIVDSRIN------DWKIKIQDTVADNASCGVFVI 169
HpaH     KKDLSGPNCTIFDVLDATDYVIPALEIIDARIEQFDSKTKVPRRVFDTISDNAANAGVVL 173
BphE2    GRSLKGPGVTIFDVLEATDFVVPAAEIIDARIQRVSEITKSRRKVEDTIADNAASAGVVV 173
            *        ::  : :   .  *::.:*        .    . ..::***:    :
```

```
VPH     GDQAVSPRQVDLVTCGMLVEKNGQLLSTGAGAAALGSPVNCVAWLANTLGHFGIALKAGE 227
MhpD    GGPAQRPAGLDLKNCAMKMTRNNEEVSSGRGSECLGHPLNAAVWLARKMASLGEPLRTGD 226
4OD     GGRMANLEDVDLRTLGVVMEKNGEVVELGAGAAVLGHPLSSVAMLANLLAERGEHIPAGT 230
TodJ    GSTPKRLCDFDSRQAGMVMERQGIPVSSGVGAACLGAPLNAVLWLARVMARAGRPLRTGD 232
BphE    GSTPKRLCDFDARQAGMVMERQGVPVSSGVGSACLGSPLNAMLWLAKVMARAGRPLRAGD 232
AmnF    GSTPISPRGLDLSLVGMCLSRRGEPVSTGAGAACLGTPLNAVVWLARTMSRLGKPLRAGE 226
DmpE    GDQAVSPRQVDLVTCGMVVEKNGHIISTGAGAAALGSPVNCVAWLANTLGRFGIALKAGE 227
NahL    GDSLVDPRKVDLNTCGMILEKNGEIVATGSGAAALGAPANAVAWLANTLGSLDIPLQAGE 226
AtdE    GDKAVSPREVDLVTCGMVVEKNGAIISTGAGAAALGSPVNCVTWLANTLGQFGIR----- 222
TdnG    GDRLVDPRDVDLGTCGMVLEKNGEIVATGAGAAALGHPANAVAWLANTLGRLGIALEAGE 228
CdoH    GDRLVDPRDVDLGTCGMVLEKNGDIVATGAGAAALGHPANAVAWLANTLGAHGIALEAGE 228
BphX1   GAARVPPADLDVRAIDAKLTRNGEVVAEGRSDAVLGNPATAVAWLAGKVESFGVRLRKGD 227
TesE    GKQHTDPASLDLAAAAMQMSKNGQPAGSGLGSAVQGHPAEAVAWLANTLGAFGIPFKAGE 229
HpaH    GGRAIKPMDVDLRRVAAVLYRNGVVEESGVSAAVLNNPIKGVAWLANKLHPYGVTLKAGE 233
BphE2   SGRPVRPDAFDLRWVGAVLSKNAMVEETGIAAGVLNHPANGIVWLVKRLARWGEGIEAGE 233
        .        .*       : :.      * .    . *      *.  :   .

VPH-XylJ        VILSGSLVPLEPVKAGDFMRVEIGGIGSASVRFI--------- 261
MhpD            IILTGALGPMVAVNAGDRFEAHIEGIGSVAATFSSAAPKGSLS 269
4OD-XylI        FIMTGGITAAVAVAPGDNITVRYQGLGSVSARFV--------- 264
TodJ            TVLSGALGPMVPVAGGDVFDVRIAGLGSVTAAFAKA------- 268
BphE            TVLSGALGPMVPVAGGDVFDVRIAGLGSVTAVFAKE------- 268
AmnF            LILSGALGPMVAVKPGDVFECHINGVGSVRTEFESNQMNGVAA 269
DmpE            VILSGSLVPLEPVKAGDVMRVDIGGIGSASVRFT--------- 261
NahL            VILSGSLAIMVPVKAGDNLRVTIGGIGGCSVRFV--------- 260
AtdE            ----------------------------------------
TdnG            VVLSGSLGIMVPVQAGDNLRVTIGGIGGCSVRFL--------- 262
CdoH            VVLSGSLGIMVPVQAGDNLRVTIGGIGGCSVRFI--------- 262
BphX1           IVLPGSCTFAVEARAGDEFVADFTGLGLVRLSFE--------- 261
TesE            VILSGSLAPLVPAAAGDRFDMVIEGMGTCSIQFTE-------- 264
HpaH            VILGGSFTRPVAARRGDTFHVDYHELGSISMQFV--------- 267
BphE2           IVLGGSFTRPVEAGPGDVFHADYGPLGSFSFRFG--------- 267
```

Figure 2.31. Sequence alignment of VPH and MhpD with 13 other homologous enzymes generated using CLUSTAL-W. Active-site residues that were mutated highlighted in (green). Glutamate residues involved in metal-binding highlighted in (magenta). From top to bottom, VPH- *Pseudomonas putida mt-2*, MhpD- *Escherichia coli*, 4OD- *Pseudomonas putida mt-2*, TodJ- *Pseudomonas putida F1*, BphE- *Burkholderia cepacia*, AmnF- *Burkholderia xenovorans LB400*, DmpE- *Pseudomonas sp. CF600*, NahL- *Azoarcus sp. BH72*, AtdE- *Acinetobacter sp. YAA*, TdnG- *Pseudomonas putida*, CdoH- *Comamonas sp. JS765*, BphX1- *Mycobacterium tuberculosis H37Rv*, TesE- *Comamonas testosteroni*, HpaH- *Pasteurella multocida subsp. multocida str. Pm70*, and BphE2- *Rhodococcus sp. RHA1*.
(*) indicates residues in that column are all identical. (:) indicates conserved substitutions. (.) indicates semi-conserved substitutions. Symbols are located below the appropriate residue(s).

site (Figure 2.1). Examination of the area near the glutamate triad identified four other residues, Lys-60, Leu-72, Asp-78, and Ser-160 (Ser-161 in VPH), that may play a role in catalysis. Based on the arrangement of these residues a working hypothesis for the catalytic mechanism is proposed in Scheme 10. The first step in catalysis is removal of the proton from the enol (**2**) to generate the conjugated ketone (**3**). Lys-60 is near the glutamate triad and may be capable of abstracting a proton from **2**. The combination of this lysine and the metal ion could act as an electron sink to bind, position, and polarize the carboxyl group and oxygen at the C-2 position of the substrate (**2**) for catalysis. The metal ion is proposed to play more of a role in binding and positioning the substrate than participating in the catalytic reaction. Activation of a water molecule for nucleophilic attack is accomplished by the carboxylate side chain of Asp-78. The Michael addition of water on C-4 of **3** forms an enolate intermediate stabilized by interaction with the Mg^{2+} ion and the positively charged side chain of Lys-60. Subsequent ketonization of the intermediate with protonation at the C-3 position may be assisted by Ser-160 (Ser-161 in VPH) generating the product (**4**).

The genes for 4OD and VPH have previously been cloned into a single plasmid and expressed as part of a 4OD/VPH coexpression system to generate the complex. To examine VPH activity independently, a critical residue within 4OD was mutated to render the decarboxylase inactive but still allow formation of the functional complex (i.e. E109Q-4OD/VPH). These two plasmids were used as templates in generating the four VPH mutants as a complex with 4OD: E109Q-4OD/K60A-VPH, 4OD/L72A-VPH, E109Q-4OD/D78N-VPH, and 4OD/S161A-VPH. Because the K60A and D78N

mutations in VPH had such low levels of activity, the E109Q-4OD/VPH plasmid was chosen as the template to eliminate any potential for 4OD activity to interfere with the kinetic determinations. The MhpD gene inserted into pET-24a vector was used as a template in producing the four MhpD mutants: K60A-MhpD, L72A-MhpD, D78N-MhpD, and S160A-MhpD.

Based on the proposed mechanism, the four residues were mutated in both enzymes and the corresponding mutants were analyzed for their effects on the overall reaction as well as the possibility of uncoupling the catalytic steps (i.e. ketonization of **2** and the subsequent Michael addition of water to **3**). The kinetic parameters for the K60A mutant were determined to investigate its proposed role as a catalytic base in abstracting a proton from the C-2 hydroxyl of **2**. This mutation resulted in a greatly reduced activity but with little change in K_m as compared to wild-type for both VPH and MhpD, leading to the conclusion that Lys-60 is essential for catalysis. Without effective deprotonation the rate of ketonization of **2** to **3** is reduced. Another major part of the loss in activity may be due to the removal of optimal hydrogen bonding and/or electrostatic interactions with the enolate intermediate formed at the 2-oxo position of the partially hydrated substrate, making the Michael addition of water at the C-4 position less favorable.

A key observation for the K60A mutant is that it is the only mutant that showed evidence for the production of **3**. In aqueous solution **2** readily ketonizes to form an equilibrium mixture of **2**, **3**, and **5**. The formation of the α,β-unsaturated ketone is the slowest to form (4.5 nM min^{-1}) and not usually observed in the time frame of a kinetic assay (Scheme 2). In our enzymatic studies the rate of conversion of **2** to **4** is such that **3**

is usually never detected under UV assay conditions. Thus, the K60A mutation does not eliminate the catalytic production of **3** but does reduce the hydration reaction enough to allow a detectable amount to accumulate. NMR analysis supports **3** as the major product (90% by integration), but also shows the production of **4** (albeit a very small amount, 10% by integration)[1]. In this study of the K60A mutants of VPH and MhpD, we have successfully obtained evidence for an uncoupling of the tautomerization reaction in converting **2** to **3** from the hydration reaction with **3** to generate **4**. The observations made for the K60A mutants of VPH and MhpD with HPD (compounds **2**-**4**) were similar to those made using the related substrate Me-HPD (compounds **6**-**8**), although at a much slower rate.

From these observations and the proposed mechanism (Scheme 10), additional insight into the mechanism can be obtained. Mutation of Lys-60 may result in the C-2 hydroxyl of **2** interacting with the bound metal ion rendering the proton more acidic and easier to remove. Hence, the catalytic conversion of **2** to **3** continues to be observed (although at a much slower rate). Another possibility is that the smaller side chain of the K60A mutant may create enough space for a water molecule(s) to move in and interact with the C-2 hydroxyl group. This weak polarizing effect may allow the enzyme to continue to catalyze the 1,5-keto-enol tautomerization reaction. At the same time, elimination of the charged Lys-60 may also reduce the rate of hydration by removing a positively charged residue from assisting in the polarization of the C-2 carbonyl group

[1] The non-enzymatic reaction using **2** had a ratio of **3** to **4** (0.9:0.1) after the overnight incubation period.

during hydration. Hence, a build-up of **3** is observed, followed by a slower production of **4**.

The role of Asp-78 in the mechanism was investigated by analyzing the kinetic properties of the asparagine mutation. The D78N mutant of both VPH and MhpD showed little change in K_m but had much larger decreases in k_{cat}, suggesting an important role for Asp-78 in catalysis. Based on its position in the proposed active site and the assumption that aspartate would be negatively charged, Asp-78 is a likely candidate to activate a water molecule for nucleophilic attack (Scheme 10). Hence, elimination of the negatively charged carboxylate group by the D78N mutation would disrupt the Michael addition of water to **3** and reduce the catalytic rate. The NMR analysis of the VPH and MhpD mutants revealed that both **3** (54% by integration) and **4** (46% by integration) are present as products. Consequently, although replacing aspartate with asparagine slows down the catalytic rate it does not eliminate it entirely, so the water molecule is still capable of intermittently adding to the C-4 position. The observations made for the D78N mutants of VPH and MhpD with HPD (compounds **2**-**4**) were similar to those made using the substrate analogue, Me-HPD (compounds **6**-**8**).

The Ser-160 to an Ala mutation was generated in MhpD (S161A in VPH) to examine its effect of hydrogen bonding to a water molecule for protonation at the C-3 position of **3** (Scheme 10). The kinetic parameters for the Ser-160 (or Ser-161) mutants gave mixed results. The S160A-MhpD and S161A-VPH mutants retain only ~5-10% of the activity observed for wild-type in converting **2** to **4** and **6** to **8**, and have a comparable K_m value to that of wild-type. The only exception was that the S160A-MhpD with **6**

retains 30% of the activity observed for wild-type and a K_m value that is twice as high. These results suggest that Ser-160 and Ser-161 are important residues for activity. The NMR analysis shows evidence for the production of **3** (35% by integration) and **4** (65% by integration) during the catalytic reaction.

Generation of the α,β–unsaturated ketone and hydrated product combined with the decrease in catalytic rate shows that Ser-160 could be responsible for activating a water molecule to protonate C-3 during the Michael addition of water. If Ser-160 only affected the protonation at C-3 during the 1,3-keto-enol reaction then the catalysis of **2** to **3** should be observed (as is the case from the NMR analysis). However, since production of **3** is not observed by UV detection then the hydration reaction must still be fast enough to process most of **3** to **4** before it can accumulate. Generation of **4** provides evidence for the protonation of C-3, although at a slower rate. Thus, Ser-160 could hydrogen bond to a water molecule to assist in proton donation or perhaps donate a proton directly from its side chain hydroxyl group. Whatever role it may play, the evidence shows that without this important residue the rate of the reaction is significantly lowered. The observations made for S160A-MhpD and S161A-VPH with HPD (compounds **2**-**4**) were similar to those made using the substrate analogue, Me-HPD (compounds **6**-**8**).

The last mutation examined whether a difference in size of the side chain of Leu-72 affected the reaction (Scheme 10). Accordingly, the L72A mutant was constructed. Of the four mutations examined, the L72A mutant of MhpD has only a minor effect on the kinetic parameters, with comparable k_{cat} and K_m values to that of wild-type converting **2** to **4** and **6** to **8**. Yet, L72A-VPH maintains only ~3-13% of the activity observed for

wild-type with **2** and **6**, but does have similar K_m values. These results suggest that the Leu-72 residue may be more important for catalysis in VPH than it is in MhpD. The mutation in MhpD has no effect on the catalytic rate or the binding of the substrates, so that Leu-72 plays no role in catalysis. However, the Leu-72 residue in VPH may play a role in aligning the substrate within the active site or stabilizing the enzyme to undergo effective catalysis. Whatever role it may play the L72A mutation has a negative impact. The NMR analysis of the reaction using **2**, shows the presence of **3** (14% by integration), but the majority of product is **4** (86% by integration). Thus, the L72A mutants of MhpD and VPH catalyze the 1,5-keto-enol tautomerization and hydration reactions. The observations made for L72A-MhpD and L72A-VPH with HPD (compounds **2**-**4**) were similar to those made using the substrate analogue, Me-HPD (compounds **6**-**8**).

Three compounds structurally similar to HPD (**2**) were tested as potential inhibitors of VPH and MhpD. The first compound is 2-oxo-3-pentynoate (2-OP, **10**) (Figure 2.4), which could be a potent irreversible inhibitor (Scheme 5) (10) or a substrate (Scheme 6) (11). In this experiment, the 4OD/VPH complex was incubated with an excess of **10** and its activity was monitored with **2** over time. VPH was not inhibited by **10** and there was no evidence for the hydration reaction. It seems reasonable to assume that the electrophilic **10** would readily react in some form with an active-site nucleophile (such as Lys-60 or Asp-78) once inside the active site. One would also predict that **10** being a five carbon molecule (although more linear) would be similar in size to the physiological substrate (**2**) of VPH. However, the results of the inhibition study suggest

that **10** is not binding in the active site in a conformation that would allow a hydration or inactivation reaction to occur.

A second study examined inhibition of VPH by 3-bromopropiolic acid (**11**), a mechanism-based irreversible inhibitor of CaaD (11) and *cis*-3-chloroacrylic acid dehalogenase (*cis*-CaaD) (21). VPH was not inhibited by **11**. Like **10**, it seems likely that the electrophilic **11** would also readily react with an available nucleophile (such as Lys-60 or Asp-78) once inside the active-site. In this case **11** is smaller (only a three carbon chain) than HPD (**2**). Here again the results of the inhibition study suggest that **11** is not binding in the active site in a conformation that would allow inactivation to occur.

Another affinity labeling inhibitor, oxirane-2-carboxylate (**12**), of *cis*-CaaD was used to test for inhibition, but only with MhpD (12). Oxirane-2-carboxylate is a chiral molecule with both enantiomers, (*R*) and (*S*)-**12**, being examined as potential inhibitors. In this study, MhpD was incubated with an excess of (*R*)-**12** and (*S*)-**12** in separate reactions and activity was monitored with **2** over time. MhpD was not inhibited by (*R*)-**12** or (*S*)-**12**. The predictions for these two inhibitors are similar to those for **10** and **11**. In this case, MhpD behavior mirrors that of VPH with the results of the inhibition study suggesting that (*R*)-**12** and (*S*)-**12** are probably not binding in the active site in a conformation that would allow inactivation to occur.

Finally, a compilation of all the results indicate that three of the four residues examined (Lys-60, Asp-78, and Ser-160 [or 161]) play an important role in the catalytic mechanism of VPH and MhpD. Both Lys-60 and Asp-78 are the most critical residues and are almost certainly directly involved in catalysis. Leu-72 proved to be a more

important residue in VPH than MhpD in affecting the catalytic rate. All four mutants of VPH and MhpD had negligible changes in K_m values as compared to the wild-type protein, demonstrating that the mutations had less of an effect on substrate binding than on the catalytic rate. Despite the important information gained in this study, limitations are still apparent, such as the lack of evidence for a definitive active site in MhpD identified by a bound ligand, no effective inhibitor in affinity-labeling critical active site residues, and the lack of a complementary structure of VPH for comparison. These are all still important pieces of information that need to be investigated to acquire a complete understanding of the catalytic mechanism of VPH and MhpD.

ACKNOWLEDGMENTS

We thank Steve D. Sorey (Department of Chemistry, The University of Texas at Austin) for his expert assistance in acquiring the NMR spectra, and Dr. William H. Johnson, Jr. (Division of Medicinal Chemistry, The University of Texas at Austin) for synthesizing needed compounds and interpreting the NMR spectra.

REFERENCES – CHAPTER 2

1. Harayama, S., Lehrbach, P.R., and Timmis, K.N. (1984) Transposon mutagenesis analysis of meta-cleavage pathway operon genes of the TOL plasmid of *Pseudomonas putida mt-2*. *J. Bacteriol 160,* 251-255.

2. Harayama, S., Rekik, M., Ngai, K.L., and Ornston, L.N. (1989) Physically associated enzymes produce and metabolize 2-hydroxy-2,4-dienoate, a chemically unstable intermediate formed in catechol metabolism via meta cleavage in *Pseudomonas putida*. *J. Bacteriol. 171*, 6251-6258.

3. Stanley, T.M., Johnson Jr., W.H., Burks, E.A., Hwang, C-C, Cook, P.F., and Whitman, C.P. (2000) Expression and stereochemical and isotope effect studies of active 4-oxalocrotonate decarboxylase. *Biochemistry 39*, 718-726.

4. (a) Pollard, J.R., Rialland, D., and Bugg, T.D. (1998) Substrate selectivity and biochemical properties of 4-hydroxy-2-keto-pentanoic acid aldolase from *Escherichia coli*. *Appl. Environ. Microbiol. 64*, 4093-4094. (b) Pollard, J.R. and Bugg, T.D. (1998) Purification, characterisation and reaction mechanism of monofunctional 2-hydroxypentadienoic acid hydratase from *Escherichia coli*. *Eur. J. Biochem. 251*, 98-106.

5. Lian, H. and Whitman, C.P. (1994) Stereochemical and Isotopic Labeling Studies of 4-Oxalocrotonate Decarboxylase and Vinylpyruvate Hydratase: Analysis and Mechanistic Implications. *J. Amer. Chem. Soc. 116*, 10403-10411.

6. Timm, D.E., Mueller, H.A., Bhanumoorthy, P., Harp, J.M., and Bunick, G.J. (1999) Crystal structure and mechanism of a carbon-carbon bond hydrolase. *Structure 7*, 1023-1033.

7. Tame, J.R., Namba, K., Dodson, E.J., and Roper D.I. (2002) The crystal structure of HpcE, a bifunctional decarboxylase/isomerase with a multifunctional fold. *Biochemistry 41*, 2982-2989.

8. Lian, H. and Whitman, C.P. (1993) Ketonization of 2-hydroxy-2,4-pentadienoate by 4-oxalocrotonate tautomerase: implications for the stereochemical course and the mechanism. *J. Amer. Chem. Soc. 115*, 7978-7984.

9. Whitman, C.P., Aird, B.A., Gillespie, W.R., and Stolowich, N.J. (1991) Chemical and enzymic ketonization of 2-hydroxymuconate, a conjugated enol. *J. Amer. Chem. Soc. 113*, 3154-3162.

10. Johnson, W.H., Jr., Czerwinski, R.M., Fitzgerald, M.C., and Whitman, C.P. (1997) Inactivation of 4-oxalocrotonate tautomerase by 2-oxo-3-pentynoate. *Biochemistry 36*, 15724-15732.

11. Wang, S.C., Person, M.D., Johnson, W.H., Jr., and Whitman, C.P. (2003) Reactions of trans-3-chloroacrylic acid dehalogenase with acetylene substrates: consequences of and evidence for a hydration reaction. *Biochemistry 42*, 8762-8773.

12. Poelarends, G.J., Serrano, H., Johnson, W.H., Jr., and Whitman, C.P. (2004) Stereospecific alkylation of cis-3-chloroacrylic acid dehalogenase by (*R*)-oxirane-2-carboxylate: analysis and mechanistic implications. *Biochemistry 43*, 7187-7196.

13. Sambrook, J. and Russell, D.W. (2001) *Molecular Cloning: A Laboratory Manual, Third Edition*, Cold Spring Harbor Laboratory, Cold Spring Harbor, NY.

14. Waddell, W.J. (1956) A simple ultraviolet spectrophotometric method for the determination of protein. *J. Lab. Clin. Med. 48*, 311-314.

15. Ho, S.N., Hunt, H.D., Horton, R.M., Pullen, J.K., and Pease, L.R. (1989) Site-directed mutagenesis by overlap extension using the polymerase chain reaction. *Gene 77*, 51-59.

16. Portsmouth, D., Stoolmiller, A.C., and Ables, R.H. (1967) Studies on the mechanism of action of 2-keto-3-deoxy-L-arabonate dehydratase. *J. Biol. Chem. 242*, 2751-2759.

17. Burks, E. A., Johnson, W. H., Jr., and Whitman, C. P. (1998) Stereochemical and Isotopic Labeling Studies of 2-Oxo-hept-4-ene-1,7-dioate Hydratase: Evidence for an Enzyme-Catalyzed Ketonization Step in the Hydration Reaction. *J. Am. Chem. Soc. 120*, 7665-7675.

18. Schwab, J.M. and Henderson, B.S. (1990) Enzyme-catalyzed allylic rearrangements. *Chem. Rev. 90*, 1203-1245.

19. Schwab, J.M. and Klassen, J.B. (1984) Steric course of the allylic rearrangement catalyzed by β-hydroxydecanoylthioester dehydrase. Mechanistic implications. *J. Am. Chem. Soc. 106*, 7217-7227.

20. Brock, D.J.H, Kass, L.R., and Bloch, K. (1967) Beta-hydroxydecanoyl thioester dehydrase. II. Mode of action. *J. Biol. Chem. 242*, 4432-4440.

21. Poelarends, G.J., Serrano, H., Person, M.D., Johnson, W.H., Jr., Murzin, A.G., and Whitman, C.P. (2004) Cloning, expression, and characterization of a cis-3-chloroacrylic acid dehalogenase: insights into the mechanistic, structural, and evolutionary relationship between isomer-specific 3-chloroacrylic acid dehalogenases. *Biochemistry 43*, 759-772.

Chapter 3: The Roles of Active site Residues in the Catalytic Mechanism of 5-(carboxymethyl)-2-Oxo-3-hexene-1,6-dioate Decarboxylase from *Escherichia coli* C: A Kinetic, NMR, and Mutational Analysis

INTRODUCTION

5-(carboxymethyl)-2-Oxo-3-hexene-1,6-dioate decarboxylase (COHED) is part of an inducible set of enzymes known as the homoprotocatechuate meta-fission pathway in *Escherichia coli C*. The enzymes of this pathway are chromosomally encoded and may be part of a degradative route for phenylalanine and tyrosine (1). COHED is a metal ion-dependent enzyme that converts 5-(carboxymethyl)-2-oxo-3-hexene-1,6-dioate (**1**) to 2-oxo-4-heptene-1,7-dioate (**3**) using Mg^{2+} (Scheme 1) (2). Based on stereochemical and isotope labeling studies, it has been proposed that COHED initially catalyzes the decarboxylation of (*5R*)-**1** to generate the 4Z isomer 2-hydroxy-2,4-heptadiene-1,7-dioate (**2**). The 1,3-keto-enol tautomerization of (*4Z*)-**2** results in the stereochemical incorporation of a deuterium at the C-3 position generating (*3S*)-**3** (in ^2H_2O) (3).

Scheme 1

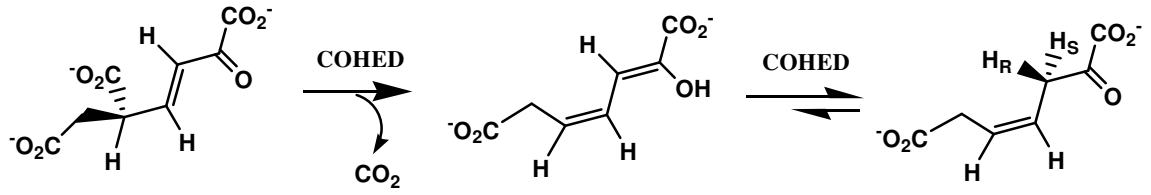

The crystal structure of COHED (with Ca^{2+}) has been solved and the enzyme has been identified as a member of the FAH (fumarylacetoacetate hydrolase) superfamily (4). COHED is a monomeric protein, which consists of two domains, an N-terminal domain (residues 1-200) and a C-terminal domain (residues 221-429) (Figure 3.1). It has been postulated that the N-terminal domain of COHED is responsible for tautomerization and the C-terminal domain (the Ca^{2+} binding site) is responsible for the decarboxylation (4).

The structural alignment of COHED with FAH identified potential active site residues in COHED. The C-terminal domain of COHED contains the EXE motif of Glu-276 and Glu-278 that may be part of a metal binding triad along with Asp-307 (Figure 3.1). Thus, Glu-276 and Glu-278 could be critical structural and/or catalytic residues, participating in the binding of the Mg^{2+} ion in the catalytic reaction. Lys-110 of COHED occupies the same position as Lys-153 of FAH, which acts as part of an oxyanion hole and a proton donor (Figure 3.2). Thus, based on its positioning, Lys-110 may stabilize the enol formation of **2** (Scheme 2A) and/or donate a proton to the C-3 position in the formation of **3** (Scheme 2B). Individual mutations of these three residues were constructed and the consequences of the mutations on the overall reaction were examined. Herein, the results for the K110Q, E276Q, and E278Q mutants of COHED are reported.

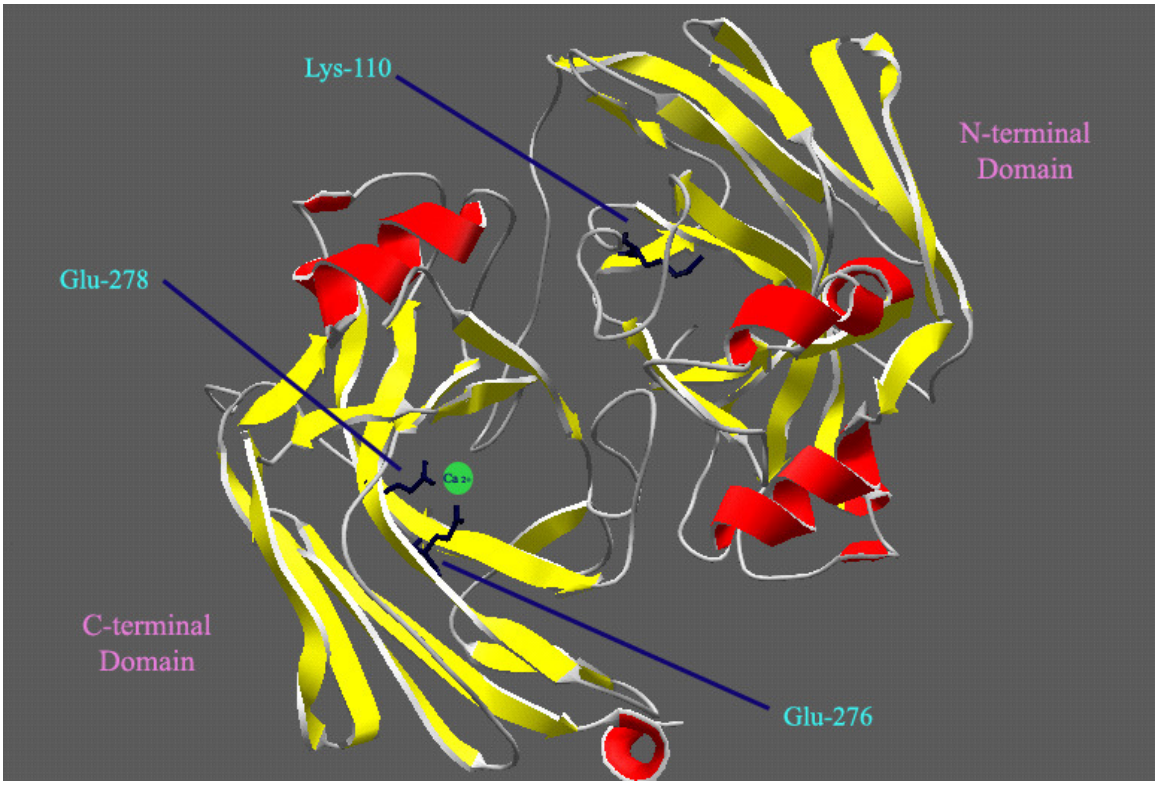

Figure 3.1. Ribbon diagram of COHED monomer with select active site residues identified (PDB code 1gtt) (4).

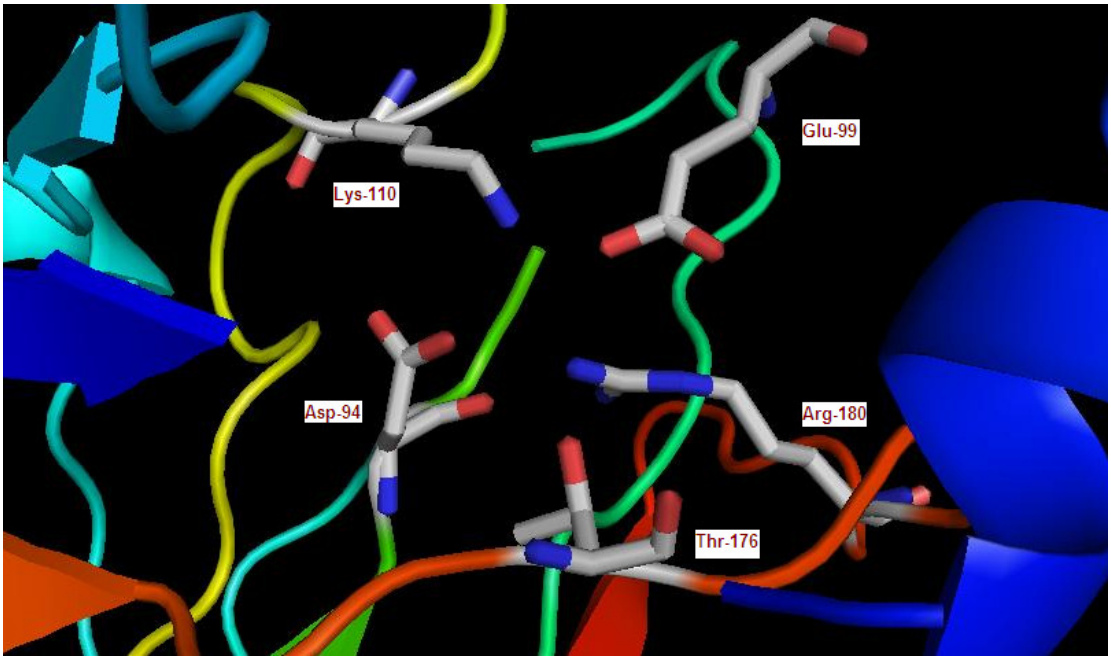

Figure 3.2. Close-up view of proposed active-site residues in N-terminal domain of COHED (PDB code 1gtt) (4).

Scheme 2

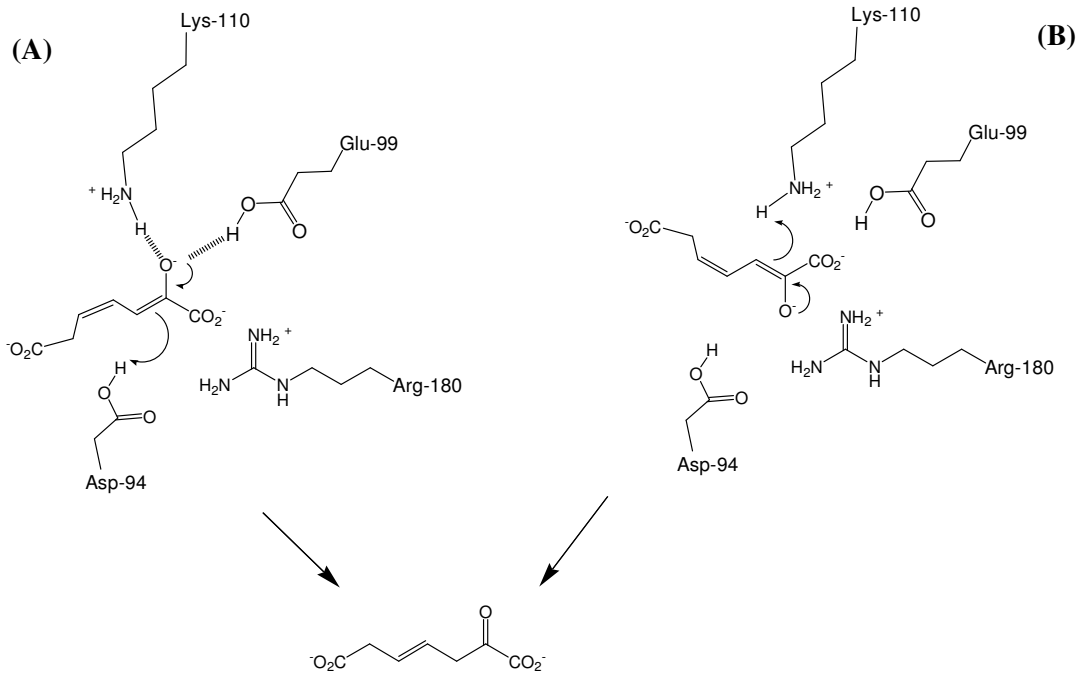

MATERIALS AND METHODS

Materials. All reagents, buffers, media components, and solvents were obtained from Sigma-Aldrich Chemical Co. (St. Louis, MO), Fisher Scientific Inc. (Fair Lawn, New Jersey), or Becton Dickinson Microbiology Systems (Sparks, MD) with the following exceptions. Literature procedures were used for the syntheses of 5-(carboxymethyl)-2-hydroxymuconate (**4**) (1,5), 2-hydroxy-2,4-heptadiene-1,7-dioate (**2**) (1,6), 2-oxo-1,7-heptadioate (**12**) (7), and 3-bromopropiolic acid (**16**) (8). The YM-10 ultrafiltration membranes and the Amicon stirred cells were obtained from Millipore Corp. (Billerica, MA). Restriction enzymes, PCR reagents, and the Expanded High Fidelity PCR System were obtained from Roche Diagnostics Corp. (Indianapolis, IN). The QIAprep Spin Miniprep Kit and MinElute Kit were obtained from Qiagen, Inc. (Valencia, CA). The QuikChange II Site-Directed Mutagenesis Kit was acquired from Stratagene (La Jolla, CA). Oligonucleotides for DNA amplification or mutant construction were synthesized by Invitrogen (Carlsbad, CA).

Bacterial Strains and Plasmids. *Escherichia coli* strain DH5α (Invitrogen, Carlsbad, CA) was used for cloning and isolation of plasmids. *E. coli* strain BL21-Gold(DE3), obtained from Stratagene, was used for recombinant protein expression. The expression vector pET24a-(+) was obtained from Novagen, Inc. (Madison, WI). The template for the construction of the COHED mutants, pET24a-COHED, was constructed by Dr. Susan C. Wang [Wang, S.C. and Whitman, C.P. (2008) unpublished results].

General Methods. Techniques for cloning and DNA manipulation were based on methods described elsewhere (9), or as suggested by the manufacturer. The PCR was

carried out in a Perkin-Elmer DNA thermocycler (Model 480) obtained from Perkin Elmer Inc. (Wellesley, MA). DNA sequencing was performed by the DNA Core Facility in the Institute for Cellular and Molecular Biology (ICMB) at the University of Texas at Austin. Plasmid DNA was introduced into cells by electroporation using a Cell-Porator Electroporation System (Whatman Biometra, Göttingen, Germany). HPLC was performed on a Waters (Milford, MA) 501/510 system or a Beckman System Gold HPLC (Fullerton,CA) using either a TSKgel DEAE-5PW anion-exchange (150 × 21.5 mm) or a TSKgel Phenyl-5PW hydrophobic interaction (150 × 21.5 mm) column (Tosoh Bioscience, Montgomeryville, PA). Gel filtration chromatography was carried out on a Spectra/Chrom Aqueous column (2.5 × 100 cm) obtained from Spectrum Chromatography (Houston, TX) using Sephadex G-75 resin. Protein was analyzed by sodium dodecyl sulfate polyacrylamide gel electrophoresis (SDS-PAGE) under denaturing conditions on gels containing 15% polyacrylamide. Protein concentrations were determined by the method of Waddell (10). Absorbance data were obtained on an Agilent 8453 Diode Array spectrophotometer (Agilent Technologies, Palo Alto, CA). The kinetic data were fitted by nonlinear regression using the Grafit program (Erithacus Software Ltd., Horley, U.K.) obtained from Sigma Chemical Co. Nuclear magnetic resonance (NMR) spectra were recorded in 100% H_2O on a Varian Unity INOVA-500 spectrometer using selective presaturation of the water signal with a 2 s presaturation interval. The lock signal is dimethyl-d_6 sufoxide (DMSO- d_6). Chemical shifts are standardized to the DMSO- d_6 signal at 2.49 ppm.

Construction of the COHED Mutants. The three single mutants of COHED (K110Q, E276Q, and E278Q) were prepared using pET24a-COHED as the template. Site-directed mutations were introduced using the QuikChange II Site-Directed Mutagenesis Kit. Accordingly, the K110Q mutant of COHED was generated by the PCR using oligonucleotides 5'-GCAATCAAAGCACAATGTCGTGATGGA-3' and 5'-TCCATCACGACATTGTGCTTTGATTGC-3' (Primer-1 and 2, respectively). Primer-1 has 12 coding sequence bases, three bases corresponding to the glutamine mutation (underlined), and another 12 bases of coding sequence. Primer-2 has 12 complementary sequence bases, three bases corresponding to the glutamine mutation (underlined), and another 12 bases of complementary sequence.

The E276Q mutant of COHED was constructed using the oligonucleotides 5'-TACATGCACTACCAAGCGGAGCTGGTG-3' and 5'-CACCAGCTCCGCTTGGTAGTGCATGTA-3' (Primer-3 and 4, respectively). Primer-3 has 12 coding sequence bases, three bases corresponding to the glutamine mutation (underlined), and another 12 bases of coding sequence. Primer-4 has 12 complementary sequence bases, three bases corresponding to the glutamine mutation (underlined), and another 12 bases of complementary sequence.

The E278Q mutant of COHED was generated using the oligonucleotides 5'-CACTACGAAGCGCAGCTGGTGGTAGTT-3' and 5'-AACTACCACCAGCTGCGCTTCGTAGTG-3' (Primer-5 and 6, respectively). Primer-5 has 12 coding sequence bases, three bases corresponding to the glutamine mutation (underlined), and another 12 bases of coding sequence. Primer-6 has 12 complementary

sequence bases, three bases corresponding to the glutamine mutation (underlined), and another 12 bases of complementary sequence.

Overexpression and Purification of K110Q-, E276Q-, E278Q-, and wild-type COHED. Each mutant construct was transformed into competent *E. coli* BL21-Gold (DE3) cells by electroporation. Transformants were grown at 37ºC on LB/Kn (50 µg/mL) plates. A single colony was used to inoculate 50 mL of LB/Kn (50 µg/mL) media in a 125 mL Erlenmeyer flask. After overnight growth at 37ºC, a 30 mL aliquot of overnight culture was used to inoculate 6 – 2L Erlenmeyer flasks containing 500 mL of LB/Kn (50 µg/mL) medium (3 L total). The cells were grown to an OD_{600} of 0.6-0.8 (~ 3 h), induced by the addition of 0.5 mM of IPTG, and allowed to grow for another 5 h. Cells were harvested by centrifugation (8 min at 7500*g*) and stored at -20ºC. The enzymes were purified by a modification of a published procedure (11). Accordingly, in a typical purification experiment, the cells from 3 L of culture were thawed and suspended in 16 mL of 50 mM triethanolamine buffer, pH 7.3 (Buffer A), containing 5 mM $MgCl_2$, disrupted by sonication, and centrifuged (1.5 hours at 60,000*g*). The supernatant was filtered through a 0.2 µm-pore diameter filter and applied to a TSKgel DEAE-5PW column (150 × 21.5 mm) that has been pre-equilibrated with Buffer A. The column was washed with 50 mL of Buffer A, and retained proteins were eluted with an increasing linear gradient (0 to 0.5 M NaCl) in Buffer A (300 mL) at a flow rate of 5 mL/min. Fractions (8 mL) that showed the highest COHED activity were pooled and concentrated to ~20 mL using an Amicon stirred cell equipped with a YM10 (10,000 MW cutoff, respectively) ultrafiltration membrane. The protein typically eluted in

fractions #5-9 (corresponding to protein eluting in the void volume) and fractions #17-22. During collection, each fraction was made 5 mM $MgCl_2$. Subsequently, the concentrate was made 1.2 M using solid $(NH_4)_2SO_4$ and the resulting solution was stirred for 60 min. at 4 ºC. After centrifugation (30 min at 17,000*g*), the supernatant was loaded onto the TSKgel Phenyl-5PW column (150 × 21.5 mm) that had previously been equilibrated with Buffer B [10 mM HEPES buffer, 1.2 M $(NH_4)_2SO_4$, pH 7.3]. The column was washed with 50 mL of Buffer B, and retained proteins were eluted with a decreasing linear gradient of 1.2 to 0 M $(NH_4)_2SO_4$ in Buffer C (10mM HEPES buffer, pH 7.3, 250mL) at a flow rate of 5mL/min. Fractions (8 mL) with the highest COHED activity were pooled and concentrated to ~3 mL using an Amicon stirred cell equipped with a YM10 ultrafiltration membrane. The protein typically eluted in fractions #25-32. The fractions collected were made 5 mM $MgCl_2$ during collection. The concentrated protein was loaded onto a Sephadex G-75 column (2.5 × 100 cm) equilibrated with 20 mM HEPES buffer, pH 7.3. Fractions (8 mL) were collected and sufficient $MgCl_2$ (from a 1 M stock solution) was added to give a 5 mM concentration in each tube. The protein normally eluted in fractions #26-34. These fractions were assayed for activity and the purity (>95%) was determined by SDS-PAGE. The purified enzymes were filtered through a 0.2 µm-pore diameter filter and stored at 4 ºC. The K110Q mutant yielded ~75% less protein than that produced by wild-type COHED, while the other two mutants (E276Q and E278Q) yielded comparable amounts to that of wild-type.

Enzyme Assays and Steady-State Kinetics. The enzyme kinetic assays were performed in 20 mM Na_2HPO_4 buffer containing 5mM $MgCl_2$, pH 7.3, following the

decrease in absorbance at 236 nm corresponding to the decarboxylation of 5-(carboxymethyl)-2-oxo-3-hexene-1,6-dioate (**1**, ε = 4500 $M^{-1}cm^{-1}$) (Scheme 3). An aliquot of enzyme (40 µL – 2 mL) was diluted into buffer (40 mL) and incubated for 1 h. Subsequently, a 1 mL-portion of the diluted enzyme was transferred to a cuvette. An aliquot of the enzyme 5-(carboxymethyl)-2-hydroxymuconate isomerase, CHMI, (1 µL of an 8 mg/mL stock) was also added to each cuvette to convert **4** to **1**. The assay was initialized by the addition of a small quantity of **4** (20 – 210 µM) from a 10 or 35 mM stock solution made up in ethanol. The amount of enzyme in each 1-mL cuvette ranged from 15 nM to 13 µM.

Scheme 3

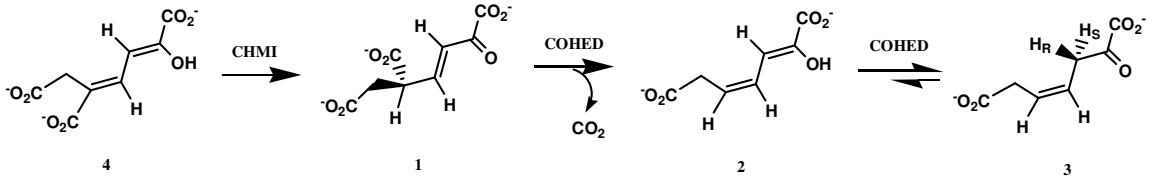

The enzyme kinetic assays using 2-hydroxy-2,4-heptadiene-1,7-dioate (HHDD, **2**, Scheme 3) as a substrate were performed in 20 mM Na_2HPO_4 buffer containing 5mM $MgCl_2$, pH 7.3, following the decrease in absorbance at 276 nm corresponding to the ketonization of HHDD (**2**, ε = 11,000 $M^{-1}cm^{-1}$) to **3**. An aliquot of enzyme (8 µL – 2 mL) was diluted into buffer (40 mL) and incubated for 1 h. Afterward, a 1 mL-portion of the diluted enzyme was transferred to a cuvette and assayed for activity by the addition of a

small quantity of substrate (20 – 210 μM) from a 10 or 35 mM stock solution made up in ethanol. The amount of enzyme in each 1-mL cuvette ranged from 3.0 nM to 5.8 μM. The chemical rate of ketonization (**2** to **3**, Scheme 4) was determined by following the decrease in absorbance at 276 nm for five different concentrations of **2**. The plot of change in absorbance at 276 nm versus substrate concentration gave a linear fit determination that was used to calculate the chemical rate at different substrate concentrations. The chemical rate of ketonization (**2** to **3**) was subtracted from the observed enzymatic rate.

Scheme 4

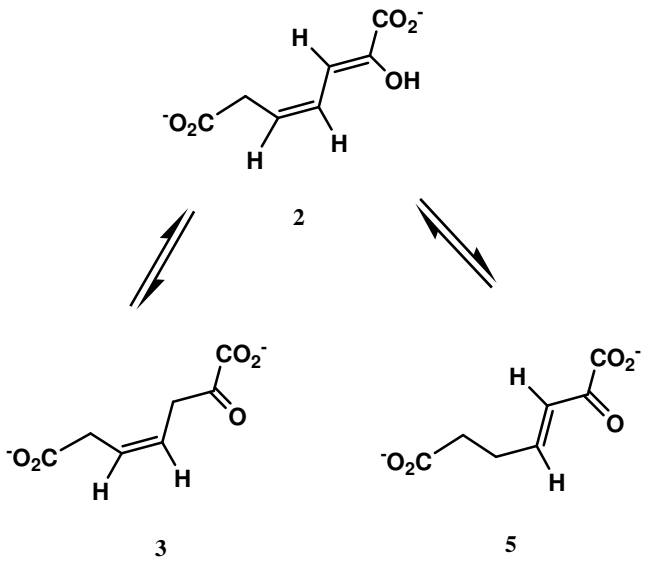

The enzyme kinetic assays using 2-hydroxy-2,4-pentadienoate (HPD, **6**, Scheme 5) as a substrate were performed in 20 mM Na_2HPO_4 buffer containing 5mM $MgCl_2$, pH 7.3, following the decrease in absorbance at 267 nm corresponding to the ketonization of

HPD (**6**, ε = 10,000 $M^{-1}cm^{-1}$) to **7**. An aliquot of enzyme (40 - 320 μL) was diluted into buffer (40 mL) and incubated for 1 h. Afterward, a 1 mL-portion of the diluted enzyme was transferred to a cuvette and assayed for activity by the addition of a small quantity

Scheme 5

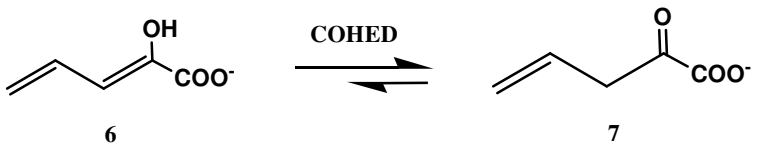

6 **7**

of substrate (20 – 240 μM) from a 10 or 40 mM stock solution made up in ethanol. The amount of enzyme in each 1-mL cuvette ranged from 470 nM to 2.9 μM. The chemical rate of ketonization (**6** to **7**, Scheme 6) was determined by following the decrease in absorbance at 267 nm for five different concentrations of **6**. The plot of change in absorbance at 267 nm versus substrate concentration gave a linear fit determination that was used to calculate the chemical rate at different substrate concentrations. The chemical rate of ketonization (**6** to **7**) was subtracted from the observed enzymatic rate.

Scheme 6

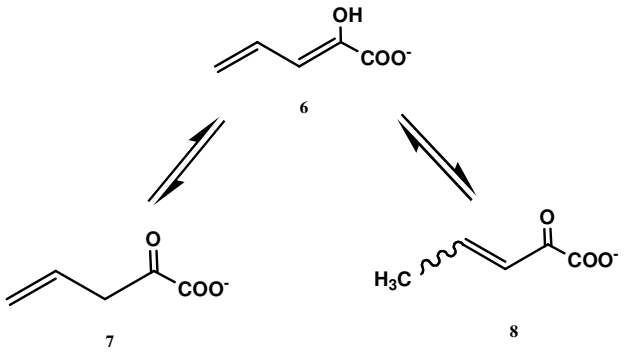

The enzyme kinetic assays using 2-oxo-3-hexenedioate (**10**, Scheme 7) as a substrate were performed in 20 mM Na_2HPO_4 buffer containing 5mM $MgCl_2$, pH 7.3, following the decrease in absorbance at 236 nm corresponding to the decarboxylation of **10** to **6**. An aliquot of enzyme (40-80 µL) was diluted into buffer (40 mL) and incubated for 1 h. Afterward, a 1 mL-portion of the diluted enzyme was transferred to a

Scheme 7

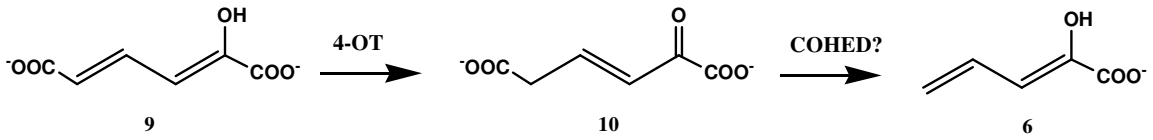

cuvette. An aliquot of the enzyme 4-oxalocrotonate tautomerase (4-OT, 1 µL of a 2 mg/mL stock) was also added to each cuvette to convert **9** to **10**. The assay was initiated by the addition of a small quantity of **9** (60 – 300 µM) from a 60 mM stock solution made up in ethanol. The amount of enzyme in each 1-mL cuvette ranged from 4.2 µM to 8.4 µM.

Kinetic parameters were determined by plotting initial rate of formation of **2** or **3** versus substrate concentration. Those data points were then fit by non-linear regression to give the V_{max} and K_m values (Figure 3.3). The V_{max} value was divided by the enzyme concentration in the cuvette to give the k_{cat} value.

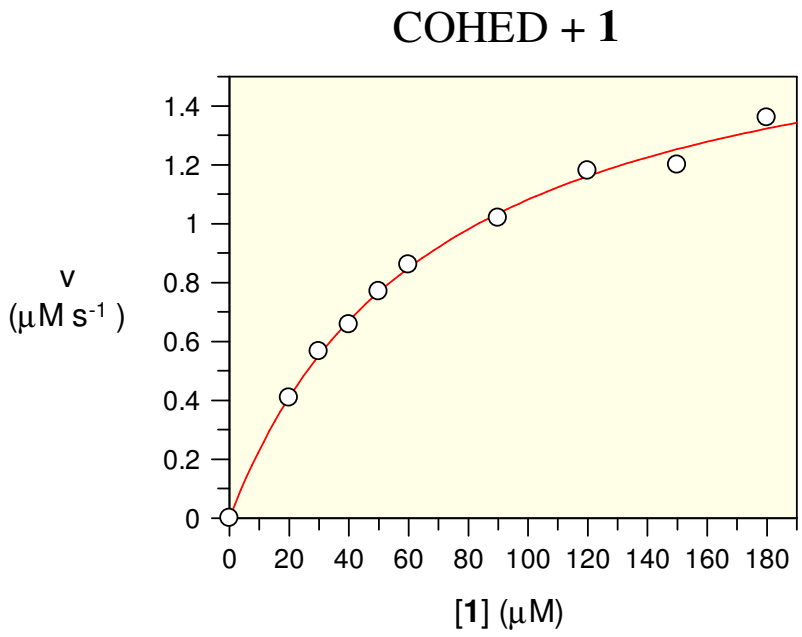

Parameter	Value	Std. Error
Vmax	1.83	0.05
Km	69.54	4.65

Enzyme Concentration – 15 nM ε_{236nm}= 4500 $M^{-1}cm^{-1}$

$$k_{cat} = \frac{1.83\ \mu M\ s^{-1}}{1.5 \times 10^{-2}\ \mu M} = 122\ s^{-1}$$

Figure 3.3. Michaelis-Menten plot for the COHED-catalyzed reaction converting **1** to **2** and sample calculation of kinetic parameters.

Mass Spectral Analysis of COHED. The mass of COHED was determined using an LCQ electrospray ion trap mass spectrometer (ThermoFinnigan, San Jose, CA),

housed in the Analytical Instrumentation Facility Core in the College of Pharmacy at the University of Texas at Austin. The protein (~1 mg/mL) was loaded onto a PD-10 Sephadex G-25 gel filtration column, which had previously been equilibrated with 100 mM NH_4HCO_3 buffer (pH 8.0). Using gravity flow, the protein was eluted in the same buffer. Fractions (0.5 mL) were analyzed for the presence of protein by UV absorbance at 215 nm. The appropriate fraction containing the purified protein was submitted for analysis by electrospray ionization mass spectrometry (ESI-MS).

*^{1}H NMR Spectroscopic Detection of **2** and **3***. An NMR tube contained an amount of **4** (4 mg, 0.02 mmol) dissolved in DMSO-d_6 (30 µL) and added to 100 mM Na_2HPO_4 buffer (0.6 mL, pH~9.2). The final pH of the solution was ~ 7. Subsequently, aliquots of COHED (100 µL of a 20 mg/mL solution in 20 mM Na_2HPO_4 buffer containing 5mM $MgCl_2$, pH 7.3) and CHMI (5 µL of an 8 mg/mL solution in 50 mM HEPES buffer, pH 7.3) were added to the reaction mixture. The concentration of **4** in the NMR tube was 19 mM. The spectrum was recorded after the reaction was allowed to go to completion (30 min). Samples of the three COHED mutants (K110Q-, E276Q-, and E278Q-COHED) were prepared separately. **2**: ^{1}H NMR (H_2O, 500 MHz) δ 2.95 (2H, d, H6), 5.52 (1H, m, H5), 6.09 (1H, d, H3), 6.22 (1H, dd, H4). **3**: ^{1}H NMR (H_2O, 500 MHz) δ 2.78 (2H, d, H6), 3.36 (2H, d, H3), 5.43 (1H, m, H4), 5.65 (1H, m, H5).

Effect of Metal Ions on the COHED Activity. The enzyme (~1 mg/mL) was purified without any metals added during the purification process. COHED was incubated for 15 min at 22 ºC in 20 mM MES buffer (pH ~6.0), which was made 10 mM in various metal ions ($CaCl_2$, $CoSO_4$, $MnCl_2$, $MgCl_2$, $ZnSO_4$, NaCl, KCl). In a separate

control experiment, the same concentration of COHED was incubated without any metal ion under otherwise identical conditions. Subsequently, an aliquot (1 µL) was removed, diluted 1000-fold into the assay buffer, and the specific activities were determined using the assay with a saturating concentration of **1** in 20 mM Na_2HPO_4 buffer, pH 7.3. The COHED activity was measured in the presence of the various metal ions (at 10 mM) as well as in the absence of these metal ions. The optimal Mg^{2+} concentration was determined by incubation of varying concentrations of $MgCl_2$ (25 µM – 10 mM) with enzyme for 10 min at 22 ºC and then assayed (using a saturating concentration of **1**) as described above.

Inhibition Studies of COHED. Stock solutions of substrate analogs and inhibitors were made up in 100 mM Na_2HPO_4 buffer, pH ~9.2. The addition of the inhibitor as a free acid to the buffer adjusted the pH of the aqueous stock solutions to ~7. The concentrations of the stock solutions were as follows: 2-oxo-1,7-heptadioate (**12**), 100 and 200 mM; 2-oxo-3-bromo-1,7-heptadioate (**13)** and 3-pentynoate (**14)**, 50 mM; 3-bromopyruvate (**15)** and 3-bromopropiolic acid (**16**), 100 mM (Figure 3.4).

A quantity of COHED (30 µL of a 1.5 mg/mL solution) was diluted into 30 mL of 20 mM Na_2HPO_4 buffer, 5 mM $MgCl_2$, pH 7.3, and allowed to equilibrate at 22 ºC for 1 h. The inhibitors were added to the enzyme stock solutions to give the desired final concentrations (0 – 400 µM). After a 5-min incubation period, 1-mL aliquots were removed and assayed in the presence of varying concentrations of **4** (40 – 400 µM). An aliquot of CHMI (1 µL of an 8 mg/mL stock) was also added to each cuvette to convert **4**

to **1**. In addition, another 1-mL aliquot was removed from some of the enzyme/inhibitor stock solutions and assayed in the presence of **2** (40 – 400 μM).

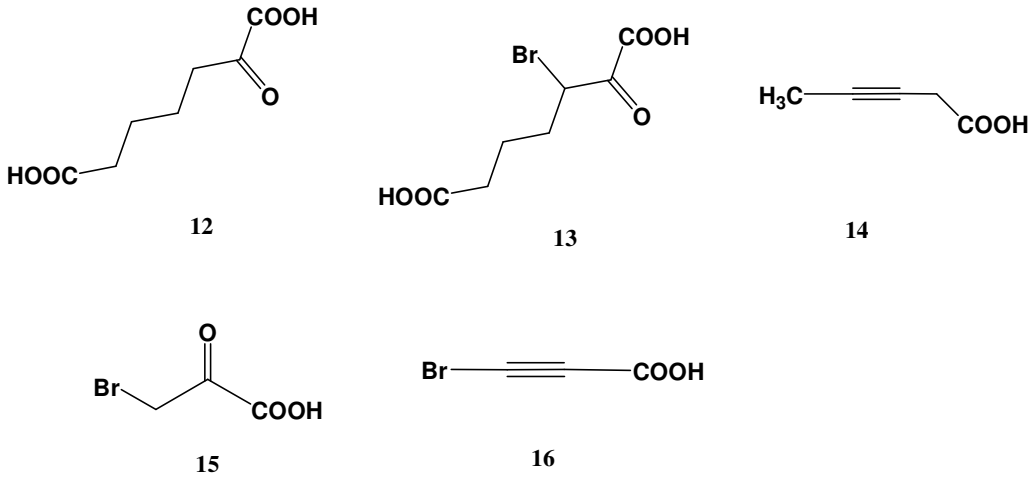

Figure 3.4. Potential Inhibitors of COHED as described in the text.

*COHED and K110Q-COHED-catalyzed Exchange of the C-3 Protons of 2-Oxo-1,7-heptadioate (**12**) with ^2H_2O.* Three separate reactions (0.6 mL) measuring the buffer-catalyzed, K110Q-COHED-catalyzed, and COHED-catalyzed rate of exchange of the proton at C-3 of 2-oxo-1,7-heptadioate (**12**) with ^2H_2O were performed in 100 mM $Na_2[^2H]PO_4$ buffer, pH ~9.2. The reactions were followed by ^1H NMR spectroscopy. The addition of **12** as the free acid dissolved in DMSO-d_6 (30 μL) to 100 mM $Na_2[^2H]PO_4$ buffer (0.6 mL, pH ~9.2) lowered the pH of each reaction to 7.1. The final concentration of **12** in each of the experiments was 23 mM and each of the ^1H NMR spectra was acquired at 5-min intervals for 2 h. In the experiment measuring the K110Q-COHED-catalyzed exchange, the reaction was initiated by the addition of enzyme (100

μL of a 20 mg/mL solution in 20 mM Na[$^2H_2$]PO_4 buffer, 5 mM $MgCl_2$, pH ~7). In the COHED-catalyzed exchange, the sample contained a given amount of enzyme (100 μL of a 24 mg/mL solution in 20 mM Na[$^2H_2$]PO_4 buffer, 5 mM $MgCl_2$, pH ~7). The intensity of the resonance observed at C-3 (δ = 2.56 ppm) was measured at timed intervals. The initial intensity of the resonance observed at 5 min was set equal to two protons. Subsequent measurements were divided by this initial intensity to give the fraction of the protons remaining. The observed rate constants were determined from a linear regression analysis of the data obtained from the decrease in the signal intensity as a function of time.

RESULTS

Construction, Expression, and Purification of K110Q-, E276Q-, E278Q-, and wild-type COHED. The K110Q, E276Q, and E278Q mutants of COHED were created by mutagenic primer-directed replication using the commercial mutagenesis QuikChange II Site-Directed Mutagenesis Kit. Each mutation was generated by the PCR using the plasmid pET24a-COHED as the template, the appropriate primers, and PCR reagents. The resulting constructs were sequenced to confirm that only the desired mutation had been introduced. The plasmid containing the mutant gene was then transformed into the *E. coli* strain BL21-Gold(DE3) and the gene was expressed, producing a soluble and active form of the protein. Purification of the recombinant protein involved a four-step protocol (using three columns), which typically provides 100 mg of purified protein (per liter of culture) for E276Q-, E278Q-COHED, and COHED. However, the K110Q-COHED mutant yielded ~15 mg of homogeneous enzyme per liter of culture. Analysis by SDS-PAGE gave a single band at 47 kDa. COHED was analyzed by ESI-MS and the spectrum showed a single peak corresponding to a mass of 47096 ± 2 Da (calculated 47108 Da).

*Kinetic Properties of COHED with **1**, **2**, and **6**.* The kinetic parameters for COHED and the corresponding mutants (K110Q-, E276Q-, and E278Q-COHED) were determined for the decarboxylation of **1** (Figures 3.5-3.8). All four enzymes show activity using **1** and the kinetic parameters are listed in Table 3.1. Wild-type COHED has a K_m value of 66 ± 4 μM and a k_{cat} value of 120 ± 3 s^{-1}. This results in a $k_{cat}/K_m = 1.8 \times 10^6$ $M^{-1}s^{-1}$. The E276Q-COHED mutant shows an 1800-fold decrease in k_{cat}, a 3-fold

increase in K_m, and a 5300-fold decrease in k_{cat}/K_m. The E278Q-COHED mutant shows a 2800-fold decrease in k_{cat}, a 3-fold decrease in K_m, and a 900-fold decrease in k_{cat}/K_m. The K110Q-COHED mutant shows the smallest changes in the kinetic parameters with all values being just slightly lower than those observed for wild-type.

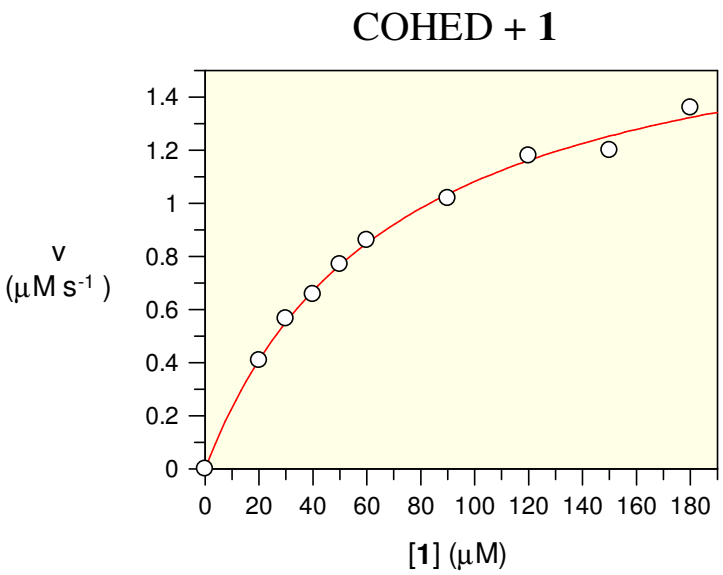

Figure 3.5. Michaelis-Menten plot for the initial rate of formation of **2** versus substrate concentration for the COHED-catalyzed reaction converting **1** to **2**.

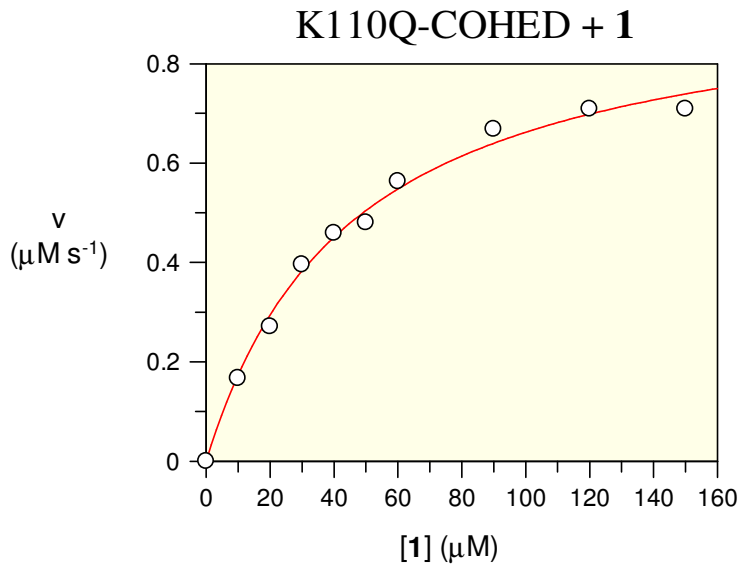

Figure 3.6. Michaelis-Menten plot for the initial rate of formation of **2** versus substrate concentration for the K110Q-COHED-catalyzed reaction converting **1** to **2**.

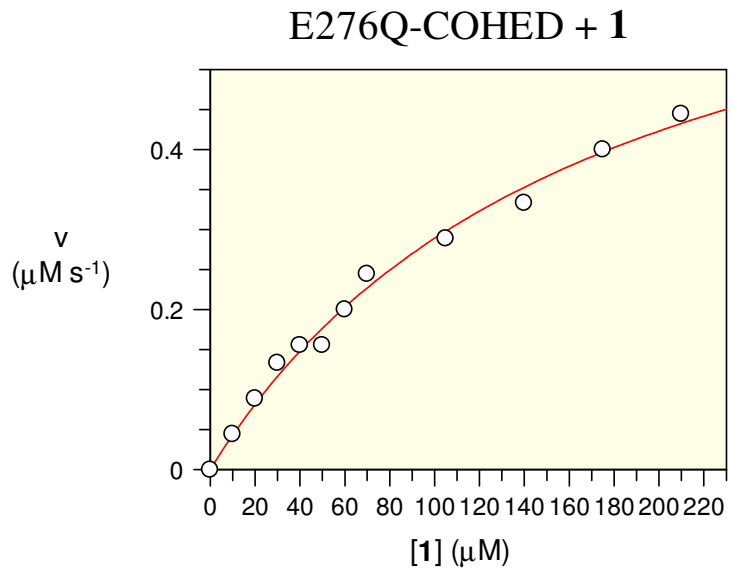

Figure 3.7. Michaelis-Menten plot for the initial rate of formation of **2** versus substrate concentration for the E276Q-COHED-catalyzed reaction converting **1** to **2**.

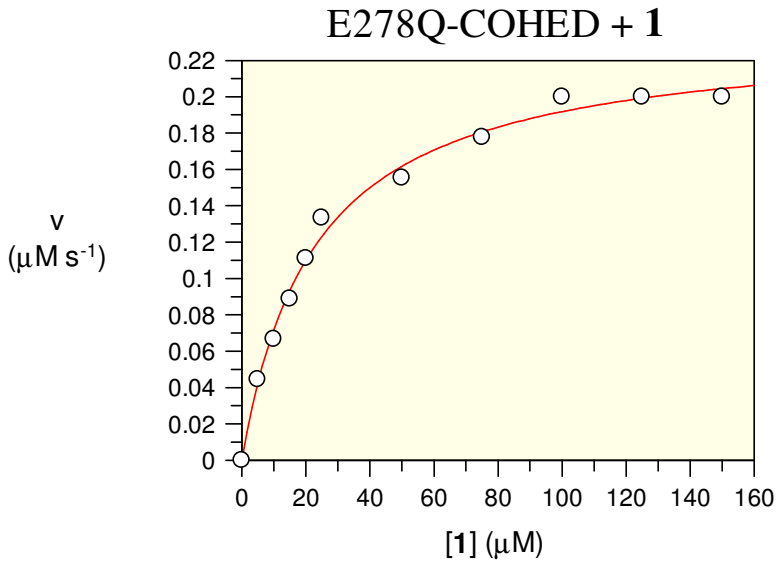

Figure 3.8. Michaelis-Menten plot for the initial rate of formation of **2** versus substrate concentration for the E278Q-COHED-catalyzed reaction converting **1** to **2**.

Table 3.1: Kinetic Parameters for COHED and corresponding mutants with 1

Enzyme	k_{cat} (s^{-1})	K_m (μM)	k_{cat}/K_m ($M^{-1}s^{-1}$)
COHED	120 ± 3	66 ± 4	$1.8\times10^6 \pm 1.2\times10^5$
K110Q-COHED	87 ± 5	50 ± 6	$1.7\times10^6 \pm 2.2\times10^5$
E276Q-COHED	0.067 ± 0.004	199 ± 30	340 ± 63
E278Q COHED	0.042 ± 0.0005	21 ± 1	2000 ± 143

The rate of ketonization of **2** to **3** by COHED and the corresponding mutants (K110Q-, E276Q-, and E278Q-COHED) was measured by following the loss in absorbance at 276 nm (Figures 3.9-3.13). All four enzymes show activity using **2** and the kinetic parameters are shown in Table 3.2. Wild-type COHED has a k_{cat} value of 360 ± 13 s^{-1} and a K_m value of 62 ± 8 μM resulting in a $k_{cat}/K_m = 5.8 \times 10^6$ $M^{-1}s^{-1}$. E276Q-COHED shows a 1400-fold decrease in k_{cat}, a 2-fold decrease in K_m, and k_{cat}/K_m is reduced by 730-fold. The E278Q-COHED mutant shows a 2600-fold decrease in k_{cat}, a slight decrease in K_m, and a 1700–fold decrease in k_{cat}/K_m. The K110Q-COHED mutant exhibits a 2-fold decrease in k_{cat}, a slight decrease in K_m, and a 1.5-fold decrease in k_{cat}/K_m.

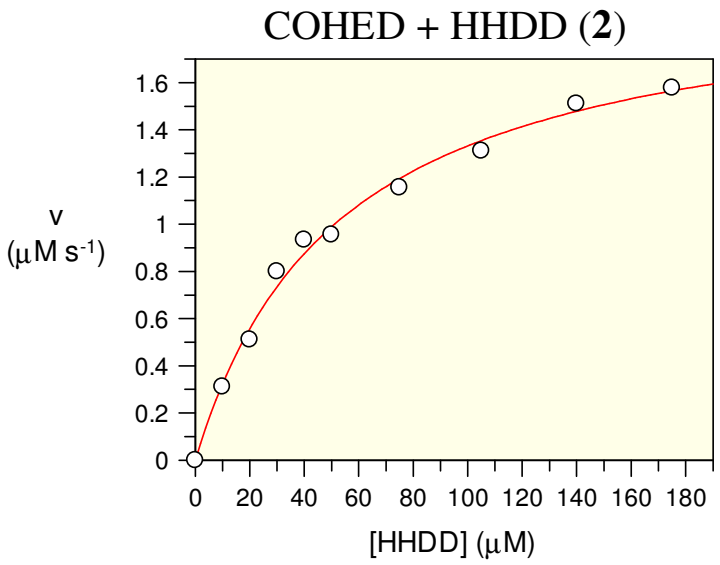

Figure 3.9. Michaelis-Menten plot for the initial rate of formation of **3** versus substrate concentration for the COHED-catalyzed reaction converting **2** to **3**.

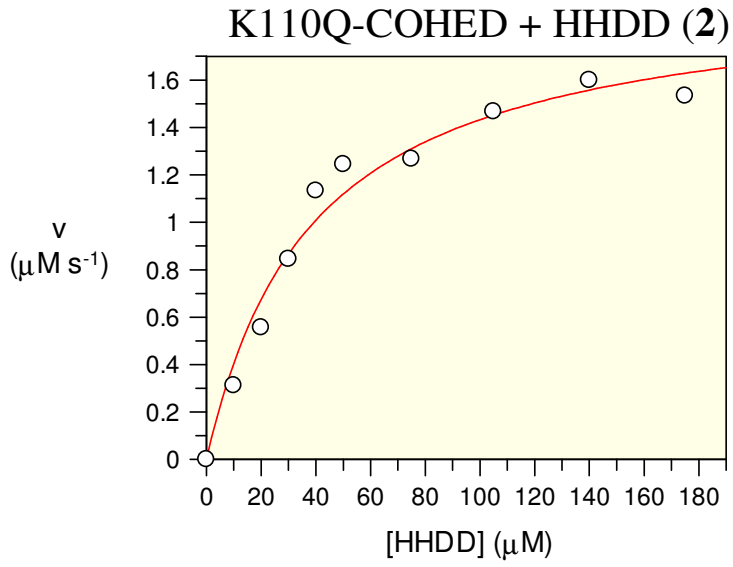

Figure 3.10. Michaelis-Menten plot for the initial rate of formation of **3** versus substrate concentration for the K110-COHED-catalyzed reaction converting **2** to **3**.

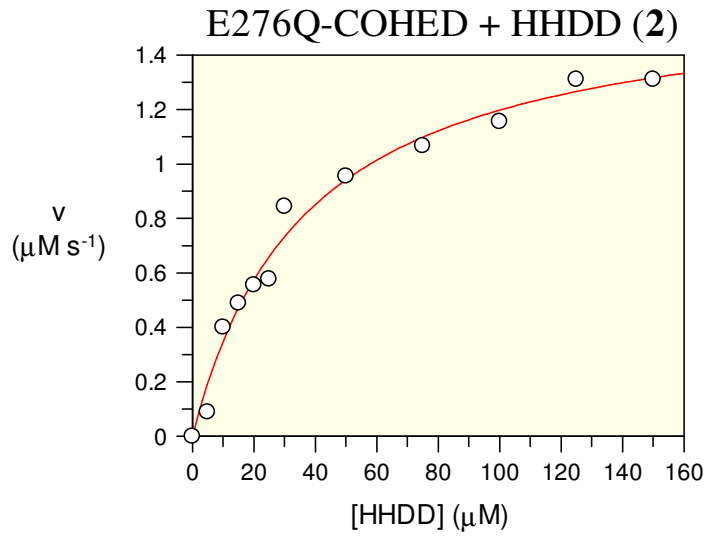

Figure 3.11. Michaelis-Menten plot for the initial rate of formation of **3** versus substrate concentration for the E276Q-COHED-catalyzed reaction converting **2** to **3**.

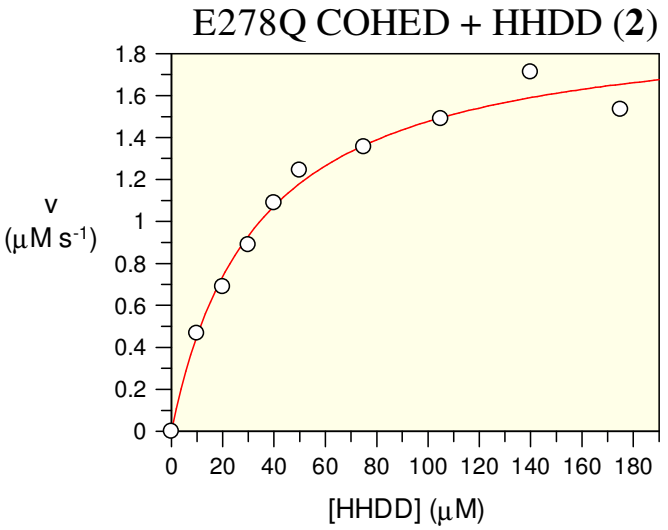

Figure 3.12. Michaelis-Menten plot for the initial rate of formation of **3** versus substrate concentration for the E278Q-COHED-catalyzed reaction converting **2** to **3**.

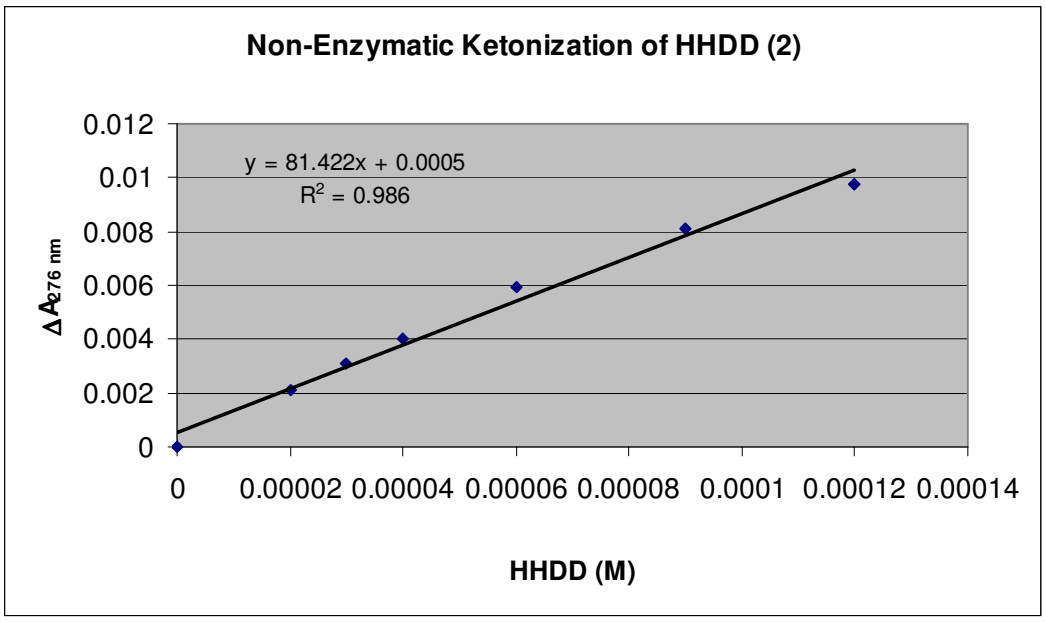

Figure 3.13. Plot of the non-enzymatic change in absorbance at 276 nm versus substrate concentration with a linear fit determination for the 1,3-keto-enol tautomerization of HHDD (**2**) to **3**.

Table 3.2: Kinetic Parameters for COHED and corresponding mutants with 2

Enzyme	k_{cat} (s^{-1})	K_m (μM)	k_{cat}/K_m ($M^{-1}s^{-1}$)
COHED	360 ± 13	62 ± 8	$5.8\times10^6 \pm 1.1\times10^6$
K110Q-COHED	190 ± 12	50 ± 7	$3.7\times10^6 \pm 6.0\times10^5$
E276Q-COHED	0.26 ± 0.01	33 ± 4	7900 ± 1300
E278Q COHED	0.14 ± 0.006	41 ± 5	3400 ± 550

The kinetic parameters for COHED and the corresponding mutants (K110Q-, E276Q-, and E278Q-COHED) for the ketonization of the alternate substrate **6** to **7** (Scheme 5) were measured by following the loss in absorbance at 267 nm (Figures 3.14-

3.16). Only wild-type COHED and the K110Q-COHED mutant show activity using **6**. The kinetic parameters are shown in Table 3.3. Wild-type COHED has a k_{cat} value of 0.93 ± 0.05 s^{-1} and a K_m value of 46 ± 6 μM resulting in a $k_{cat}/K_m = 2.0 \times 10^4$ $M^{-1}s^{-1}$. The K110Q-COHED mutant shows only a slight decrease in k_{cat}, a 2-fold increase in K_m, and a 3-fold decrease in k_{cat}/K_m. The E276Q- and E278Q-COHED mutants had no measurable activity with **6**.

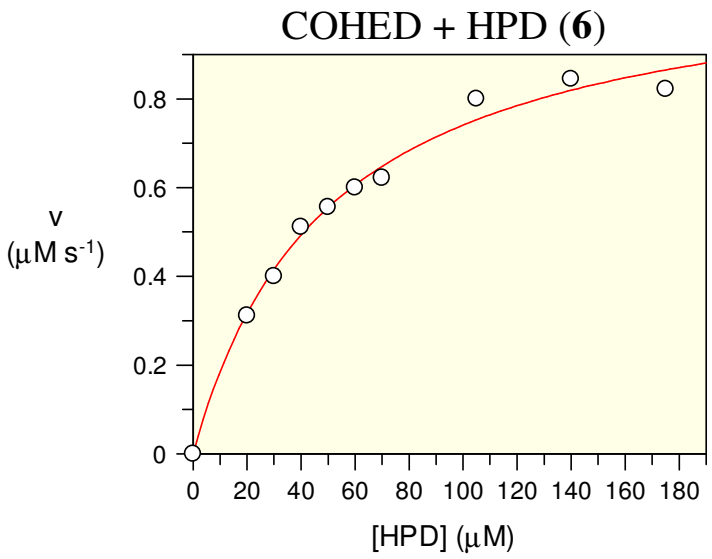

Figure 3.14. Michaelis-Menten plot for the initial rate of formation of **7** versus substrate concentration for the COHED-catalyzed reaction converting **6** to **7**.

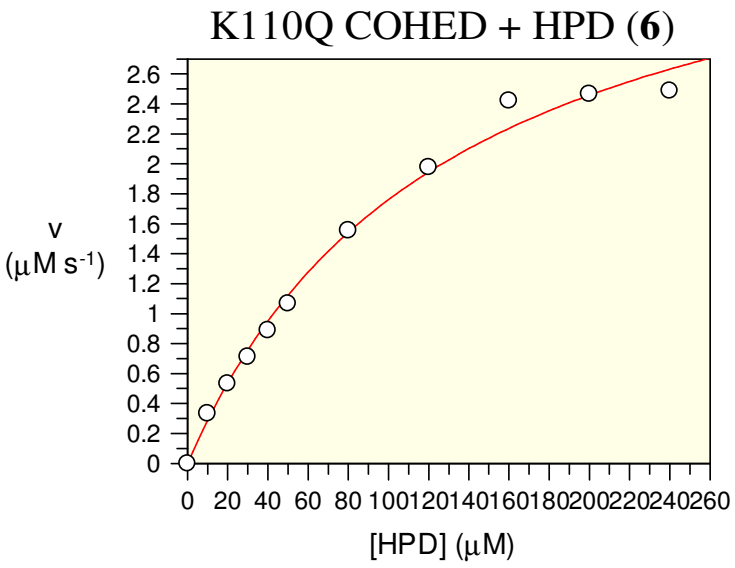

Figure 3.15. Michaelis-Menten plot for the initial rate of formation of **7** versus substrate concentration for the K110Q-COHED-catalyzed reaction converting **6** to **7**.

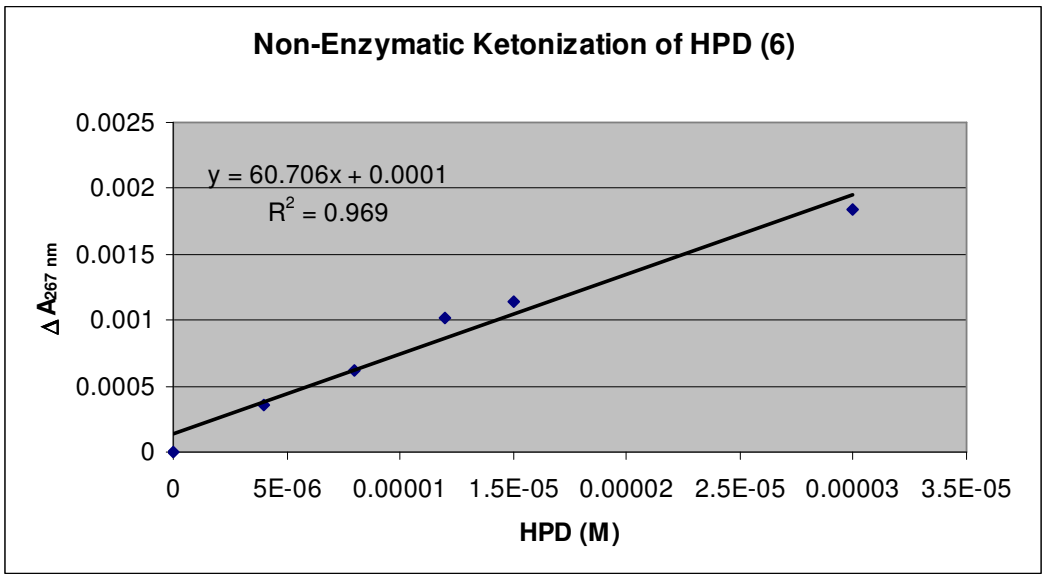

Figure 3.16. Plot of the non-enzymatic change in absorbance at 267 nm versus substrate concentration with a linear fit determination for the 1,3-keto-enol tautomerization of HPD (**6**) to **7**.

Table 3.3: Kinetic Parameters for COHED and corresponding mutants with 6

Enzyme	k_{cat} (s^{-1})	K_m (μM)	k_{cat}/K_m ($M^{-1}s^{-1}$)
COHED	0.93 ± 0.05	46 ± 6	$2.0\times10^4 \pm 3.1\times10^3$
K110Q-COHED	0.62 ± 0.05	100 ± 20	6200 ± 1500
E276Q-COHED	No activity		
E278Q COHED	No activity		

COHED and the three mutants (K110Q-, E276Q-, and E278Q-COHED) were tested for activity using **10** (Scheme 7). Neither the wild-type enzyme nor the mutants showed any decarboxylase activity after a 4-hr incubation period with **10**.

Activity of COHED with Metal Ions. The specificity of COHED for metals was examined. The decarboxylase activity of COHED using **1** was measured in the presence

of Mg^{2+}, Mn^{2+}, Ca^{2+}, Zn^{2+}, and Co^{2+}. No activity was observed when COHED was incubated with Na^{+} and K^{+} (Table 3.4 and Figure 3.17). COHED showed the highest decarboxylase activity using Mg^{2+} and Zn^{2+}. The optimal metal ion concentration for COHED activity was determined by incubating COHED with varying concentrations of $MgCl_2$ (25 μM – 10 mM). The lowest concentration of Mg^{2+} ion required to give full activity was ~1 mM with a K_m value for Mg^{2+} binding of 342 μM (Figure 3.18).

Table 3.4: Relative Activity of COHED with different metal ions

Metal (10mM)	Relative Activity (U/mg)
Mg^{2+}	60
Mn^{2+}	36
Ca^{2+}	24
Zn^{2+}	80
Co^{2+}	26
Na^{+}	No activity
K^{+}	No activity

COHED - 1.3×10^{-3} mg mL^{-1} $\varepsilon_{236} = 4500\ M^{-1}cm^{-1}$

$$A = \varepsilon l c$$

$$\Delta c = \frac{\Delta A}{\varepsilon * l} = \frac{0.0059\ Au\ s^{-1}}{4500\ M^{-1}cm^{-1} * 1cm} = 1.31 \times 10^{-6}\ M\ s^{-1}$$

$$1.31\ \mu mol\ L^{-1}\ s^{-1} \left(\frac{1\ L}{1000\ mL}\right)\left(\frac{60\ s}{1\ min}\right) = 0.079\ \mu mol\ mL^{-1}\ min^{-1}$$

$$\frac{0.079\ \mu mol\ mL^{-1}\ min^{-1}}{1.3 \times 10^{-3}\ mg\ mL^{-1}} = 60\ U\ mg^{-1}$$

Figure 3.17 Sample calculation of relative activity determination for COHED when incubated with **1** (saturation conditions) and 10 mM Mg^{2+}. The calculation uses Beer's Law where A is absorbance, ε is molar absorbtivity, l is path length of the sample, and c is the concentration of substrate.

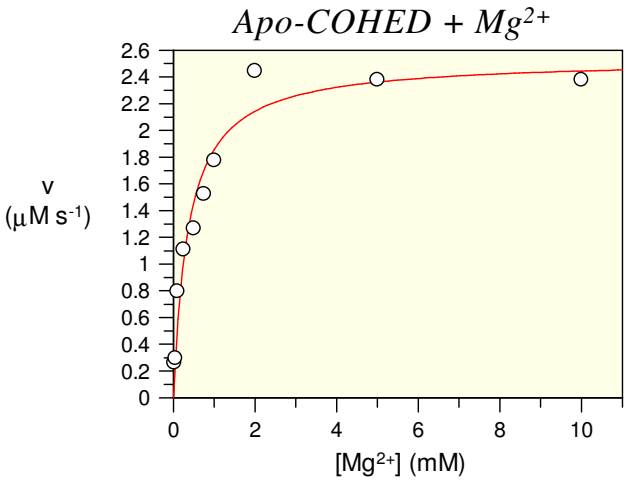

Figure 3.18 Michaelis-Menten plot for the initial rate of formation of **3** versus Mg^{2+} concentration for the COHED-catalyzed reaction converting **1** to **3**.

*Inhibition Studies of COHED with **12-16**.* Five compounds were examined as potential inhibitors of COHED. The first compound was 2-oxo-1,7-heptadioate (**12**, Figure 3.4), the alkane equivalent of **3**, which could act as a competitive inhibitor. In this experiment 1.5 µg/mL (32 nM) of COHED was incubated with varying concentrations of **12** (0 – 300 µM), and COHED activity was measured with **1**. As the concentration of **12** increased the initial rate decreased. The data were fit with a non-linear regression analysis and shows that **12** is a competitive inhibitor with a K_i value of 86 µM (Figure 3.19).

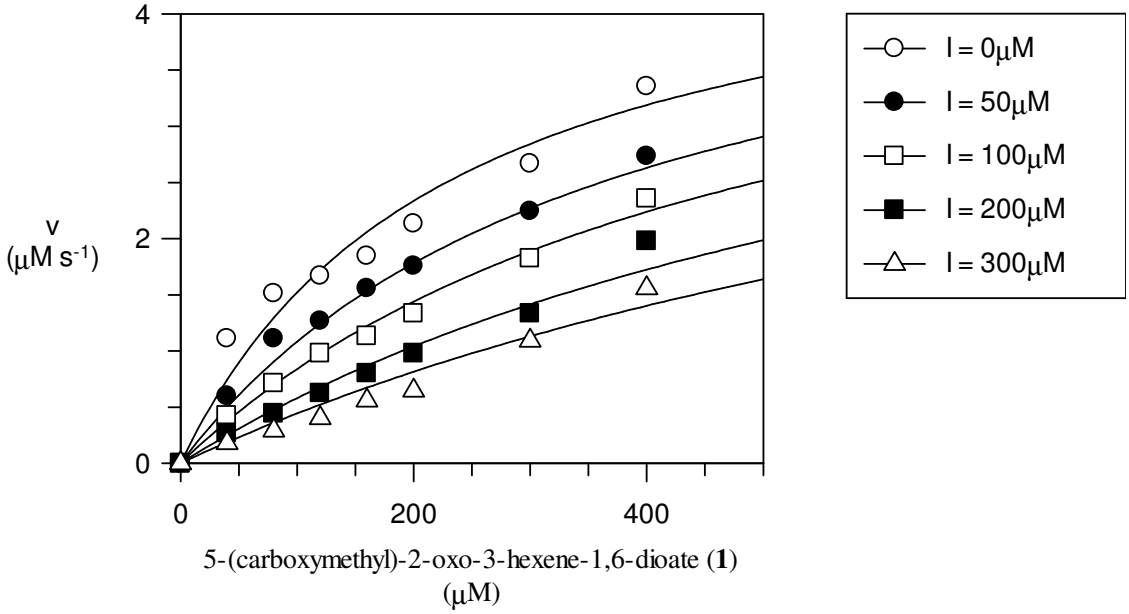

Figure 3.19. Competitive inhibition kinetics of COHED with **12**. Michaelis-Menten plot of the initial rate of formation of **3** versus substrate concentration for the COHED-catalyzed reaction converting **1** to **3**. The reaction mixtures were incubated with varying concentrations of **12.**

A potential mechanism-based inhibitor, 3-bromopropiolic acid (**16**, Figure 3.4) (12) was also examined. A hydration reaction converts 3-bromopropiolic acid (**16**) to a species that inactivates *trans*-3-chloroacrylic acid dehalogenase (CaaD). Hydration generates a potent acylating agent that forms a covalent bond with the active site Pro-1 (Scheme 8) (8).

Scheme 8

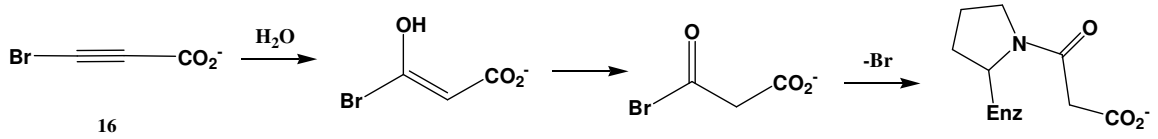

16

In this experiment 1.5 µg/mL (32 nM) of COHED was incubated with varying concentrations of **16** (0 – 400 µM). COHED activity was measured with **1** and **2**, separately, after a 5-min incubation period and then after an overnight incubation period. COHED was not inhibited by **16** and retained full activity after the incubation period.

An additional set of experiments examined the effects of three other compounds (**13-15**, Figure 3.4) on COHED. Accordingly, COHED (1.5 µg/mL [32 nM]) was incubated with varying concentrations (0 – 400 µM) of each compound. COHED activity was measured with **1** and **2**, separately, after a 5-min incubation period and then after an overnight incubation period. 2-Oxo-3-bromo-heptandioate (**13**) was found to have comparable kinetic values to those measured for **12**. As the concentration of **13** increased the initial rate decreased. The preliminary data were fit with a non-linear regression analysis that suggests a competitive nature of the inhibition (Figure 3.20).

Thus, **13** may also be a competitive inhibitor of COHED. COHED (1 mg, 16 μM) was incubated with an excess amount of **13** (4 mg, 12 mM [253 Da]) and the remaining

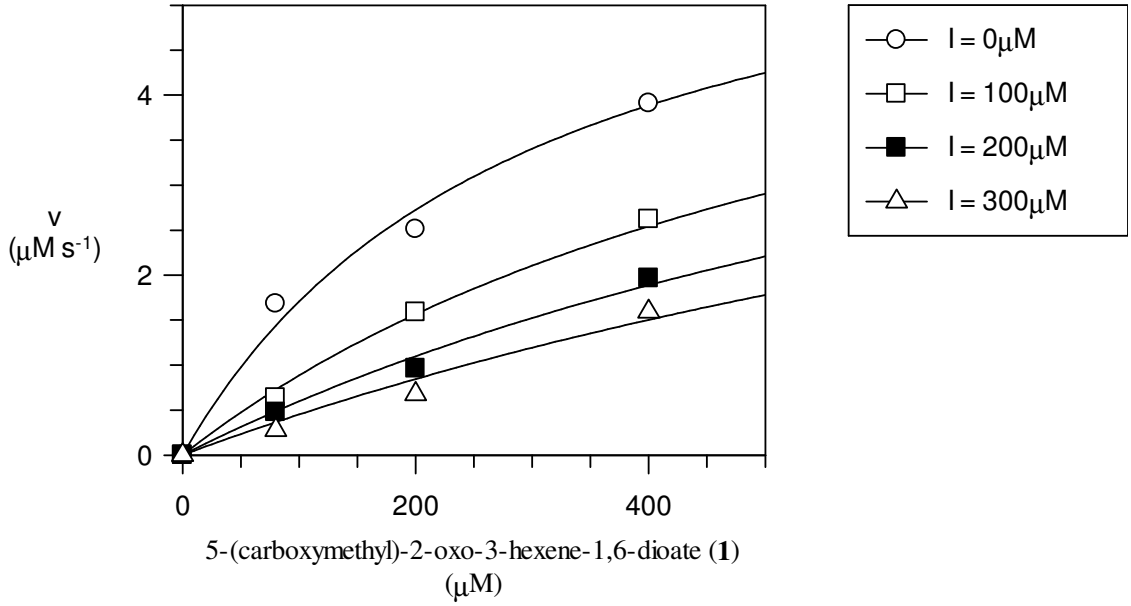

Figure 3.20. Competitive inhibition kinetics of COHED with **13**. Michaelis-Menten plot of the initial rate of formation of **3** versus substrate concentration for the COHED-catalyzed reaction converting **1** to **3**. The reaction mixtures were incubated with varying concentrations of **13.**

enzymatic activity was determined. Irreversible inhibition by **13** could result from the attack of an active-site nucleophile at the C-3 position displacing the bromine in an S_N2-type reaction. The mass spectrometry data showed a mass of 47096 Da for COHED and a mass of 47168 Da for COHED and **13**, after an overnight incubation period. The difference is 72 Da. This difference does not correspond to any mass associated with the

incorporation of **13** (173 Da, loss of bromine) or of a cleavage product of **13** bound to the enzyme. After the COHED/**13** incubation mixture was diluted 1000-fold, COHED still had full activity.

In another experiment 1.5 μg/mL (32 nM) of COHED was incubated with varying concentrations of 3-pentynoate, **14** (0 – 200 μM). COHED activity was measured with **1** and **2**, separately, after a 5-min incubation period and then after an overnight incubation period. COHED was not inhibited by **14** and retained full activity after the incubation period.

In this last inhibition study COHED (1 mg, 16 μM) was incubated with an excess amount of 3-bromopyruvate (**15**, 4 mg, 19 mM [167 Da]) and the remaining enzymatic activity was determined. Irreversible inhibition by **15** could result from the attack of an active-site nucleophile at the C-3 position displacing the bromine in an S_N2-type reaction. The mass spectrometry data for COHED with **15** were inconclusive. After the COHED/**15** incubation mixture was diluted 1000-fold, COHED still retained full activity after the incubation period.

*COHED and K110Q-COHED-catalyzed Exchange of the C-3 Protons of **12** with ^2H_2O.* The exchange of the C-3 protons for deuterons of the alternate substrate, **12**, was followed by ^{1}H NMR spectroscopy in the presence of COHED, K110Q-COHED, and in the absence of enzyme (Scheme 9). The decrease in signal intensity at 2.58 ppm as a function of time followed a first-order rate of decay for each process (Figure 3.21).

Scheme 9

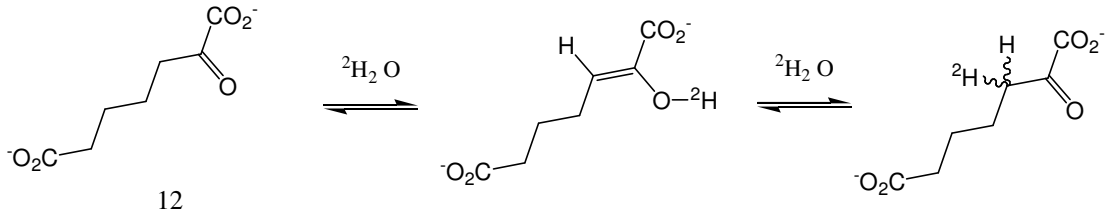

12

The signal at 2.56 ppm corresponds to the C-3 proton (7). For the nonenzymatic process, the rate was 0.0014 min^{-1} (in 100 mM $Na_2[^2H]PO_4$ buffer, pH 7.2). For the COHED-catalyzed process, the rate was 0.0039 min^{-1} (using 70 µM of COHED). The K110Q mutant had a rate of 0.0017 min^{-1} (using 60 µM of K110Q- COHED). Hence, the

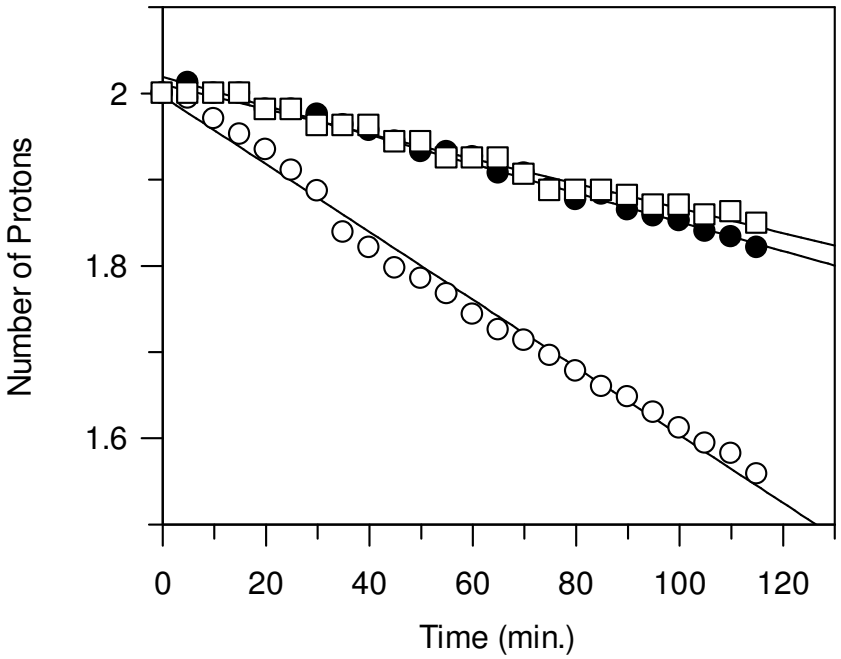

Figure 3.21. Rate of the buffer-, K110Q-COHED-, and COHED catalyzed C-3 proton exchange with solvent deuterons of 2-oxo-1,7-heptadioate (**12**). Each time point of the buffer-catalyzed exchange (open squares), K110Q-COHED catalyzed exchange (filled circles), and COHED catalyzed exchange (open circles) represents the fraction of protons remaining at C-3 of **12**.

COHED-catalyzed rate is 3-fold faster than the rate for the nonenzymatic and K110Q-COHED reactions (which are essentially the same). The K110Q mutation eliminates the ability of COHED to exchange the C-3 proton. COHED clearly accelerates the exchange, which is consistent with an enzyme-catalyzed enolization and subsequent ketonization at C-2 (Scheme 9).

DISCUSSION

The structure of COHED shows two separate domains, the C-terminal (residues 221-429) and the N-terminal (residues 1-200). It is proposed that decarboxylation of **1** takes place in the C-terminal domain and the ketonization of **2** occurs in the N-terminal domain (4). The two domains share 34% sequence identity with highly similar structures, including a central cavity located at equivalent positions within each domain.

The C-terminal and N-terminal domains of COHED can be superpositioned with the two catalytic C-terminal domains of the FAH homodimer with an rms deviation of 0.65Å for 46 select residues surrounding the FAH active site (4). FAH was crystallized with product (fumarate and acetoacetate) bound in the active sites of the C-terminal domains (12). Thus, the structural overlap of FAH and COHED allowed residues in the substrate binding site of FAH to be compared with equivalent residues in COHED. The C-terminal domain of COHED has a triad of carboxyl groups coordinated to the Ca^{2+} ion (similar to the metal binding site of FAH), while the N-terminal domain did not contain a bound metal ion (4). The decarboxylase activity of COHED is reported to be magnesium dependent, and the protein loses activity in the absence of magnesium (3, 6). Hence, the metal binding domain (C-terminal domain) was postulated as the site of decarboxylase activity, while the N-terminal domain would catalyze the ketonization reaction.

COHED catalyzes the decarboxylation of a vinylogous analog of a β–keto acid. The general mechanism for β–decarboxylases involves a metal ion or Schiff base formation (13, 14). The formation of a Schiff base lowers the energy of decarboxylation by permiting facile protonation of the nitrogen (an imine, **18**, Scheme 10). The

protonated nitrogen atom acts as an electron sink drawing electron density towards itself during the decarboxylation reaction. One example of Schiff base catalysis is that of acetoacetate decarboxylase, which catalyzes the decarboxylation of acetoacetic acid (**17**) to acetone and carbon dioxide (Scheme 10) (14, 15). Based on previous studies, a Schiff base mechanism has been ruled out for COHED because there is no loss of activity upon incubation with substrate (**1**) and $NaBH_4$, and no incorporation of ^{18}O in **3** (at C-2) when the reaction is carried out in $H_2{}^{18}O$ (Johnson, W.H., Jr. and Whitman, C.P., unpublished).

Scheme 10

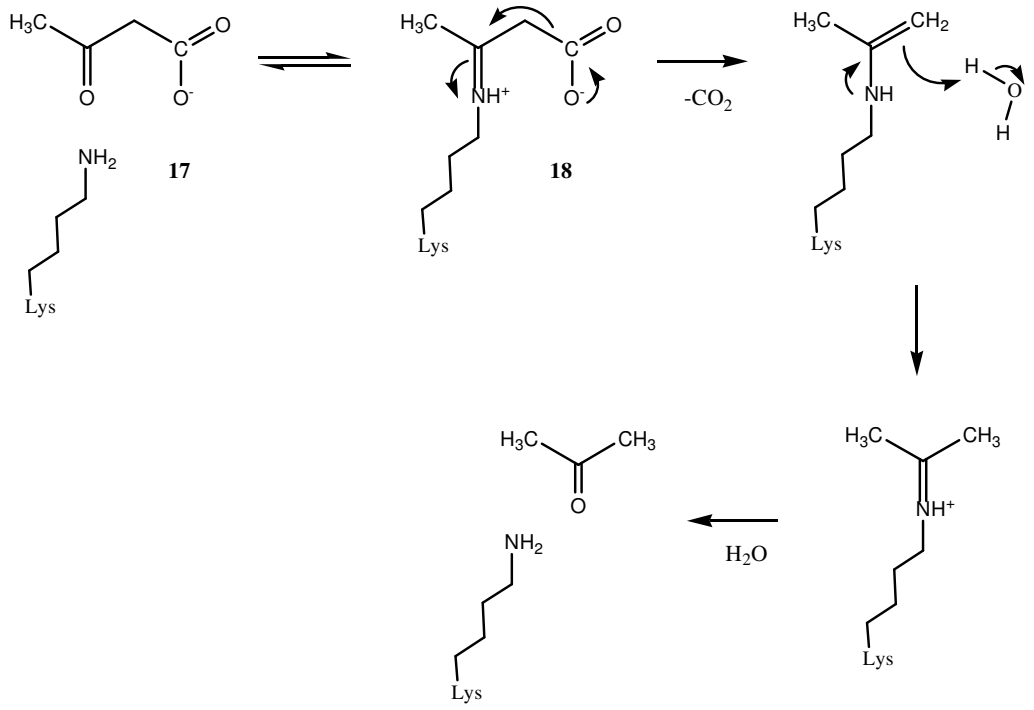

The second type of mechanism for β–decarboxylases requires a metal ion cofactor to assist in catalysis. The metal ion electrostatically stabilizes the incipient negative

charge and helps orient the substrate in a conformation that is catalytically favorable. An example of this type of metal-dependent catalysis involves the decarboxylation of (*S*)-α-acetolactate (**19**) by α-acetolactate decarboxylase to give (*R*)-acetoin (**20**, Scheme 11). The Mg^{2+} ion stabilizes the formation of the enol intermediate and positions it for catalysis, followed by ketonization at C-2 to generate an inversion of stereochemistry at C-3 in the product (**20**) (16). COHED, as a metal-dependent decarboxylase, may catalyze

Scheme 11

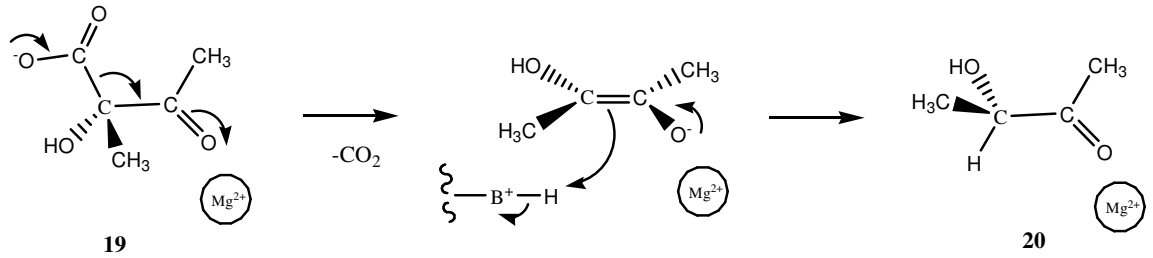

a similar reaction. Upon decarboxylation, the C-2 carbonyl of **1** could stabilize the incipient carbanion by forming the corresponding enolate intermediate (Scheme 12). The resulting negative charge of the enolate would be stabilized by electrostatic interaction with the metal ion cofactor (Mg^{2+}). Subsequent ketonization of **2** would protonate the C-3 position of **3**. Although some mechanistic and stereochemical studies have been carried out (1-3) and the COHED crystal structure (with only Ca^{2+} bound) has been solved (4), the identity of the active site residues that participate in the chemistry remain unknown. These results shed light on the two domains in COHED and identified potential active site residues that function in the conversion of **1** to **3**.

Scheme 12

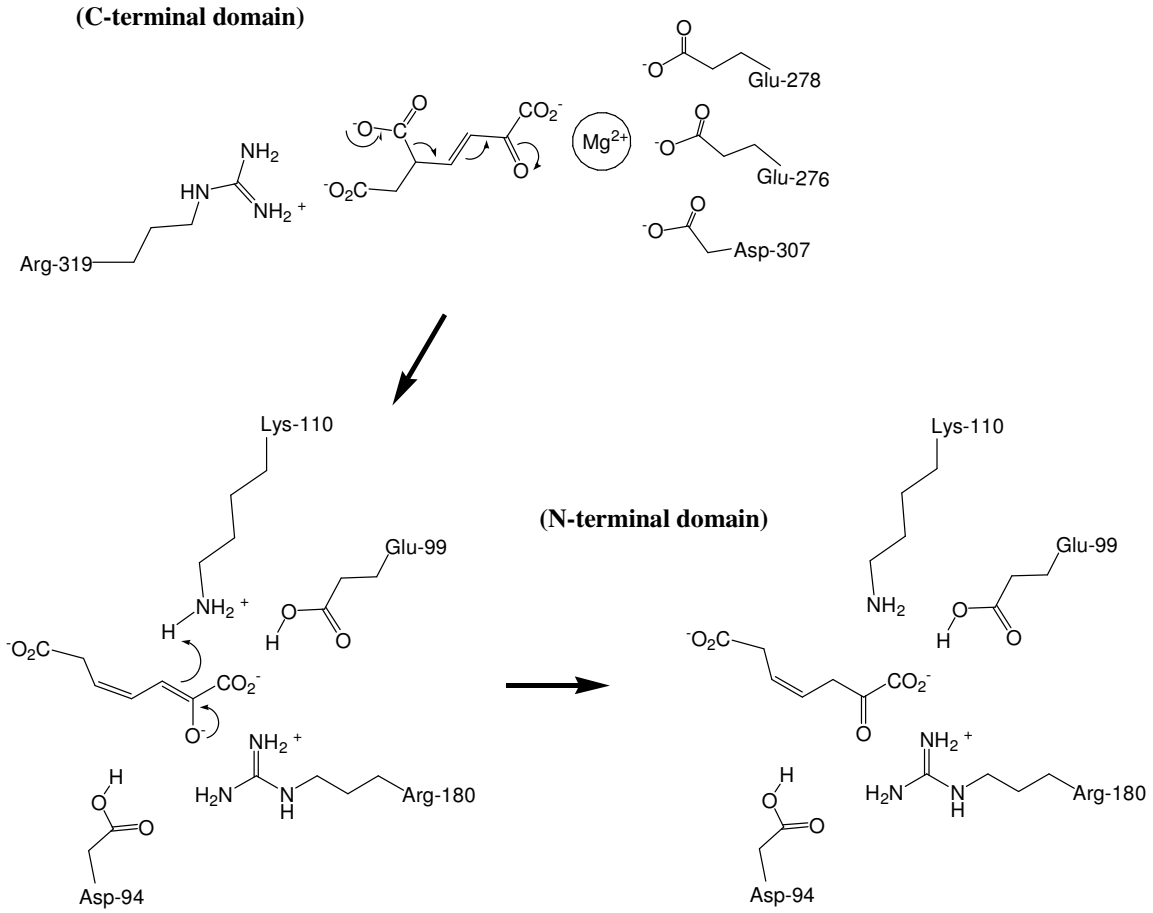

The gene for COHED was used as a template in generating the three active site mutants: K110Q-COHED, E276Q-COHED, and E278Q-COHED. The corresponding mutants were analyzed for their effects on the overall reaction as well as the possibility of uncoupling the catalytic steps (i.e. decarboxylation of **1** to **2** and the ketonization of **2** to **3**). By mutating either Glu-276 or Glu-278, two potential metal binding ligands in the C-terminal domain, the decarboxylation reaction might be affected while the ketonization (**2** to **3**) could remain unchanged. The kinetic parameters for the E276Q and E278Q

mutants were determined and showed greatly reduced activity for both reactions when examined with **1** and **2**. The only large difference in K_m value was observed for the E276Q mutant with **1** which yielded a value 3-fold higher than that of wild-type. From these results it can be concluded that both Glu-276 and Glu-278 are essential for activity.

Since Glu-276 and Glu-278 may be part of the metal binding site in COHED, these results indicate that without effective binding of the metal ion within the active site of the C-terminal domain neither the decarboxylation reaction nor the 1,3-keto-enol tautomerization reaction (postulated as being in the N-terminal domain) can be effectively catalyzed. Consequently, these results suggest that the reactions do not take place in separate domains. The metal ion may interact with the C-1 carboxylate group of **1** positioning it in the correct orientation for effective decarboxylation. Thus, without the bound metal ion the carboxylate group may not be positioned in an orientation conducive to decarboxylation. The metal ion may also play a role in polarizing the C-2 carbonyl group, so a loss of the metal ion would eliminate the inductive effect of withdrawing electron density from C-5 and reduce the rate of decarboxylation (Scheme 12).

Despite these initial observations with E276Q- and E278Q-COHED, two separate catalytic domains may still exist. The missing metal ion may affect the structural conformation of COHED preventing active-site residues in either domain from proper interaction with the substrates (**1** or **2**). Thus, without proper binding of the metal ion neither domain may be capable of catalyzing its specific reaction.

A metal ion is critical for COHED activity. In a related set of studies, the importance of metal specificity was determined for COHED with a number of divalent and monovalent metal ions. These metal studies demonstrated a preference for divalent metal ions with Zn^{2+} and Mg^{2+} having comparable relative activities when incubated with COHED. The optimal concentration of Mg^{2+} ion required for full activity was ~1 mM.

The role of the third potential active site residue Lys-110 (N-terminal domain) in the mechanism was investigated by analyzing the kinetic properties of the K110Q mutant. K110Q-COHED showed only a 1-2-fold decrease in k_{cat} and K_m values for both **1** and **2**. A substrate analog, **12**, was also examined with K110Q-COHED and COHED. When COHED is incubated with varying concentrations of **12** it was found to be a competitive inhibitor, indicating binding at the active site. However, when the COHED reaction was carried out in ^2H_2O the ^1H NMR spectrum showed an accelerated rate of deuterium exchange at the C-3 position. Thus, **12** is actually a substrate analog for COHED. The K110Q-mutant and the non-enzymatic reaction show the same rate of exchange. Hence, these studies show that Lys-110 is responsible for proton exchange at the C-3 position of **12**. If these results are an indication of how COHED interacts with **2**, then the results show evidence for an uncoupling of the decarboxylation reaction from the ketonization reaction. Using **12** to directly measure the rate of proton exchange at C-3 provides more definitive evidence, than the results for the E276Q- and E278Q-COHED mutants, which only show a decrease in activity for **2**. Thus, the C-3 exchange data presents a stronger case for catalysis occurring in two domains and lend support for the N-terminal domain catalyzing the 1,3-keto-enol tautomerization of **2** to **3**. Consequently,

if Lys-110 does protonate the C-3 position of **2**, then there must be some kind of compensating interaction either from a neighboring active site residue or a water molecule that is still capable of donating a proton at C-3 during ketonization of **2**. That may explain why only a slight decrease in the kinetic parameters is observed between the K110Q-mutant and wild-type COHED with the physiological substrates (**1** and **2**).

Wild-type COHED and the three mutants were also examined with two substrate analogs, **6** and **10**, to determine the importance of the carboxymethyl moiety and the carboxylate group at C-6 to the kinetic parameters. In the first experiment, COHED and the three mutants were incubated with 2-hydroxy-2,4-pentadienoate (HPD, **6**), which is a truncated analog of **2** where the carboxymethyl group has been removed. Only COHED and K110Q-COHED showed activity using **6** but with lower k_{cat} values than those measured for **2**, while the K_m values were comparable. These results indicate that **6** is capable of binding within the active-site of COHED (presumably at the N-terminal domain), but catalysis of the 1,3-keto-enol tautomerization reaction is not very efficient, signifying the importance of the carboxymethyl group. There are two possible roles for this carboxymethyl group. First, the binding of the C-7 carboxylate group within the active-site may induce a conformational change in the enzyme which facilitates catalysis. Second, the C-7 carboxylate group may interact with an active site residue(s) which assist in properly positioning the substrate (**2**) for effective interaction with the catalytic residues. This potential noncovalent, electrostatic interaction would affect the catalytic reaction and may account for the significant difference between the enzyme's activity utilizing the dicarboxylated dienol (**2**) compared to its activity using the

monocarboxylated dienol (**6**). Without this "handle" to determine the exact positioning of the substrate the molecule is free to assume different conformations within the active site. Most of these conformations are catalytically unfavorable, which may account for the 300-fold decrease observed in the corresponding k_{cat}/K_m values. A similar situation has been observed in 4-oxalocrotonate tautomerase, an enzyme of the catechol meta-fission pathway and a homologue of CHMI (the enzyme that precedes COHED). 4-OT catalyzes a 1,5-keto-enol tautomerization reaction using 2-hydroxymuconate (**9**), an analog of **4** without the carboxymethyl group (Scheme 7) (17). A comparison of the kinetic properties of 4-OT with **9** to those of 4-OT with **6** determined that the k_{cat}/K_m value between the two substrates was 10^4–fold larger for the physiological substrate, **9**. It was concluded that the higher value of k_{cat}/K_m was due primarily to a decrease in the overall kinetic barrier for the conversion of **9** provided by the C-6 carboxylate group interacting with an active-site arginine residue (17).

A second experiment examined COHED and the three mutants with 2-oxo-3-hexenedioate (**10**), an analog of **1** (without the carboxymethyl group), to observe the effect the loss of the carboxymethyl group has on the kinetic parameters of the decarboxylation reaction (Scheme 7). In this case, no activity was observed for COHED or for any of the mutants. These results are another indication of the importance the carboxymethyl group may have on COHED catalysis. The reasons for the lack of activity using **10** are similar to those discussed previously for **6**. However, another possibility is that the carboxylate group at the C-6 position may interact with surrounding

active site residue(s), which prevents decarboxylation. Alternatively, this type of interaction may alter the conformation of **10** within the active site not allowing catalysis.

The importance of three active site residues (Lys-110, Glu-276, and Glu-278), the Mg^{2+} ion, and the carboxymethyl group to COHED catalysis have been established. Some evidence supported the idea of two separate catalytic domains in COHED, but additional data is necessary. Consequently, attention focused on finding a suitable irreversible inhibitor.

Four compounds similar to **2** were tested as potential inhibitors of COHED. The first compound examined was 3-bromopropiolic acid (**16**), a mechanism-based irreversible inhibitor of CaaD (8) and its homolog *cis*-3-chloroacrylic acid dehalogenase (*cis*-CaaD) (Figure 3.4) (18). In this experiment, COHED was incubated with an excess of **16** and its activity was monitored with **1** and **2** after 24 hours. COHED was not inhibited by **16**. It seems reasonable to assume that the electrophilic **16** would readily react with an available active site nucleophile once inside the proposed active site(s). One would also predict that **16** being a smaller molecule (only a three carbon chain) than the physiological substrate (**2**) would easily fit into either of the active-site(s) of COHED. However, the results of the inhibition study suggest that **16** is not binding in the active site in a conformation that would allow inactivation to occur.

Another potential affinity labeling inhibitor, 2-oxo-3-bromo-heptadienoate (**13**) was examined (Figure 3.4). The evidence for **13** as a probable competitive inhibitor demonstrates it can bind at the active site(s). However, kinetic measurments showed that once the inhibitor is removed COHED is active. Thus, **13** does not irreversibly inhibit

the enzyme. One other potential affinity labeling inhibitor, 3-bromopyruvate (**15**) was examined as an irreversible inhibitor of COHED (Figure 3.4). Unlike **12** and **13**, 3-bromopyruvate did not act as a competitive inhibitor toward COHED and did not irreversibly inhibit the enzyme either. Like **16**, the results of the inhibition study suggest that **15** is not binding in the active site in a conformation that would allow inactivation to occur.

Based on the results of the four potential inhibitors (**13-16**) tested, no irreversible inhibitor has been identified for COHED. Perhaps a future examination of the crystal structure of COHED with **12** bound in the active site(s) may shed light on identifying possible interactions of these three active site residues with the substrate, recognizing other active site residues involved in catalysis, and determining additional mechanistic insight toward uncoupling the decarboxylation and ketonization reactions. Further investigations of other potential inhibitors and mutagenesis studies would continue to contribute toward a better understanding of the catalytic mechanism of COHED.

ACKNOWLEDGMENTS

We thank Steve D. Sorey (Department of Chemistry, The University of Texas at Austin) for his expert assistance in acquiring the NMR spectra, and Dr. William H. Johnson, Jr. (Division of Medicinal Chemistry, The University of Texas at Austin) for synthesizing needed compounds and interpreting the NMR spectra.

REFERENCES – CHAPTER 3

1. (a) Sparnins, V.L., Chapman, P.J., and Dagley, S. (1974) Bacterial degradation of 4-hydroxyphenylacetic acid and homoprotocatechuic acid. *J. Bacteriol. 120*, 159-167. (b) Jenkins, J.R. and Cooper, R.A. (1988) Molecular cloning, expression, and analysis of the genes of the homoprotocatechuate catabolic pathway of Escherichia coli C. *J. Bacteriol. 170*, 5317-5324.

2. Johnson, W.H., Jr., Hajipour, G., and Whitman, C.P. (1992) Characterization of a dienol intermediate in the 5-(carboxymethyl)-2-oxo-3-hexene-1,6-dioate decarboxylase reaction. *J. Am. Chem. Soc. 114*, 11001-11003.

3. Johnson, W.H., Jr., Hajipour, G., and Whitman, C.P. (1995) The stereochemical course of 5-(carboxymethyl)-2-oxo-3-hexene-1,6-dioate decarboxylase from *Escherichia coli* C. *J. Am. Chem. Soc. 117*, 8719-8726.

4. Tame, J.R., Namba, K., Dodson, E.J., and Roper D.I. (2002) The crystal structure of HpcE, a bifunctional decarboxylase/isomerase with a multifunctional fold. *Biochemistry 41*, 2982-2989.

5. Roper, D.I. and Cooper, R.A. (1990) Purification, properties, and nucleotide sequence of 5-(carboxymethyl)-2-hydroxymuconate isomerase of *Escherichia coli* C. *FEBS Lett 266*, 63-66.

6. Garrido-Pertierra, A. and Cooper, R.A. (1981) Identification and purification of distinct isomerase and decarboxylase enzymes involved in the 4-hydroxyphenylacetate catabolic pathway of *Escherichia coli*. *Eur. J. Biochem. 117*, 581-584.

7. Burks, E. A., Johnson, W. H., Jr., and Whitman, C. P. (1998) Stereochemical and Isotopic Labeling Studies of 2-Oxo-hept-4-ene-1,7-dioate Hydratase: Evidence for an Enzyme-Catalyzed Ketonization Step in the Hydration Reaction. *J. Am. Chem. Soc. 120*, 7665-7675.

8. Wang, S.C., Person, M.D., Johnson, W.H., Jr., and Whitman, C.P. (2003) Reactions of trans-3-chloroacrylic acid dehalogenase with acetylene substrates: consequences of and evidence for a hydration reaction. *Biochemistry 42*, 8762-8773.

9. Sambrook, J. and Russell, D.W. (2001) *Molecular Cloning: A Laboratory Manual, Third Edition*, Cold Spring Harbor Laboratory, Cold Spring Harbor, NY.

10. Waddell, W.J. (1956) A simple ultraviolet spectrophotometric method for the determination of protein. *J. Lab. Clin. Med. 48*, 311-314.

11. Stanley, T.M., Johnson Jr., W.H., Burks, E.A., Hwang, C-C, Cook, P.F., and Whitman, C.P. (2000) Expression and stereochemical and isotope effect studies of active 4-oxalocrotonate decarboxylase. *Biochemistry 39*, 718-726.

12. Timm, D.E., Mueller, H.A., Bhanumoorthy, P., Harp, J.M., and Bunick, G.J. (1999) Crystal structure and mechanism of a carbon-carbon bond hydrolase. *Structure 7*, 1023-1033.

13. (a) Pedersen, K.J. (1934) The decomposition of α-nitrocarboxylic acids - with some remarks on the decomposition of β-ketocarboxylic acids. *Phys. Chem. 38*, 559-571. (b) Pedersen, K.J. (1938) Amine catalysis of the ketonic decomposition of α,α-dimethylacetoacetic acid. *J. Am. Chem. Soc. 60*, 595-601.

14. Westheimer, F.H. (1963) The mechanism of the enzymic decarboxylation of acetoacetic acid. *Proc. Chem. Soc.*, 253-261.

15. O'Leary, M.H. and Westheimer, F.H. (1968) Acetoacetate decarboxylase. Selective acetylation of the enzyme. *Biochemistry 7*, 913-919.

16. Crout, D.H.G., Littlechild, J., Mitchell, M.B., and Morrey, S.M. (1984) Stereochemistry of the decarboxylation of α-acetolactate (2-hydroxy-2-methyl-3-oxobutanoate) by the acetolactate decarboxylase of *Klebsiella aerogenes*. *J. Chem. Soc. Perkin Trans. 1*, 2271-2276.

17. Lian, H., Czerwinski, R.M., Stanley, T.M., Johnson, W.H., Jr., Watson, R.J., and Whitman, C.P. (1998) The contribution of the substrate's carboxylate group to the mechanism of 4-oxalocrotonate tautomerase. *Bioorg. Chem. 26*, 141-156.

18. Poelarends, G.J., Serrano, H., Person, M.D., Johnson, W.H., Jr., Murzin, A.G., and Whitman, C.P. (2004) Cloning, expression, and characterization of a cis-3-chloroacrylic acid dehalogenase: insights into the mechanistic, structural, and evolutionary relationship between isomer-specific 3-chloroacrylic acid dehalogenases. *Biochemistry 43*, 759-772.

REFERENCES

1. Horowitz, N.H. (1945) On the evolution of biochemical syntheses. *Proc. Natl. Acad. Sci. USA 31*, 153-157.

2. Horowitz, N.H. (1965) The evolution of biochemical synthesis – retrospect and prospect, in *Evolving Genes and Proteins* (V. Bryson and H.J. Vogel, Eds.) pp 15-23, Academic Press, New York.

3. Jensen, R.A. (1976) Enzyme recruitment in evolution of new function. *Ann. Rev. Microbiol. 30*, 409-425.

4. Gerlt, J.A. and Babbitt, P.C. (2001) Divergent evolution of enzymatic function: mechanistically diverse superfamilies and functionally distinct suprafamilies. *Ann. Rev. Biochem. 70*, 209-246.

5. Lazcano, A. and Miller, S.L. (1999) On the origin of metabolic pathways. *J. Mol. Evol. 49*, 424-431.

6. Kirschner, K., Szadkowski, H., Jardetzky, T.S., and Hager, V. (1987) Phosphoribosylanthranilate isomerase-indoleglycerol-phosphate synthase from *Escherichia coli*. *Methods Enzymol. 142*, 386-397.

7. Wilmanns, M., Priestle, J.P., Niermann, T., and Jansonius, J.N. (1992) Three-dimensional structure of the bifunctional enzyme phosphoribosylanthranilate isomerase: indoleglycerolphosphate synthase from *Escherichia coli* refined at 2.0Å resolution. *J. Mol. Biol. 223*, 477-507.

8. O'Brien, P.J. and Herschlag, D. (1999) Catalytic promiscuity and the evolution of new enzymatic activities. *Chem. Biol. 6*, R91-R105.

9. Copley, S.D. (2000) Evolution of a metabolic pathway for degradation of a toxic xenobiotic; the patchwork approach. *Trends. Biochem. Sci. 25*, 261-265.

10. Xun, L. and Orser, C.S. (1991) Purification and properties of pentachlorophenol hydroxylase: a flavoprotein from *Flavobacterium* sp. Strain ATCC 39723. *J. Bacteriol. 173*, 4447-4453.

11. Xun, L., Topp, E., and Orser, C.S. (1992) Purification and characterization of a tetrachloro-*p*-hydroquinone reductive dehalogenase from a *Flavobacterium* sp. *J. Bacteriol. 174*, 8003-8007.

12. Xun, L., Resing, K., Lawson, S.L., Babbitt, P.C., and Copley, S.D. (1999) Evidence that pcpA encodes 2,6-dichlorohydroquinone dioxygenase, the ring-cleavage enzyme required for pentachlorophenol degradation in *Sphingomonas chlorophenolica* Strain ATCC 39723. *Biochemistry 38*, 7659-7669.

13. McCarthy, D.L., Navarrete, S., Willett, W.S., Babbit, P.C., and Copley, S.D. (1996) Exploration of the relationship between tetrachlorohydroquinone dehalogenase and the glutathione *S*-transferase superfamily. *Biochemistry 35*, 14634-14642.

14. Board, P.G., Baker, R.T., Chelvanayagam, G., and Jermiin, L.S. (1997) Zeta, a novel class of glutathione transferases in a range of species from plants to humans. *Biochem. J. 328*, 929-935.

15. Armstrong, R.N. (1997) Structure, catalytic mechanism, and evolution of the glutathione transferase. *Chem. Res. Toxicol. 10*, 2-18.

16. Anandarajah, K., Kiefer, P.M., Jr., Donohoe, B.S., and Copley, S.D. (2000) Recruitment of a double bond isomerase to serve as a reductive dehalogenase during biodegradation of pentachlorophenol. *Biochemistry 39*, 5303-5311.

17. Gribble, G.W. (1994) The natural production of chlorinated compounds. *Environ. Sci. Technol. 28*, 311A-319A.

18. Siuda, J.F. and DeBernardis, J.F. (1973) Naturally occurring halogenated organic compounds. *Lloydia 36*, 107-143.

19. Hofstein, H.A., Feng, Y., Anderson, V.E., and Tonge, P.J. (1999) Role of glutamate 144 and glutamate 164 in the catalytic mechanism of enoyl-CoA hydratase. *Biochemistry 38*, 9508-16.

20. Scholten, J.D., Chang, K.H., Babbitt, P.C., Charest, H., Sylvestre, M., and Dunaway-Mariano, D. (1991) Novel enzymic hydrolytic dehalogenation of a chlorinated aromatic. *Science 253*, 182-185.

21. Chang, K.H., Liang, P.H., Beck, W., Scholten, J.D., and Dunaway-Mariano, D. (1992) Isolation and characterization of the three polypeptide components of 4-chlorobenzoate dehalogenase from *Pseudomonas* sp. Strain CBS-3. *Biochemistry 31*, 5605-5610.

22. Holden, H.M., Benning, M.M., Haller, T., and Gerlt, J.A. (2001) The crotonase superfamily: divergently related enzymes that catalyze different reactions involving acyl coenzyme A thioesters. *Acc. Chem. Res. 34*, 145-157.

23. Engel, C.K., Mathieu, M., Zeelen, J.P., Hiltunen, J.K., and Wierenga, R.K. (1996) Crystal structure of enoyl-coenzyme A (CoA) hydratase at 2.5Å resolution: a spiral fold defines the CoA-binding pocket. *EMBO J. 19*, 5135-5145.

24. Benning, M.M., Taylor, K.L., Liu, R. Q., Yang, G., Xiang, H., Wesenberg, G., Dunaway-Mariano, D., and Holden, H.M. (1996) Structure of 4-chlorobenzoyl coenzyme A dehalogenase determined to 1.8Å resolution: an enzyme catalyst generated via adaptive mutation. *Biochemistry 35*, 8103-8109.

25. Yang, G., Liang, P.H., and Dunaway-Mariano, D. (1994) Evidence for nucleophilic catalysis in the aromatic substitution reaction catalyzed by (4-chlorobenzoyl)coenzyme A dehalogenase. *Biochemistry 33*, 8527-8531.

26. Taylor, K.L., Liu, R.Q., Liang, P.H., Price, J, Dunaway-Mariano, D., Tonge P.J., Clarkson, J., and Carey, P.R. (1995) Evidence for electrophilic catalysis in the 4-chlorobenzoyl-CoA dehalogenase reaction: UV, Raman, and ^{13}C-NMR spectral studies of dehalogenase complexes of benzoyl-CoA adducts. *Biochemistry 34*, 13881-13888.

27. Yang, G., Liu R.Q., Taylor, K.L., Xiang, H., Price, J., and Dunaway-Mariano, D. (1996) Identification of active site residues essential to 4-chlorobenzoyl-coenzyme A dehalogenase catalysis by chemical modification and site directed mutagenesis. *Biochemistry 35*, 10879-10885.

28. Taylor, K.L., Xiang, H., Liu, R.Q., Yang, G., and Dunaway-Mariano, D. (1997) Investigation of substrate activation by 4-chlorobenzoyl-coenzyme A dehalogenase. *Biochemistry 36*, 1349-1361.

29. Xiang, H., Dong, J., Carey, P.R., and Dunaway-Mariano, D. (1999) Product catalyzes the deamidation of D145N dehalogenase to produce the wild-type enzyme. *Biochemistry 38*, 4207-4213.

30. Glasner, M.E., Gerlt, J.A., and Babbitt, P.C. (2007) *Mechanisms of protein evolution and their application to protein engineering, in Advances in Enzymology and Related Areas of Molecular Biology, Volume 75: Protein Evolution* (Toone, E.J., Ed.) pp 193-239, John Wiley and Sons, Inc., Hoboken, New Jersey.

31. Gerlt, J.A., Babbitt, P.C., and Rayment, I. (2005) Divergent evolution in the enolase superfamily: the interplay of mechanism and specificity. *Arch. Biochem. Biophys. 433*, 59-70.

32. Babbitt, P.C., Hasson, M.S., Wedekind, J.E., Palmer, D.R.J., Barrett, W.C., Reed, G.H., Rayment, I., Ringe, D., Kenyon, G.L., and Gerlt, J.A. (1996) The enolase superfamily: a general strategy for enzyme-catalyzed abstraction of the α-protons of carboxylic acids. *Biochemistry 35*, 16489-16501.

33. Gerlt, J.A. and Raushel, F.M. (2003) Evolution of function in $(\beta/\alpha)_8$-barrel enzymes. *Curr. Opin. Chem. Biol. 7*, 252-264.

34. Babbitt, P.C. and Gerlt, J.A. (1997) Understanding enzyme superfamilies. chemistry as the fundamental determinant in the evolution of new catalytic activities. *J. Biol. Chem. 272*, 30591-30594.

35. Gerlt, J.A. and Babbitt, P.C. (1998) Mechanistically diverse enzyme superfamilies: the importance of chemistry in the evolution of catalysis. *Curr. Opin. Chem. Biol. 2*, 607-612.

36. Xiang, H., Luo, L., Taylor, K.L., and Dunaway-Mariano, D. (1999) Interchange of catalytic activity within the 2-enoyl-coenzyme A hydratase/isomerase superfamily based on a common active site template. *Biochemistry 38*, 7638-7652.

37. (a) Bayly, R.C. and Barbour, M.G. (1984) The Degradation of Aromatic Compounds by the Meta and Genisate Pathways, in *Microbiological Degradation of Organic Compounds* (Gibson, D.T., Ed.) pp 253-294, Marcel Dekker, New York. (b) Dagley, S. (1986) Biochemistry of Aromatic Hydrocarbon Degradation in *Pseudomonads*, in *The Bacteria: A Treatise on Structure and Function* (Ornston, L. Nicholas and Sokatch, J.R., Eds.) pp 527-555, Academic Press, New York. (c) Dagley, S. (1975) A Biochemical Approach to Some Problems of Environmental Pollution, in *Essays in Biochemistry Vol. 11* (Campbell, P.N., Aldridge, W.N., Eds.) pp 81-138, Academic Press, New York.

38. Shingler, V., Powlowski, J., and Marklund, U. (1992) Nucleotide sequence and functional analysis of the complete phenol/3,4-dimethylphenol catabolic pathway of Pseudomonas sp. strain CF600. *J. Bacteriol. 174*, 711-724.

39. (a) Harayama, S., Lehrbach, P.R., and Timmis, K.N. (1984) Transposon mutagenesis analysis of meta-cleavage pathway operon genes of the TOL plasmid of *Pseudomonas putida mt-2*. *J. Bacteriol 160,* 251-255. (b) Harayama, S., Rekik, M., Ngai, K.L., and Ornston, L.N. (1989) Physically associated enzymes produce and metabolize 2-hydroxy-2,4-dienoate, a chemically unstable intermediate formed in catechol metabolism via meta cleavage in *Pseudomonas putida*. *J. Bacteriol. 171*, 6251-6258.

40. Sanvoisin, J., Langley, G.J., and Bugg, T.D.H. (1995) Mechanism of Extradiol Catechol Dioxygenases: Evidence for a Lactone Intermediate in the 2,3-Dihydroxyphenylpropionate 1,2-Dioxygenase Reaction. *J. Am. Chem. Soc. 117,* 7836-7837.

41. Whitman, C.P., Aird, B.A., Gillespie, W.R., and Stolowich, N.J. (1991) Chemical and enzymic ketonization of 2-hydroxymuconate, a conjugated enol. *J. Am. Chem. Soc. 113*, 3154-3162.

42. Diaz, E. and Timmis, K.N. (1995) Identification of functional residues in a 2-hydroxymuconic semialdehyde hydrolase. A new member of the alpha/beta hydrolase-fold family of enzymes which cleaves carbon-carbon bonds. *J. Biol. Chem. 270*, 6403-6411.

43. (a) Sparnins, V.L., Chapman, P.J., and Dagley, S. (1974) Bacterial degradation of 4-hydroxyphenylacetic acid and homoprotocatechuic acid. *J. Bacteriol. 120*, 159-167. (b) Jenkins, J.R. and Cooper, R.A. (1988) Molecular cloning, expression, and analysis of the genes of the homoprotocatechuate catabolic pathway of Escherichia coli C. *J. Bacteriol. 170*, 5317-5324.

44. Hajipour, G., Johnson, W.H., Jr., Dauben, P.D., Stolowich, N.J., and Whitman, C.P. (1993) Chemical and enzymatic ketonization of 5-(carboxymethyl)-2-hydroxymuconate. *J. Am. Chem. Soc. 115*, 3533-3542.

45. (a) Garrido-Pertierra, A. and Cooper, R.A. (1981) Identification and purification of distinct isomerase and decarboxylase enzymes involved in the 4-hydroxyphenylacetate catabolic pathway of *Escherichia coli*. *Eur. J. Biochem. 117*, 581-584. (b) Roper, D.I. and Cooper, R.A. (1990) Purification, properties, and nucleotide sequence of 5-(carboxymethyl)-2-hydroxymuconate isomerase of *Escherichia coli C*. *FEBS Lett 266*, 63-66.

46. Johnson, W.H., Jr., Hajipour, G., and Whitman, C.P. (1992) Characterization of a dienol intermediate in the 5-(carboxymethyl)-2-oxo-3-hexene-1,6-dioate decarboxylase reaction. *J. Am. Chem. Soc. 114*, 11001-11003.

47. Johnson, W.H., Jr., Hajipour, G., and Whitman, C.P. (1995) The stereochemical course of 5-(carboxymethyl)-2-oxo-3-hexene-1,6-dioate decarboxylase from *Escherichia coli C*. *J. Am. Chem. Soc. 117*, 8719-8726.

48. Roper, D.I., Stringfellow, J.M., and Cooper, R.A. (1995) Sequence of the hpcC and hpcG genes of the meta-fission homoprotocatechuic acid pathway of *Escherichia coli C*: nearly 40% amino-acid identity with the analogous enzymes of the catechol pathway. *Gene 156*, 47-51.

49. Burks, E. A., Johnson, W. H., Jr., and Whitman, C. P. (1998) Stereochemical and Isotopic Labeling Studies of 2-Oxo-hept-4-ene-1,7-dioate Hydratase: Evidence for an Enzyme-Catalyzed Ketonization Step in the Hydration Reaction. *J. Am. Chem. Soc. 120*, 7665-7675.

50. Whitman, C.P., Hajipour, G., Watson, R.J., Johnson, W.H., Jr., Bembenek, M.E., and Stolowich, N.J. (1992) Stereospecific ketonization of 2-hydroxymuconate by 4-oxalocrotonate tautomerase and 5-(carboxymethyl)-2-hydroxymuconate isomerase. *J. Am. Chem. Soc. 114*, 10104-10110.

51. Tame, J.R., Namba, K., Dodson, E.J., and Roper D.I. (2002) The crystal structure of HpcE, a bifunctional decarboxylase/isomerase with a multifunctional fold. *Biochemistry 41*, 2982-2989.

52. Timm, D.E., Mueller, H.A., Bhanumoorthy, P., Harp, J.M., and Bunick, G.J. (1999) Crystal structure and mechanism of a carbon-carbon bond hydrolase. *Structure 7*, 1023-1033.

53. Pollard, J.R., Rialland, D., and Bugg, T.D. (1998) Substrate selectivity and biochemical properties of 4-hydroxy-2-keto-pentanoic acid aldolase from *Escherichia coli*. *Appl. Environ. Microbiol. 64*, 4093-4094.

54. Pollard, J.R. and Bugg, T.D. (1998) Purification, characterisation and reaction mechanism of monofunctional 2-hydroxypentadienoic acid hydratase from *Escherichia coli*. *Eur. J. Biochem. 251*, 98-106.

55. Stanley, T.M., Johnson Jr., W.H., Burks, E.A., Hwang, C-C, Cook, P.F., and Whitman, C.P. (2000) Expression and stereochemical and isotope effect studies of active 4-oxalocrotonate decarboxylase. *Biochemistry 39*, 718-726.

56. Lian, H. and Whitman, C.P. (1994) Stereochemical and Isotopic Labeling Studies of 4-Oxalocrotonate Decarboxylase and Vinylpyruvate Hydratase: Analysis and Mechanistic Implications. *J. Amer. Chem. Soc. 116*, 10403-10411.

57. Schwab, J.M. and Henderson, B.S. (1990) Enzyme-catalyzed allylic rearrangements. *Chem. Rev. 90*, 1203-1245.

58. Lian, H. and Whitman, C.P. (1993) Ketonization of 2-hydroxy-2,4-pentadienoate by 4-oxalocrotonate tautomerase: implications for the stereochemical course and the mechanism. *J. Amer. Chem. Soc. 115*, 7978-7984.

59. Johnson, W.H., Jr., Czerwinski, R.M., Fitzgerald, M.C., and Whitman, C.P. (1997) Inactivation of 4-oxalocrotonate tautomerase by 2-oxo-3-pentynoate. *Biochemistry 36*, 15724-15732.
60. Wang, S.C., Person, M.D., Johnson, W.H., Jr., and Whitman, C.P. (2003) Reactions of trans-3-chloroacrylic acid dehalogenase with acetylene substrates: consequences of and evidence for a hydration reaction. *Biochemistry 42*, 8762-8773.

61. Poelarends, G.J., Serrano, H., Johnson, W.H., Jr., and Whitman, C.P. (2004) Stereospecific alkylation of cis-3-chloroacrylic acid dehalogenase by (*R*)-oxirane-2-carboxylate: analysis and mechanistic implications. *Biochemistry 43*, 7187-7196.

62. Sambrook, J. and Russell, D.W. (2001) *Molecular Cloning: A Laboratory Manual, Third Edition*, Cold Spring Harbor Laboratory, Cold Spring Harbor, NY.

63. Waddell, W.J. (1956) A simple ultraviolet spectrophotometric method for the determination of protein. *J. Lab. Clin. Med. 48*, 311-314.

64. Ho, S.N., Hunt, H.D., Horton, R.M., Pullen, J.K., and Pease, L.R. (1989) Site-directed mutagenesis by overlap extension using the polymerase chain reaction. *Gene 77*, 51-59.

65. Portsmouth, D., Stoolmiller, A.C., and Ables, R.H. (1967) Studies on the mechanism of action of 2-keto-3-deoxy-L-arabonate dehydratase. *J. Biol. Chem. 242*, 2751-2759.

66. Schwab, J.M. and Klassen, J.B. (1984) Steric course of the allylic rearrangement catalyzed by β-hydroxydecanoylthioester dehydrase. Mechanistic implications. *J. Am. Chem. Soc. 106*, 7217-7227.

67. Brock, D.J.H, Kass, L.R., and Bloch, K. (1967) Beta-hydroxydecanoyl thioester dehydrase. II. Mode of action. *J. Biol. Chem. 242*, 4432-4440.

68. Poelarends, G.J., Serrano, H., Person, M.D., Johnson, W.H., Jr., Murzin, A.G., and Whitman, C.P. (2004) Cloning, expression, and characterization of a cis-3-chloroacrylic acid dehalogenase: insights into the mechanistic, structural, and evolutionary relationship between isomer-specific 3-chloroacrylic acid dehalogenases. *Biochemistry 43*, 759-772.

69. (a) Pedersen, K.J. (1934) The decomposition of α-nitrocarboxylic acids - with some remarks on the decomposition of β-ketocarboxylic acids. *Phys. Chem. 38*, 559-571. (b) Pedersen, K.J. (1938) Amine catalysis of the ketonic decomposition of α,α-dimethylacetoacetic acid. *J. Am. Chem. Soc. 60*, 595-601.

70. Westheimer, F.H. (1963) The mechanism of the enzymic decarboxylation of acetoacetic acid. *Proc. Chem. Soc.*, 253-261.

71. O'Leary, M.H. and Westheimer, F.H. (1968) Acetoacetate decarboxylase. Selective acetylation of the enzyme. *Biochemistry 7*, 913-919.

72. Crout, D.H.G., Littlechild, J., Mitchell, M.B., and Morrey, S.M. (1984) Stereochemistry of the decarboxylation of α-acetolactate (2-hydroxy-2-methyl-3-oxobutanoate) by the acetolactate decarboxylase of *Klebsiella aerogenes*. *J. Chem. Soc. Perkin Trans. 1*, 2271-2276.

73. Lian, H., Czerwinski, R.M., Stanley, T.M., Johnson, W.H., Jr., Watson, R.J., and Whitman, C.P. (1998) The contribution of the substrate's carboxylate group to the mechanism of 4-oxalocrotonate tautomerase. *Bioorg. Chem. 26*, 141-156.

Vita

Scott G. Miller attended the Arkansas School for Mathematics and Sciences, graduating in 1995. He attended The University of Central Arkansas from 1995 – 2000. He graduated with a Bachelor's of Science degree in May 2000, majoring in biology and chemistry. In August 2001, he enrolled in the Division of Medicinal Chemistry of the College of Pharmacy at The University of Texas at Austin. He was a doctoral student from 2001 – 2008 under the supervision of Christian P. Whitman, graduating in August 2008 with a Doctor of Philosophy in Pharmacy (Medicinal Chemistry) from the University of Texas at Austin.

Permanent Address: 6263 McNeil Drive, Apt. 1324, Austin, Texas 78729

This dissertation was typed by the author